NGU REPORT 2015.024

Pockmarks, gas flares and carbonate crusts and their relation to the tectonic and stratigraphic evolution of the Alvheim and Utsira High areas (North Sea) and the Harstad Basin (SW Barents Sea)

GEOLOGY FOR SOCIETY

SINCE 1858

GEOLOGICAL SURVEY OF NORWAY

- NGU -

GEOLOGICAL SURVEY OF NORWAY

REPORT

Geological Survey of Norway
P.O.Box 6315 Sluppen
NO-7491 TRONDHEIM
Tel.: 47 73 90 40 00

Report no.: 2015.024

ISSN: 0800-3416 (print)
ISSN: 2387-3515 (online)

Grading: Confidential until December 2016

Title: Pockmarks, gas flares and carbonate crusts and their relation to the tectonic and stratigraphic evolution of the Alvheim and Utsira High areas (North Sea) and the Harstad Basin (SW Barents Sea)

Authors: Shyam Chand, Terje Thorsnes, Aivo Lepland and Antoine Cremiere

Client: Lundin Norway AS

County:

Commune:

Map-sheet name (M=1:250.000)

Map-sheet no. and -name (M=1:50.000)

Deposit name and grid-reference:

Number of pages: 95 **Price (NOK):** 390
Map enclosures: 0

Fieldwork carried out:	**Date of report:** 1st December 2015	**Project no.:** 352200	**Person responsible:** Reidulv Bøe R. Bøe

Summary

This project aims to achieve a better understanding of shallow geological/seabed conditions and processes to support technical and environmental aspects of exploration and production in the Alvheim and Utsira High areas in the North Sea and the Harstad Basin in the SW Barents Sea.

The sub-goals of the project are:

- Cruise planning and preparations.
- Detection and mapping of water column gas flares using EM710 multibeam and HUGIN Sniffer.
- Mapping of bathymetry and identification of neotectonic features on the seafloor and their relation to the subsurface.
- Sampling of seep gas and carbonate crusts from pockmarks and adjacent seabed for a follow-up study that will assess the potential of crusts as proxies of the timing and intensity of past leakages.

Five cruises were planned and carried out in January, March, September and November 2013, and in September 2014, with the following results:

- A total of 25 gas flares from Alvheim, 21 from the Utsira High and 190 from the Harstad Basin are identified from water column data collected by multibeam echosounder in the MAREANO program and during the cruises in January, March and November 2013.
- Carbonate crusts were identified at 247 sites in the Harstad Basin using the HUGIN HUS system during the cruise in March and November 2013.
- ROV sampling was undertaken during three cruises. Carbonate crusts, seep gas and push-in sediment cores were collected from Alvheim in September 2013, seep gas was collected from the Harstad Basin in November 2013 and carbonate crusts, seep gas and push-in sediment cores were collected from the Harstad Basin and the Loppa High in September 2014.

This report summarizes the cruise results and results from work on the collected data.

Keywords: Marine geology	Gas Flare	Pockmark
Seismic	Shallow Gas	Neotectonic
Multibeam bathymetry	Backscatter	AUV

CONTENTS

1. INTRODUCTION

The study areas described in this report are located in the North Sea and the Barents Sea. The Phanerozoic history of North Sea can be divided into two major phases. The first was related to formation of the Pangean supercontinent with the Caledonian and Hercynian orogenies. During the Caledonian orogeny, the collision between the Fennoscandian Baltic shield and the Laurentian Greenland Shield led to formation of compressional structural elements that were superimposed on older Precambrian structural trends. The Caledonian structural elements are typically directed NE-SW. They were reactivated during subsequent tectonic events (Isaksen and Tonstad, 1989).

The second major tectonic phase was associated with the breakup of the Pangean supercontinent. In late Palaeozoic and early Triassic times, tensional forces acted on the whole area and resulted in the breakup of the supercontinent and the opening of the North Atlantic during the Tertiary. From Permian time onwards, extensional tectonics produced grabens and basins, and associated sea level change was the main factor controlling sedimentary processes (Isaksen and Tonstad, 1989). The tectonic movements also led to the development of important structural features in the North Sea. The Mid North Sea High is an east-west trending high dividing the North Sea into a northern and a southern basin.

During the Jurassic and earliest Early Cretaceous the North Sea was affected by a series of tectonic movements. Block faulting during rifting and erosion took place in the later part of the Jurassic (Isaksen and Tonstad, 1989). Uplift and erosion during the Late Kimmerian resulted in widespread regression which formed isolated sedimentary basins where deposition took place under dominantly anaerobic bottom water conditions (Rawson and Riley, 1982; Clausen et al., 2000). The Early Cretaceous was a period of transgression with minor regressions.

The central North Sea has source rocks of Permian to Tertiary age from which oil, gas and fluids migrate and are potentially stored in shallow hydrocarbon reservoirs. A few natural gas seeps have been reported from the North Sea (Hovland and Sommerville, 1985). During the Quaternary, the central North Sea was characterized by high sedimentation rates over short time intervals, separated by long hiatuses (Sejrup et al., 1991, Haflidason et al., 1998; Ottesen et al., 2014). Fine grained shallow water sediments dominate the Pleistocene sequence. These sediments were suggested to have been re-deposited by rivers flowing northward from the British Isles and the continent during periods of low sea level. The extreme low stands of sea level are also indicated by deeply incised river channels. The most extensive glaciations in the North Sea Basin occurred between 200 and 450 ka BP (Sejrup et al., 1991).

Pore pressure estimates in the North Sea indicate high overpressures. Horizontal stresses are high and partly related to deglaciation and flexure and partly related to compaction disequilibrium (Grollimund and Zoback, 2000). Iceberg ploughmarks are reported to be

accumulation zones of shallow gas (Haavik and Landro, 2014). Surface and subsurface expressions of gas seepage to the seabed are observed throughout the North Sea (Landrø and Strønen, 2003; Schroot et al., 2005; Forsberg et al., 2007). Subglacial tunnel valleys formed during the last glaciations are common along the seafloor and subsurface (Lonergan et al., 2006).

The Barents Sea is an epicontinental sea bounded by a sheared and rifted Tertiary margin to the west (Eldholm et al., 1984). Mesozoic and early Cenozoic sedimentation took place in intracratonic basins. After the early Eocene opening of the Norwegian Sea, the Tertiary sediment transport bypassed these basins, and depocentres were established on the continental margin (Spencer et al., 1984). The Bear Island Trough (Bjørnøyrenna) was formed by extensive glacial erosion (Nøttvedt et al., 1988; Eidvin and Riis, 1989; Vorren et al., 1991; Riis and Fjeldskaar, 1992) and the bulk of the eroded sediments were deposited on the continental slope on the Bear Island Trough Mouth Fan (Vorren et al., 1991; Faleide et al., 1996). The morphology of the Barents Sea has been interpreted as a submerged, inherited fluvial landscape, formed in preglacial times and later modified by glacial erosion (Nansen, 1904; Lastochkin, 1977; Vorren et al., 1986, 1991; Laberg et al., 2011). Drilling and coring from SW Barents Sea show that the sediments have mainly a glacial affinity, and that the main part of the erosion took place in the late Plio-Pleistocene (<2.7 Ma) (Eidvin and Riis, 1989; Eidvin et al., 1993, 1998; Mørk and Duncan, 1993; Hald et al., 1990; Knies et al., 2009).

Estimates show that about 1000 m of sedimentary rocks may have been removed by the glacial erosion (Nøttvedt et al., 1988; Vorren et al., 1991; Riis and Fjeldskaar, 1992; Løseth et al., 1992; Nyland et al., 1992). The erosion produced a prominent erosion surface, the upper regional unconformity, URU (Solheim and Kristoffersen, 1984; Vorren et al., 1986). An upper glacigenic sediment succession of varying thickness covers the URU (Solheim and Kristoffersen, 1984; Vorren et al., 1986). It reaches a maximum thickness of about 1000 m at the present shelf edge close to the Bear Island Fan, and has a secondary maximum on the inner shelf, adjacent to the Norwegian coast, where it fills a large glacial trough (the Bear Island Trough) (Vorren et al., 1989, 1990). Associated with the erosion, considerable late Cenozoic uplift took place, modeled by Riis and Fjeldskaar (1992) to be around 900-1400 m in the western Barents Sea. A major part of the Bear Island Fan is of late Pliocene and Pleistocene age (Eidvin and Riis, 1989; Eidvin et al., 1993), which implies very high erosion and sedimentation rates. High erosion rates in the mid-late Pleistocene were also inferred by Vorren et al. (1991), with 150 m regionally, and as much as 400 m locally, during the last 0.8 Ma, and by Sættem et al. (1992), who suggest erosion of 200-250 m or more for the last 0.44 Ma. Seismostratigraphic interpretations indicate that grounded glaciers may have reached the shelf break of the southern Barents Sea 5-10 times during the Pleistocene (Solheim and Kristoffersen, 1984; Vorren et al., 1988; Sættem et al., 1992

The present study is focused on three small regions along the central North Sea and southernmost part of the SW Barents Sea. The first study area lies close to the boundary of the

UK – Norway territorial waters, named Alvheim, the second study area is at the Utsira High (Fig. 1) while the third study area lies in Håkjerringdjupet in the Harstad Basin, SW Barents Sea (Fig. 2). The project's aim is to achieve a better understanding of the shallow subsurface and seabed geological conditions and processes to support technical and environmental aspects of hydrocarbon exploration within the study areas. The project has the following sub-goals:

- To detect seep-related features, including pockmarks on the seafloor and gas flares in the water column.
- To map faults and other neotectonic structures and assess their nature.
- To identify carbonate crusts at the seafloor and assess their potential as indicators of fluid flux and timing of fluid flux.

2. STUDY AREAS

The study focuses on two locations in the central North Sea and one location in the SW Barents Sea. The locations in North Sea are close to the Utsira High, close to the new giant discovery Johan Sverdrup and the Alvheim field (Fig. 1). The location in SW Barents Sea is within the Harstad Basin, in the Håkjerringdjupet depression (Fig. 2).

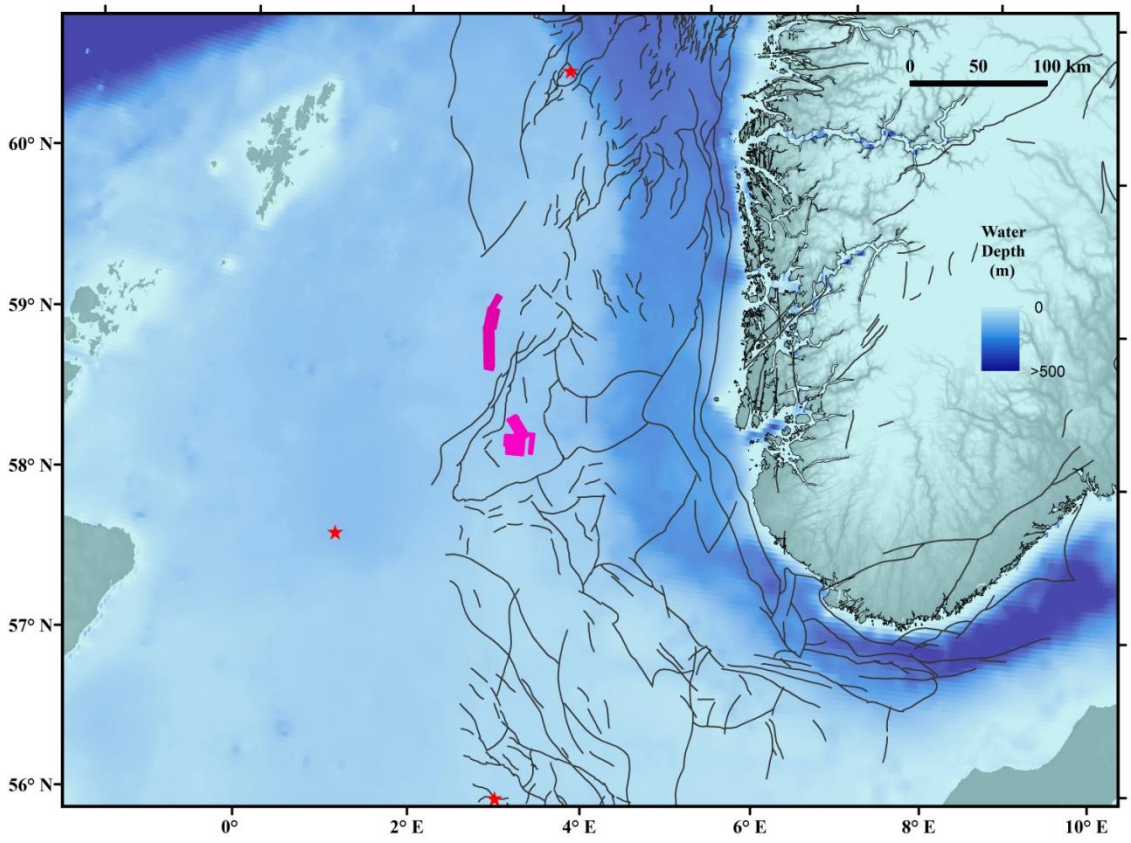

Figure 1. North Sea study areas and new multibeam bathymetry (pink polygons) obtained in the project shown on regional bathymetry. Also shown are faults (black lines) in the Norwegian part of the North Sea and previously known gas flares (red stars) (Hovland and Summerville, 1985; Hovland, 2007).

The North Sea was under the influence of glaciations several times during the Pleistocene including the Elsterian, Saalian and Weichselian glaciations (Stoker et al., 1985; Cameron et al., 1987; Wingfield, 1989, Sejrup et al., 1991; Nygård et al., 2005, Ottesen et al., 2014). The conditions during the Quaternary varied between a present day water depth of up to 150 m, lowered sea level, glacial coverage with a grounded glacier (Chappell and Shackleton 1986, Fairbanks, 1989) or even sub aerial exposure (Sejrup et al., 1991). The Quaternary morphology is dominated by buried channels, their origin attributed to sub glacial melt water transport incising the underlying sedimentary strata during periods of glacial coverage (Cameron et al., 1987; Sejrup et al., 1987; Wingfield, 1989; Gausland, 1998; Huuse and Lykke-Andersen, 2000; Huuse et al., 2003; Lonergan et al., 2006; Fichler et al., 2005). After the retreat of the glaciers, the seafloor topography was filled by marine and glaciomarine sediments (Gausland, 1998; Huuse and Lykke-Andersen, 2000).

The structure and subcrop map of the North Sea indicates many older formations of Miocene to Jurassic age outcropping under the glacial sediments towards the west and east of the study area whereas it is underlain by Pliocene sediments within the study area (Fig. 3). The region is heavily tectonised with regional faults extending in the NE-SW direction (Figs. 1 & 3). Occurrence of shallow gas as seismic anomalies (Karstens and Berndt, 2015) and high gas concentrations in sediments are reported from the study area (Hovland et al., 1987).

The SW Barents Sea region was under the influence of a thick ice sheet during the Last Glacial Maximum (LGM), inferred to be 750-1000 m thick from modeling results (Siegert et al., 2001) (Fig. 2). The glaciers retreated from this region around 18 000-20 000 cal years BP (14 000-16 000 ^{14}C yrs BP) which resulted in huge release of ice load as well as deposition of glaciomarine and marine sediments. The exact timing of the retreat is still debated, but an early retreat was suggested by Aagard Sørensen et al. (2010) based on dating of a core from Ingøydjupet. The sedimentation rates during the glaciomarine period varied between 40 and 70 cm/kyr while it settled to a modest rate of 6 cm/kyr during the last 9000 cal years BP (Aagard Sørensen et al., 2010). Studies on cores from the Loppa high (Pau et al., 2012) and carbonate crust samples (Cremiere et al., 2014) indicate that the region was ice free and pockmarks and carbonate crusts started forming by 17 000 cal years BP.

The study area is also covering the Håkjerringdjupet depression, where the basin deepens to maximum water depths of ~375 m (Fig. 2). The structure and subcrop map of the SW Barents Sea indicate the occurrence of regional faults and sedimentary formations of Cambro-Silurian to Pliocene age (Fig. 4a & b). The Troms- Finnmark Fault complex acts as a main boundary between the Finnmark Platform and the Tromsø and Harstad Basins (Fig. 4a). The sedimentary rocks underlying the URU are of mainly Pliocene age in the Harstad Basin whereas they are as old as Jurassic in Håkjerringdjupet and on the Finnmark Platform, and are generally shallowing towards the Finnmark Platform (Fig. 4b).

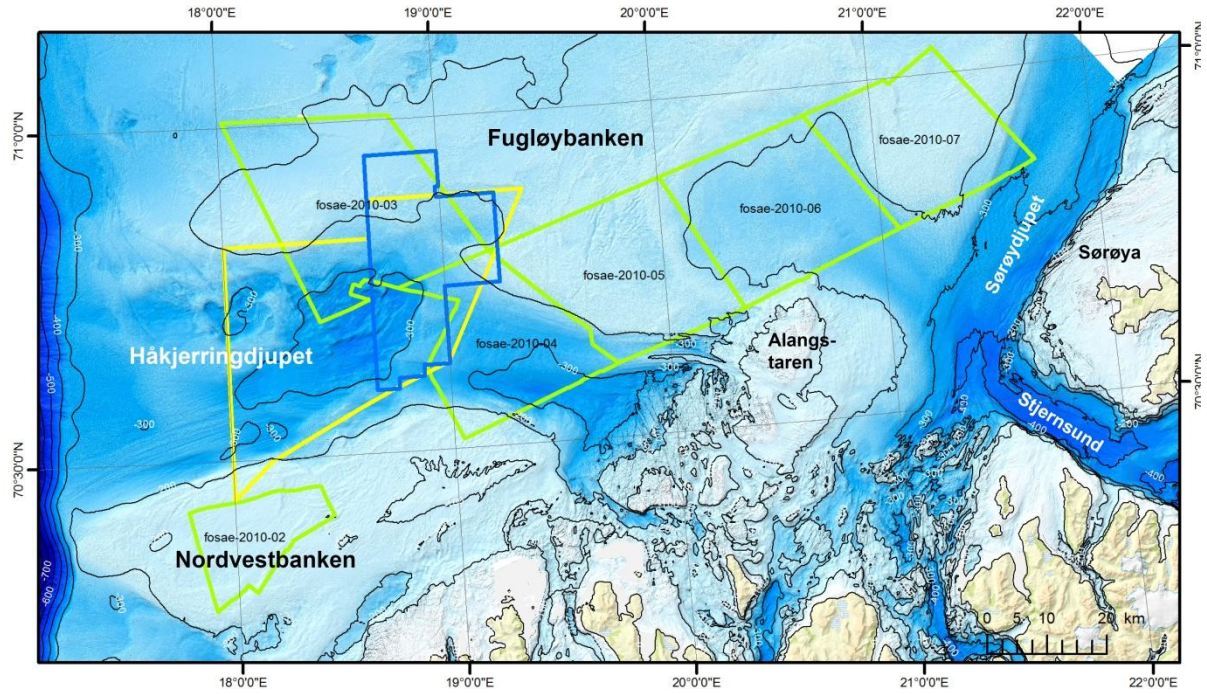

Figure *2. Bathymetry of the SW Barents Sea showing the study area in the Harstad Basin (yellow polygon). MAREANO surveys with water column data (green polygons) and hydrocarbon license block (blue polygon) are also shown.*

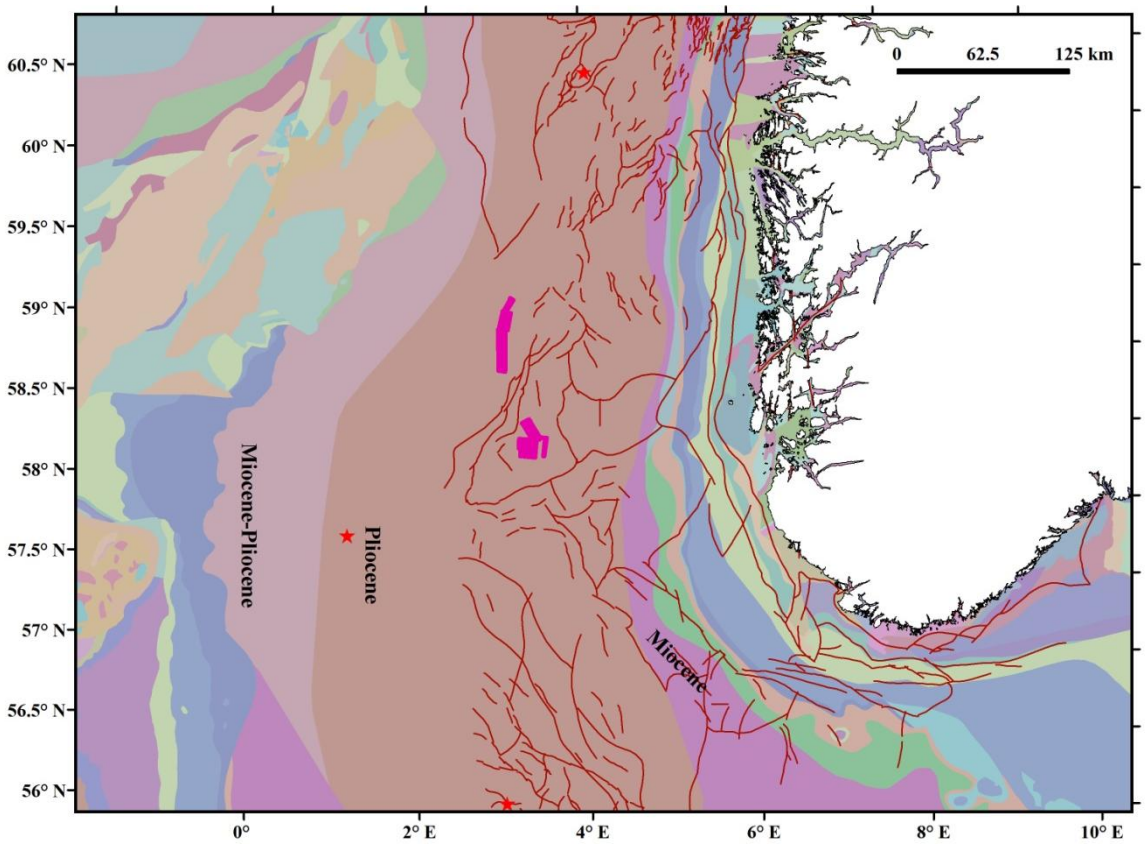

Figure *3. Structural and subcrop map of the Central North Sea (Sigmond, 1992) showing the study areas (pink polygons), faults (red lines) and previously known flare locations (red stars) (Hovland, 2007; Hovland and Sommerville, 1985) .*

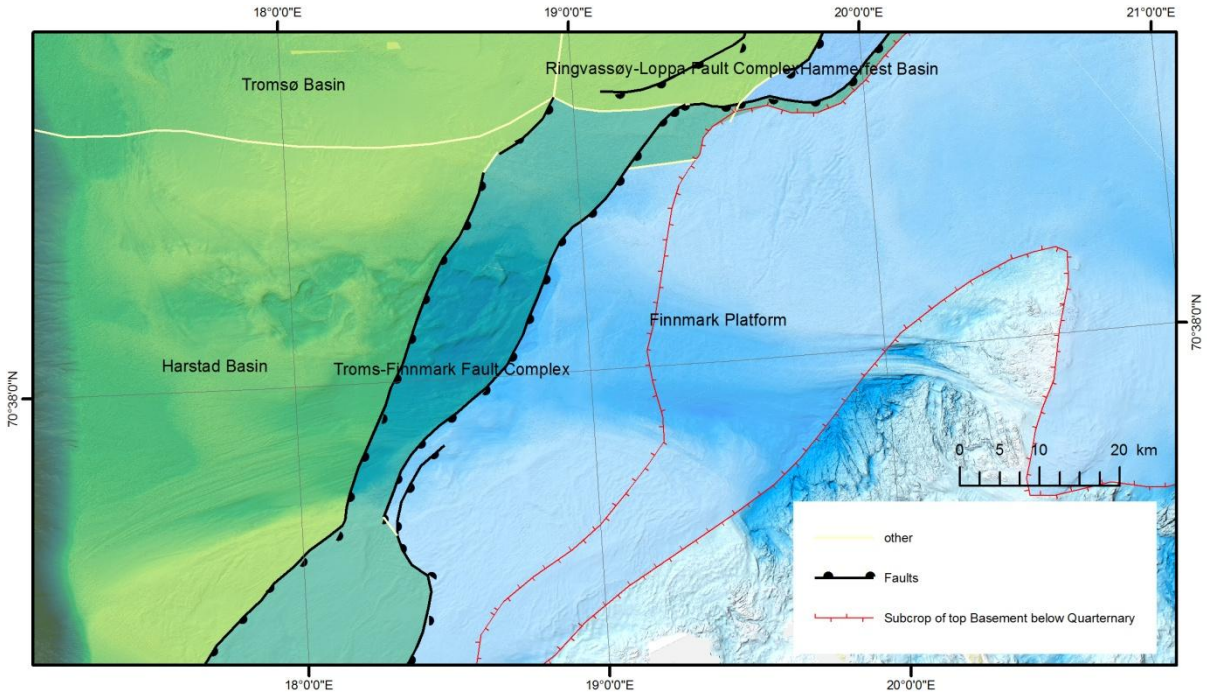

Figure 4a. Structural map of the Harstad basin showing major fault complexes and basins (Sigmond, 1992).

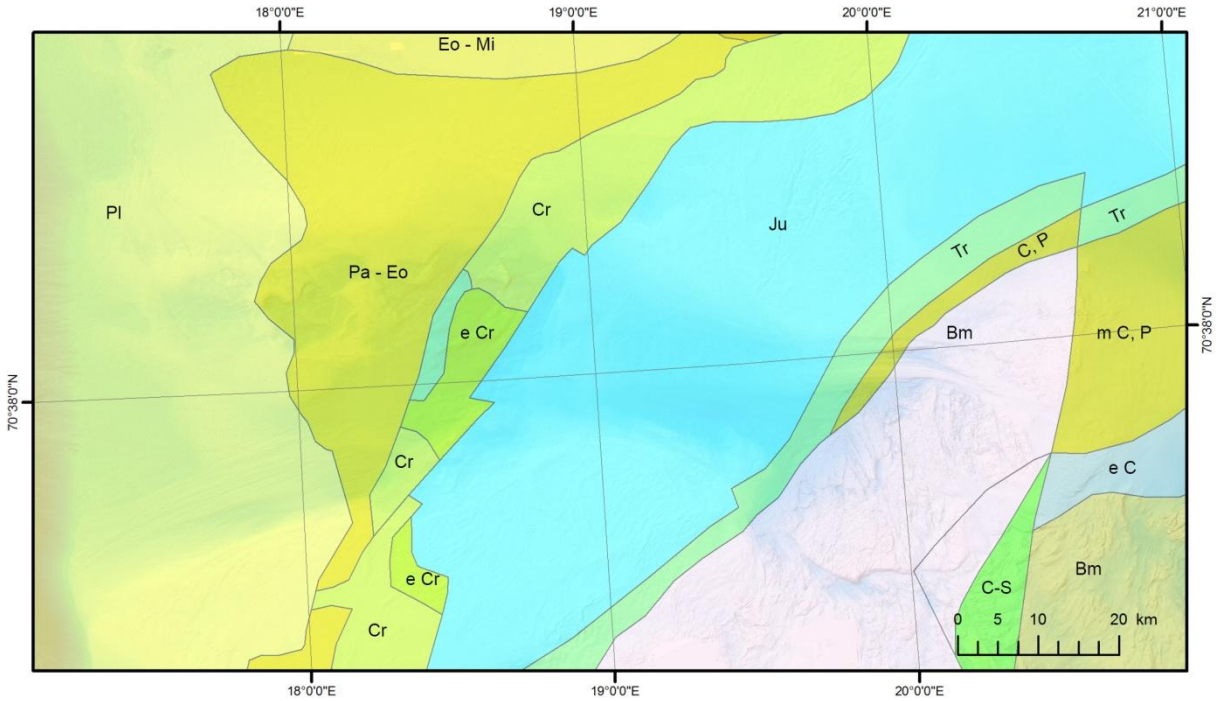

Figure 4b. Subcrop map. Bm: basement; C-S: Cambro-Silurian; e C: early Cretaceous; m C, P: mid Carboniferous, Permian; C, P: Carboniferous, Permian; Tr: Triassic; Ju: Jurassic; e Cr: early Cretaceous; Cr: Cretaceous; Pa-Eo: Paleocene-Eocene; Eo-Mi: Eocene-Miocene; Pl: Pliocene (from Sigmond 1992).

3. MATERIALS AND METHODS

3.1 Bathymetry/backscatter

The multibeam bathymetry echosounder (MBE) data in the North Sea study areas (Figs. 5 & 6) were collected by the Norwegian Defence Research Establishment (FFI) using EM710 system whereas the Harstad Basin data (Fig. 7) were collected by the MAREANO programme using EM710 and other echosounders. The main advantage of the EM710 multibeam echosounder system is that it can record water column data also. Part of the MAREANO data collected using older multibeam echosounders did not record water column data so some of the areas of interest were covered by new EM710 surveys to acquire water column data. The operating frequency used by EM710 (70-100 kHz) is also advantageous for the intermediate water depths, between 200 m and 1000 m, where other systems usually need a change in frequency. The operating frequency of 70-100 kHz and water depths of ca. 120 m give a Fresnel zone diameter (foot print) of around 4 m thus mapping 16 m^2 by each beam.

As a general rule, features smaller than the size of one fourth the wavelength cannot be resolved (Sheriff, 1980). Hence, features larger than 1 meter in diameter can be theoretically detected using the system. The water column data recorded by the system can be used for detection of active gas seeps and also detection of fauna. The presences of fish schools (air in bladder) can be easily identified and is hence useful to estimate the energy loss in the water column during detailed backscatter processing. FlederMaus (FM) Midwater package was used to process water column data for detecting and analysing gas anomalies. The MBE data can also be used to derive the seafloor reflection (i.e., backscatter) properties which will indirectly give an indication of sediment type/grain size and/or hardness of the sea bottom. The FM Geocoder package was used to process the MBE data for backscatter.

3.2 HUGIN Payloads

The HUGIN AUV was equipped with the following payloads: 1) An EdgeTech 2200 high resolution full spectrum chirp sub-bottom profiler (SBP), 2) high resolution interferometric synthetic aperture sonar (HISAS), 3) Methane Sniffer, 4) Turbidity sensor, 5) B&W photo camera. The SBP was used to profile interesting features of the immediate subsurface in very high resolution (Figs. 5b & 6b). The HUGIN HUS was flown ~10 m above the seafloor at a constant speed giving 50 cm horizontal resolution and a vertical resolution of less than 100 microseconds (~10 cm) with the SBP system. The HUGIN EdgeTech data are available to the user as Segy files, needing however a correction for water depth. The data were corrected for water depth and converting the geographic coordinates to UTM coordinates with centimeter accuracy was done using in house programs. The SegY files were converted to jpeg2000 format files using the Natural Resources Canada (NRC) software segyjp2 and visualised using segyjp2 viewer. The geographic locations of the data points were converted to ArcGIS shape files using segyjp2 viewer.

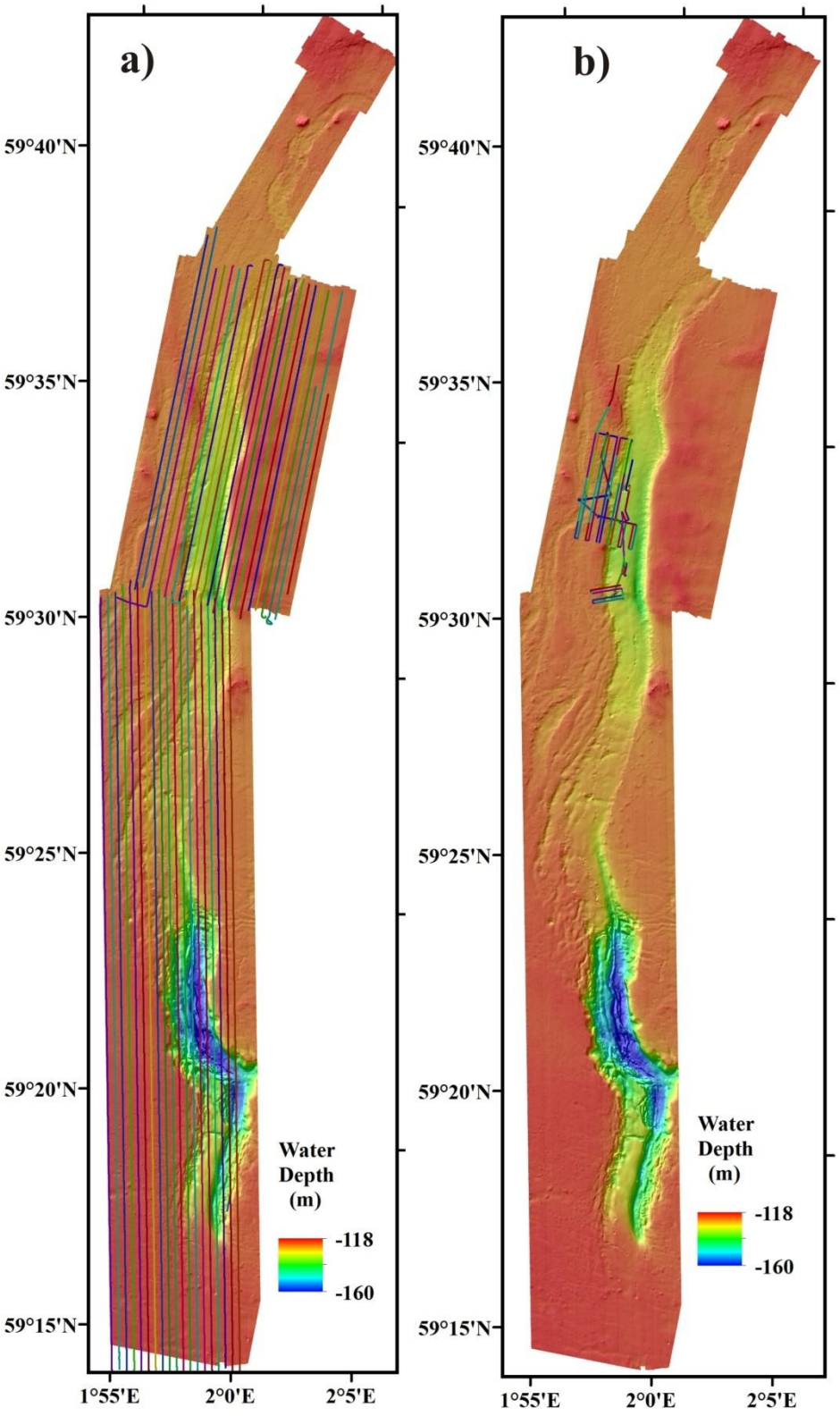

Figure 5. Bathymetry of the Alvheim study area showing the locations of a) Topas lines and b) Hugin SBP lines.

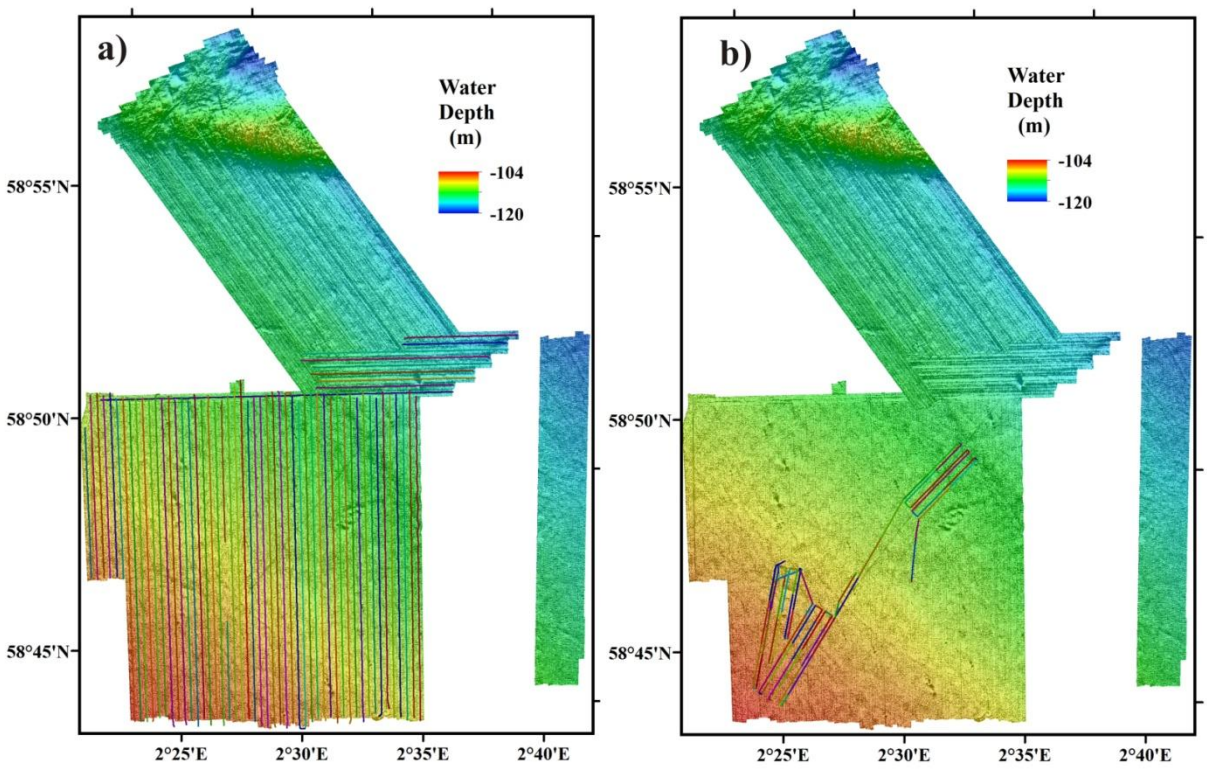

Figure 6. Bathymetry of the Utsira High area showing the locations of a) Topas lines and b) Hugin SBP lines.

The HISAS 1030 is a high resolution interferometric synthetic aperture sonar system capable of providing very high resolution images and detailed bathymetry of the seabed. The system has a range-independent resolution of approximately 3x3 cm out to a distance of 200 m from both sides of the AUV at a speed of 2 m/s. Raw, unprocessed sidescan sonar data in xtf format were ready within a few hours. Onboard processed high resolution mosaics in geotiff format were available for inspection in Reflection and/or ArcMap within 10 hours of HUGIN recovery.

Carbonate crust were identified on the SAS imagery as patchy, 1-2 m wide, irregular, low relief objects, normally in combination with pockmarks or small depressions. In some cases, the sediments around the interpreted crust fields have higher backscatter.

The methane sniffer (METS) has a methane sensitive detector located in a detector room in the sensor head. The detector room is protected against water and pressure by a silicone membrane. The gas molecules diffuse through the membrane, following the partial pressure gradient between water and detector room, according to Henry's law. Hence, the concentration in the detector room is directly correlated to the concentration in the outside water. The sensitivity in the pumped flow-through mode is 1nM – 500nM. The reaction time is within a few seconds (METS product sheet, from www.franatech.com). The T90 time (time to reach 90% of the end-value) for this version of METS is typically within 5 minutes in pumped-through mode (Michel Masson, Franatech – pers. comm.)

The methane sniffer was used to estimate the amount of leakage at locations where gas flares have been identified during previous cruises. In addition to the methane sniffer, HUGIN also carried temperature, turbidity, salinity and visibility sensors. Data set deliveries included GeoTiff files and ASCII text files. The TFish B&W camera provided very high resolution images of the seafloor. The TFish images were available co-registered with the HISAS data within hours through the Reflection software system on-board HU Sverdrup.

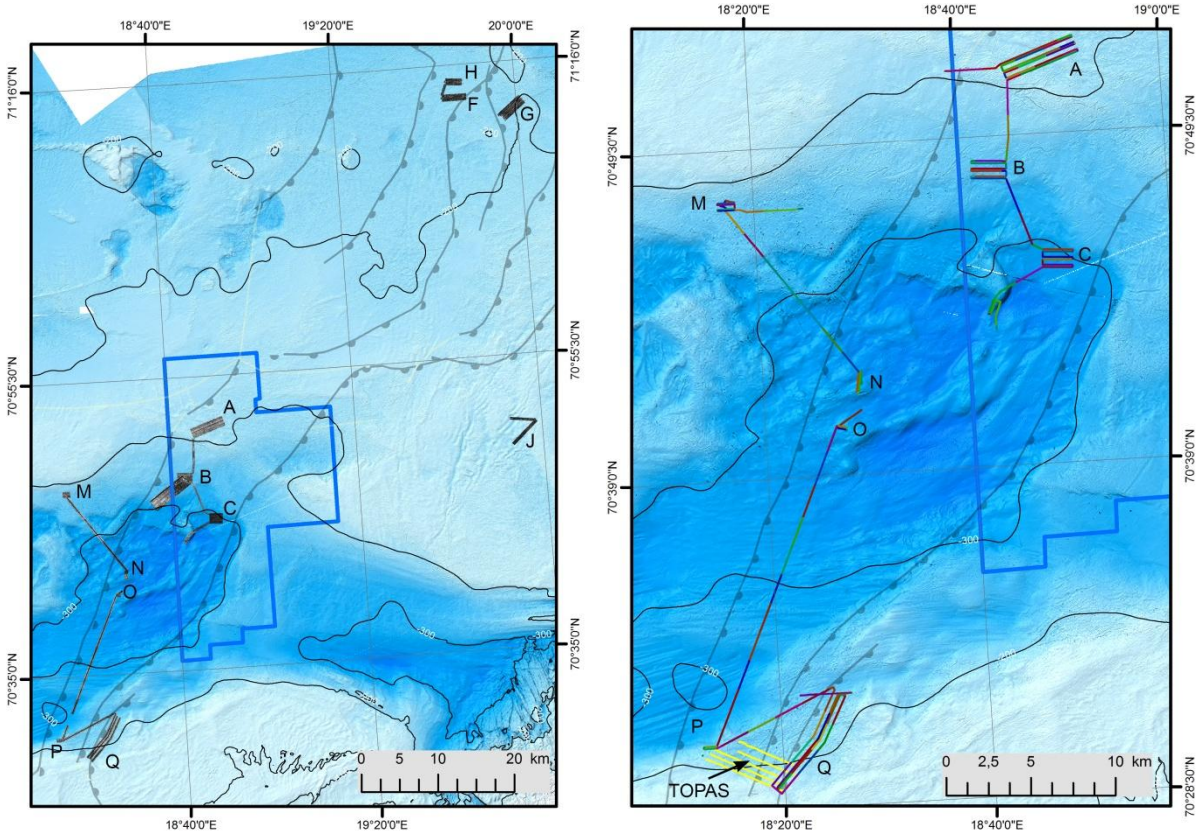

Figure 7. Bathymetry of the Harstad Basin showing the locations of a) SAS data from areas A, B, C, F, G, H, J, M, N, O, P and Q, b) Hugin SBP lines.

Table 1 - Areas covered by HISAS and/or TFish imagery.

Area name - HISAS	Area km^2	Area name - Tfish	Area m^2
A	6	**A**	16000
B	10,8	**B**	113000
C	2,3		
F	2,3		
G	4		
H	1,4		
J	1,2		
M	0,8	M	7400 + 15450
N	0,5	N	15000
O	0,4		
P	0,3		
Q	7,1		
Sum	37,1	Sum	166850

Twelve localities (Fig. 7), covering a total area of 37.1 km^2 (Table 1) were surveyed using SAS during the cruises in November 2013 and June 2014. Data were also recorded on the transits, with a total length of 43 km giving an area of c. 14.6 km^2. TFish images were collected from a total area of 166 850 m^2.

3.3 Topas

Topas data were collected along with MBE data collection during the main survey in January 2013 in the North Sea study areas. Due to interference with the multibeam system no Topas data were collected during the North Sea cruise in March 2013 (Figs. 5a & 6a). No Topas data were collected from the Harstad Basin for this project.

3.4 2D/3D seismic data

Industry 2D seismic data from all the study areas were evaluated for subsurface anomalies using Petrel software. 2D seismic available through the DISKOS database was used for all the study areas and interpreted using Petrel. A merged 3D seismic dataset covering parts of the study area in the Harstad Basin was available from Lundin Norge AS. The 3D seismic data was used for interpreting major boundaries and fluid flow features.

3.5 ROV

Seabed inspection and sampling using Remotely Operated Vehicle (ROV) was undertaken during three cruises. The Alvheim and Utsira High study areas were studied using working class ROV during a 3-day long cruise in September 2013 using a Seabed Worker vessel.

Table 2. Coordinates of materials collected by ROV from the Alvheim study area during the cruise in September 2013. The type of sampled material is indicated in the Sample ID field. Gas: gas sample; Carb: carbonate crust sample; PC: push-in core sample.

Y UTM31	X UTM31	Sample ID
6602205	435498	13C-ROV2-Gas1
6602202	435500	13C-ROV3-Carb1
6602201	435474	13C-ROV4-Gas2
6602201	435474	13C-ROV4-Carb2
6602199	435488	13C-ROV5-PC1
6602189	435473	13C-ROV5-PC2
6602189	435473	13C-ROV5-Gas3
6602192	435464	13C-ROV5-PC3

6598078	435940	13C-ROV6 -Gas4
6598051	435958	13C-ROV6-Carb3
6598215	435876	13C-ROV7-Carb4
6598226	435880	13C-ROV7-Carb5
6598043	435933	13C-ROV8-PC4
6598063	435980	13C-ROV8-PC5
6606226	435600	13C-ROV11-Carb6
6600145	435127	13C-ROV13-Carb7
6600134	435123	13C-ROV13-Carb8
6600157	435111	13-ROV14-PC6
6600146	435120	13-ROV14-PC7
6601190	434926	13C-ROV16-Carb9
6601445	434824	13C-ROV16-Carb10
6601432	434854	13C-ROV16-PC8
6601432	434854	13C-ROV16-Gas5
6602357	434696	12C-ROV17-Carb11
6596402	436918	13C-ROV18-Gas6B
6596368	436905	12C-ROV18-Carb12
6596359	436897	13C-ROV18-Gas6A
6596363	436892	13C-ROV18-PC9
6595315	437096	13C-ROV19-Gas7
6595321	437070	13C-ROV19-Carb13
6595317	437100	13C-ROV19-Gas8
6595318	437107	13C-ROV19-Carb14
6595310	437092	13C-ROV19-PC10
6594669	436921	13C-ROV21-Gas9
6594671	436933	13C-ROV21-Carb15
6594657	436923	13C-ROV21-PC11
6582960	437990	13C-ROV22-Carb16
6582967	437993	13C-ROV22-PC12
6582967	437993	13C-ROV22-Gas10
6582258	438038	13C-ROV23-Carb17
6582264	438072	13C-ROV23-Gas11
6582269	438070	12C-ROV23-PC13
6580026	438581	13C-ROV24-Carb18
6580056	438580	13C-ROV24-Carb19
6580034	438597	13C-ROV24-PC14

A total of 24 ROV dives were performed, and 19 carbonate crusts, 13 push-in cores and 11 gas samples were collected (Table 2). All these materials were obtained from the Alvheim study area that has numerous occurrences of carbonate crusts on the seafloor as well as ubiquitous patches of white microbial mats that were targeted for push-in coring. Seafloor

inspection of the Utsira High focussing on locations with indications of flares in the water column did not provide any evidence of crusts or microbial mats hence no materials were collected from the Utsira High.

The seafloor of the Harstad Basin was inspected by ROV during two cruises. The ROV work in November 2013 provided visual documentation of carbonate crusts and bubbling gas. Due to bad weather and technical limitations of the ROV system, it was possible to use ROV for collecting only one gas sample (WGS84 coordinates 70°48'21.755 and 18°42'43.834) during the November 2013 cruise. A powerful working-class ROV used during the September 2014 cruise made it possible to obtain extensive high-quality video documentation of the seafloor and to collect 22 carbonate crust samples, 14 push-in cores and 4 gas samples from five carbonate crust areas in the Harstad Basin and two areas at the Loppa High (Table 3). The BGS combined rock drill and vibrocorer RD1 was deployed eight times to obtain continuous successions through carbonate crusts (Fig. 8). Due to fragile, porous nature of carbonate crusts, they typically disintegrated during drilling and only two drilled core samples through crusts were obtained (Table 3). The RD1 system was also used to obtain one 4 m long vibrocore (Table 3).

Table 3. Coordinates of materials collected by ROV from the Harstad Basin and Loppa High areas during the cruise in September 2014. The type of sampled material is indicated in the Sample type field. Gas: gas sample; Carb: carbonate crust sample; VibroCore: c. 4 m long vibrocore sample; Drill Core: drill core through carbonate crust; PC: push-in core sample.

Lat WGS84N	Long WGS84E	Sample ID	Sample type	Area
70,7942878	18,2911925	P1411001	Carb	Harstad Basin
70,7942118	18,2911485	P1411002	Carb	Harstad Basin
70,7941868	18,2916661	P1411003	Carb	Harstad Basin
70,794155	18,2914262	P1411004	Carb	Harstad Basin
70,7941498	18,2912024	P1411005	Carb	Harstad Basin
70,7942319	18,2911299	P1411006	Gas	Harstad Basin
70,794232	18,2911299	P1411007	Gas	Harstad Basin
70,8736228	18,85556	P1411008	Carb	Harstad Basin
70,8735723	18,8545872	P1411009	Carb	Harstad Basin
70,8734634	18,8571027	P1411010	Carb	Harstad Basin
70,8731827	18,8587172	P1411011	Carb	Harstad Basin
70,8735081	18,8577689	P1411012	Carb	Harstad Basin
70,8735431	18,8565662	P1411013	Carb	Harstad Basin
70,873515	18,8572104	P1411014	PC	Harstad Basin
70,8735145	18,8572479	P1411015	PC	Harstad Basin
70,8735071	18,8574933	P1411016	PC	Harstad Basin
70,819438	19,9615145	P1411017	Carb	Harstad Basin
70,8194652	19,9615395	P1411018	Carb	Harstad Basin

70,8199751	19,9615519	P1411019	Carb	Harstad Basin
70,819457	19,9615769	P1411020	Carb	Harstad Basin
72,5673273	20,8696312	P1411031	VibroCore	Loppa High
72,5679549	20,8735859	P1411032	PC	Loppa High
72,5680632	20,8736559	P1411033	PC	Loppa High
72,5680885	20,8741248	P1411034	PC	Loppa High
72,5673178	20,8686956	P1411035	PC	Loppa High
72,5669916	20,869128	P1411036	PC	Loppa High
72,5669814	20,8691122	P1411037	PC	Loppa High
72,1578358	19,7275986	P1411043	DrillCore	Loppa High
72,1577982	19,7278794	P1411045	Gas	Loppa High
72,158008	19,7282994	P1411046	PC	Loppa High
72,1576013	19,7271156	P1411047	PC	Loppa High
72,1578025	19,7272481	P1411048	PC	Loppa High
72,1578193	19,7273186	P1411049	PC	Loppa High
70,8194547	19,9615339	P1411050	DrillCore	Harstad Basin
70,8049645	18,7084816	P1411055	Carb	Harstad Basin
70,8052173	18,7090614	P1411056	Carb	Harstad Basin
70,8050894	18,7099141	P1411057	Carb	Harstad Basin
70,8048532	18,7093554	P1411058	Carb	Harstad Basin
70,8060889	18,7134421	P1411059	Gas	Harstad Basin
70,7579383	18,8207773	P1411060	Carb	Harstad Basin
70,7579706	18,8207541	P1411061	Carb	Harstad Basin
70,7579629	18,8208102	P1411062	Carb	Harstad Basin

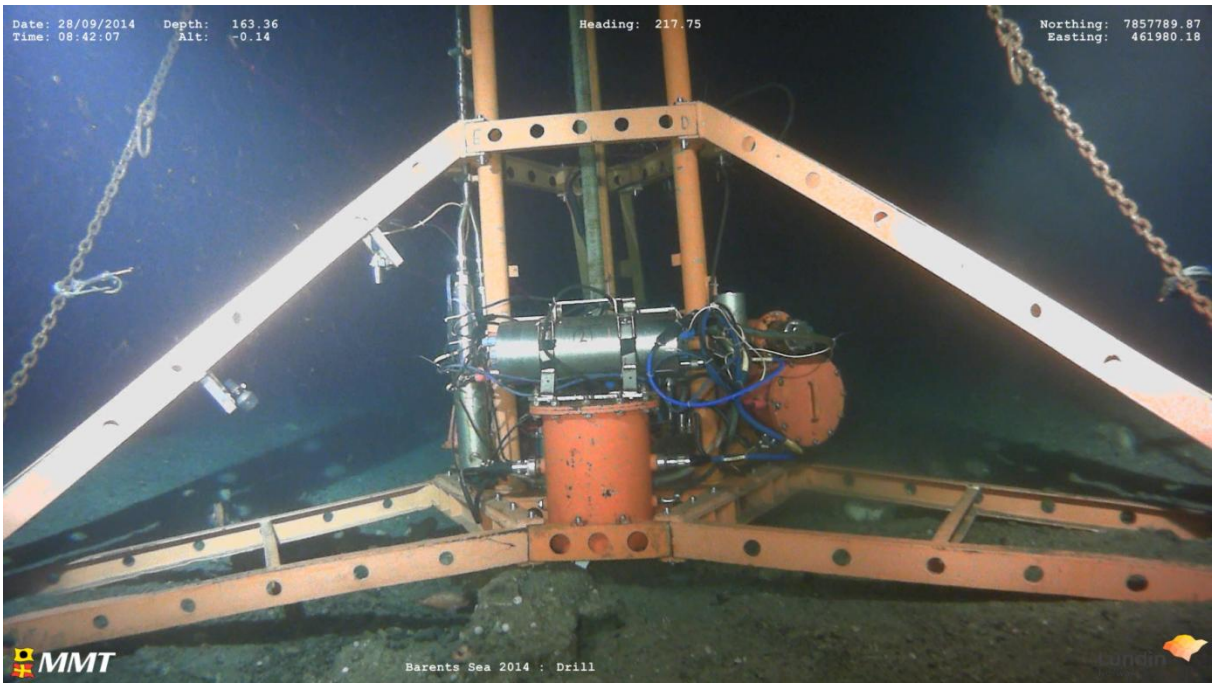

Figure 8. Photo of BGS RockDrill on the seafloor drilling at Area J within hydrocarbon exploration block license PL764.

4. POCKMARKS, GAS FLARES, CARBONATE CRUSTS, GAS HYDRATES, NEOTECTONICS AND QUATERNARY STRATIGRAPHY

4.1 General morphology and seafloor character

4.1.1 Alvheim

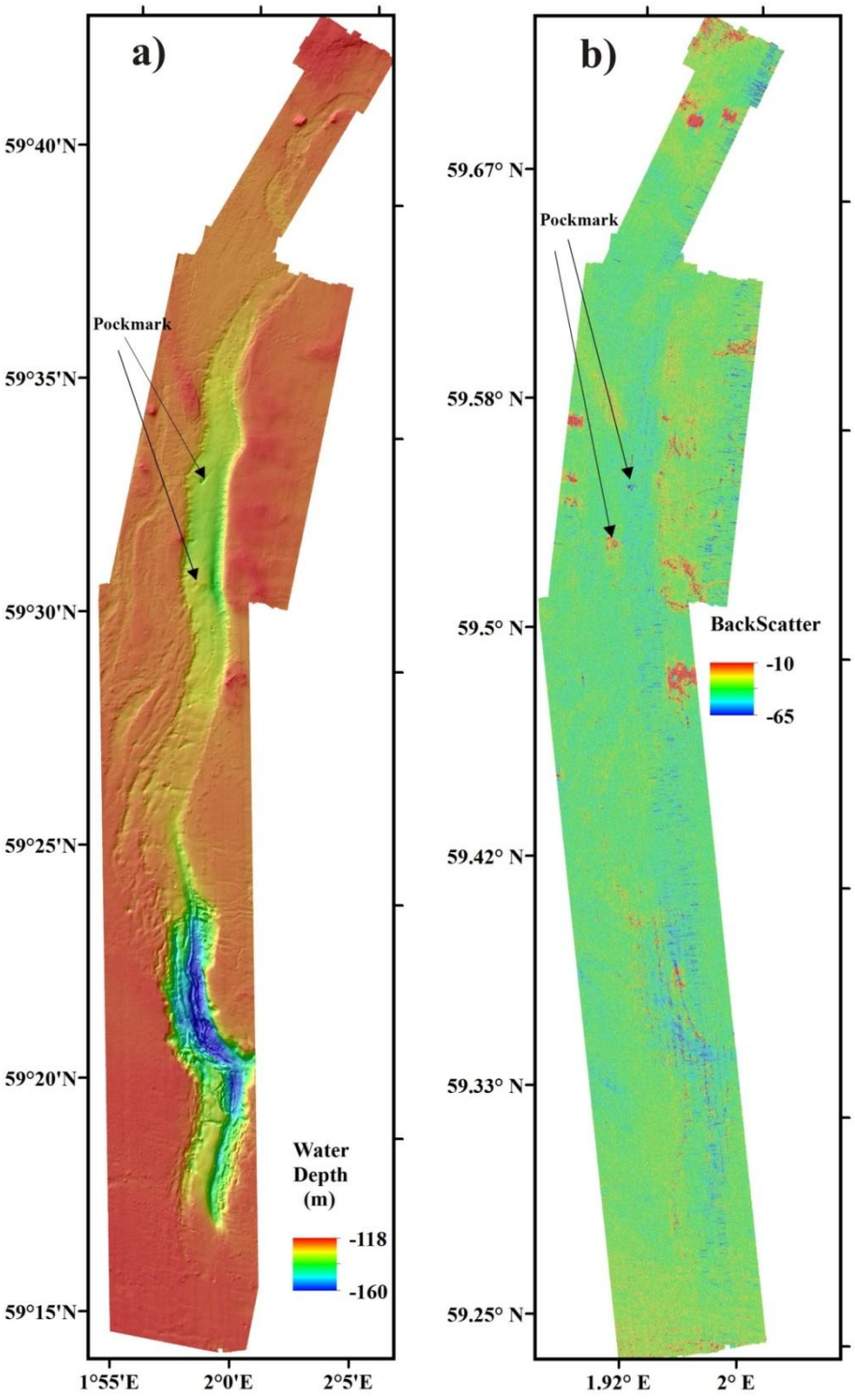

Figure 9. a) Bathymetry and b) backscatter of the Alvheim study area showing the general morphology of the seafloor and the backscatter changes associated with morphological features.

Multibeam bathymetry was collected from the Alvheim study area in January and March, 2013 (Fig. 9a). Water depths range from 113 m to 168 m with largest depths occurring within a N-S trending channel (Fig. 9a). Only few pockmarks were observed within the study area. The pockmarks occur along the boundaries of the channel and also within it as isolated depressions. The deepest part of the channel is devoid of pockmarks. The backscatter map (Fig. 9b) indicates high backscatter associated with the pockmarks and also with some mounds located along the margins of the channel (Fig. 9b). In general, the backscatter is quite uniform indicating that the upper few tens of centimeters of the seafloor shows little variation in sediment type. Seafloor investigation using AUV HUGIN indicated many furrows. The seabed is clayey and drop stones and carbonate crusts can be seen (Fig. 10a & b).

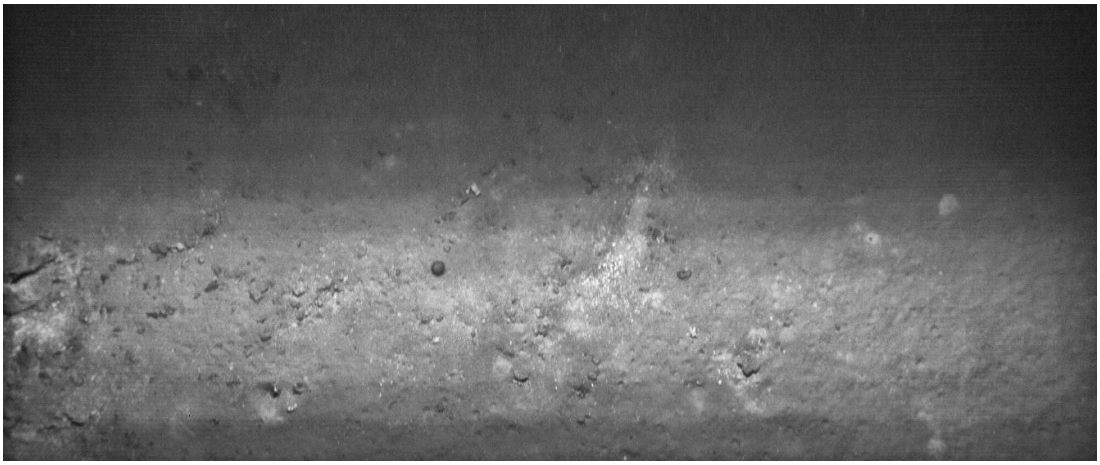

Figure 10a. HUGIN TFish photo of the seafloor at Alvheim indicating drop stones, carbonate crusts and muddy sediments.

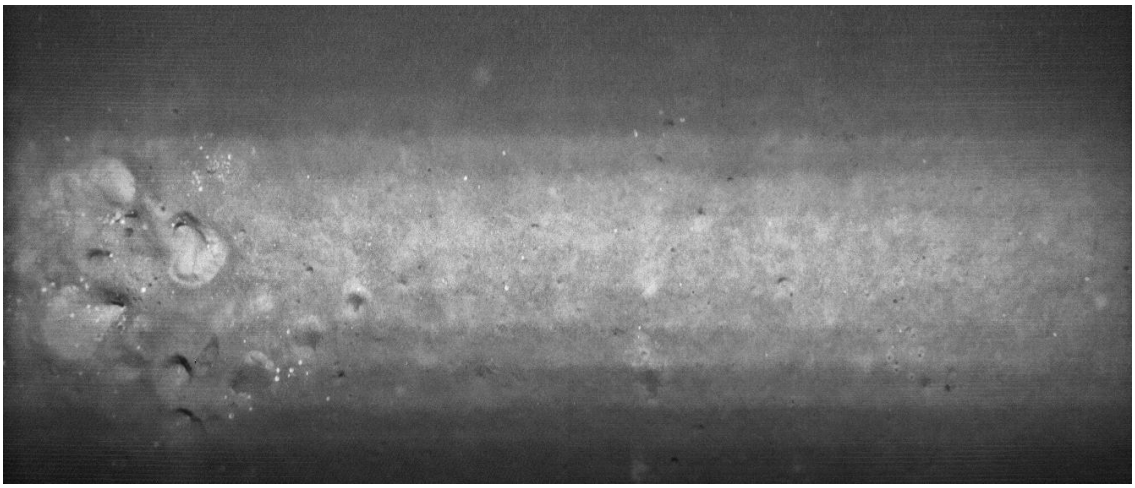

Figure 10b. HUGIN TFish photo of the seafloor at Alvheim showing many small holes which may represent gas escape features or burrows.

4.1.2 Utsira High

The morphology of the Utsira High study area is different from Alvheim. The seafloor is flat in most of the area except for the E-W trending linear ridge along the northern part (Fig. 11). Water depths range from 100 to 125 m and the E-W trending ridge along the northern part is criss-crossed by iceberg plough marks indicating only thin post glacial deposits overlying this high. The remaining areas are flat with very few morphologic features indicating a thick, soft sediment cover deposited after the glaciers retreated from this area. Some hill-hole pairs can be seen and are most probably formed by anchoring of drilling rigs on the seafloor or other human activities. Three pipelines can be seen going across the study area.

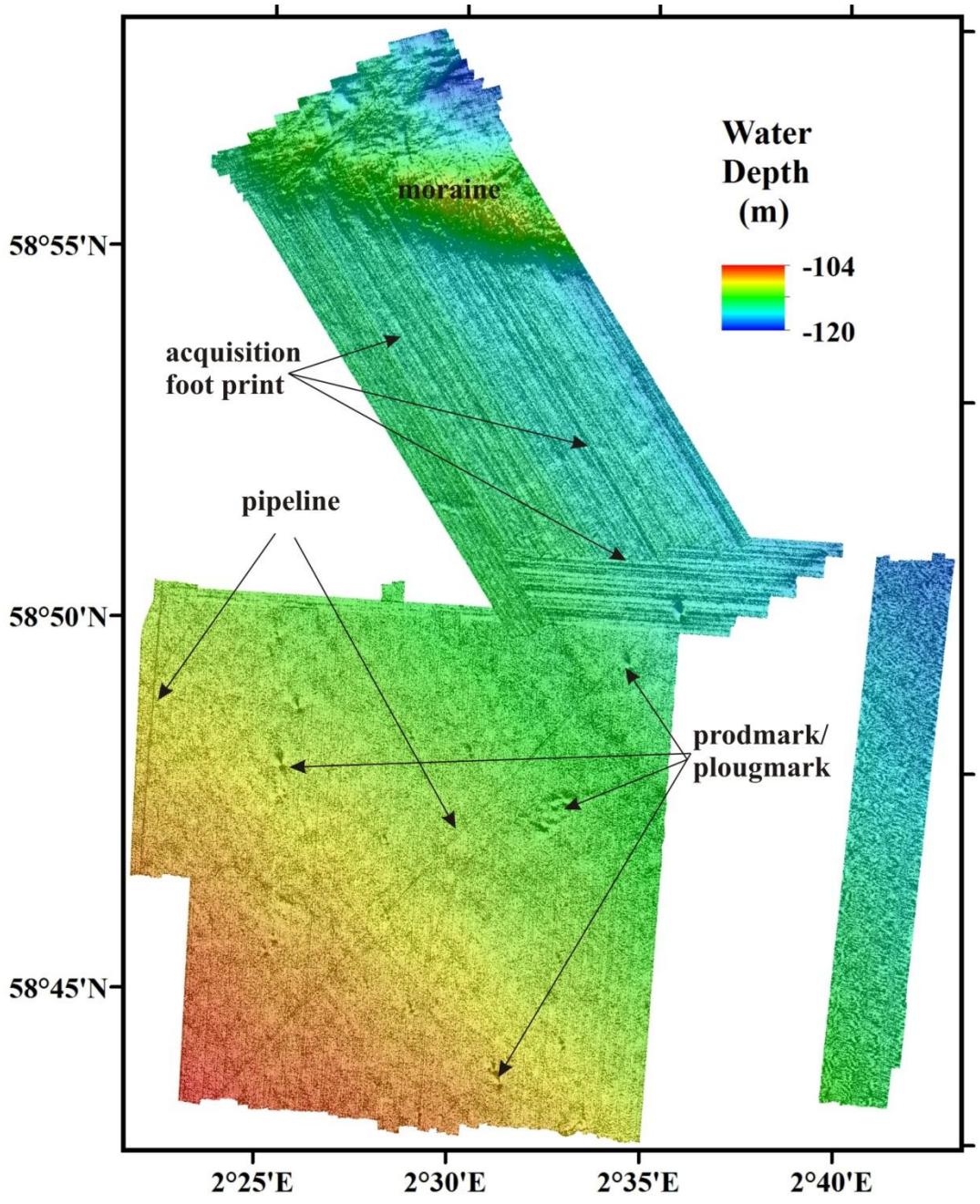

Figure 11a. Multibeam bathymetry from the Utsira High study area.

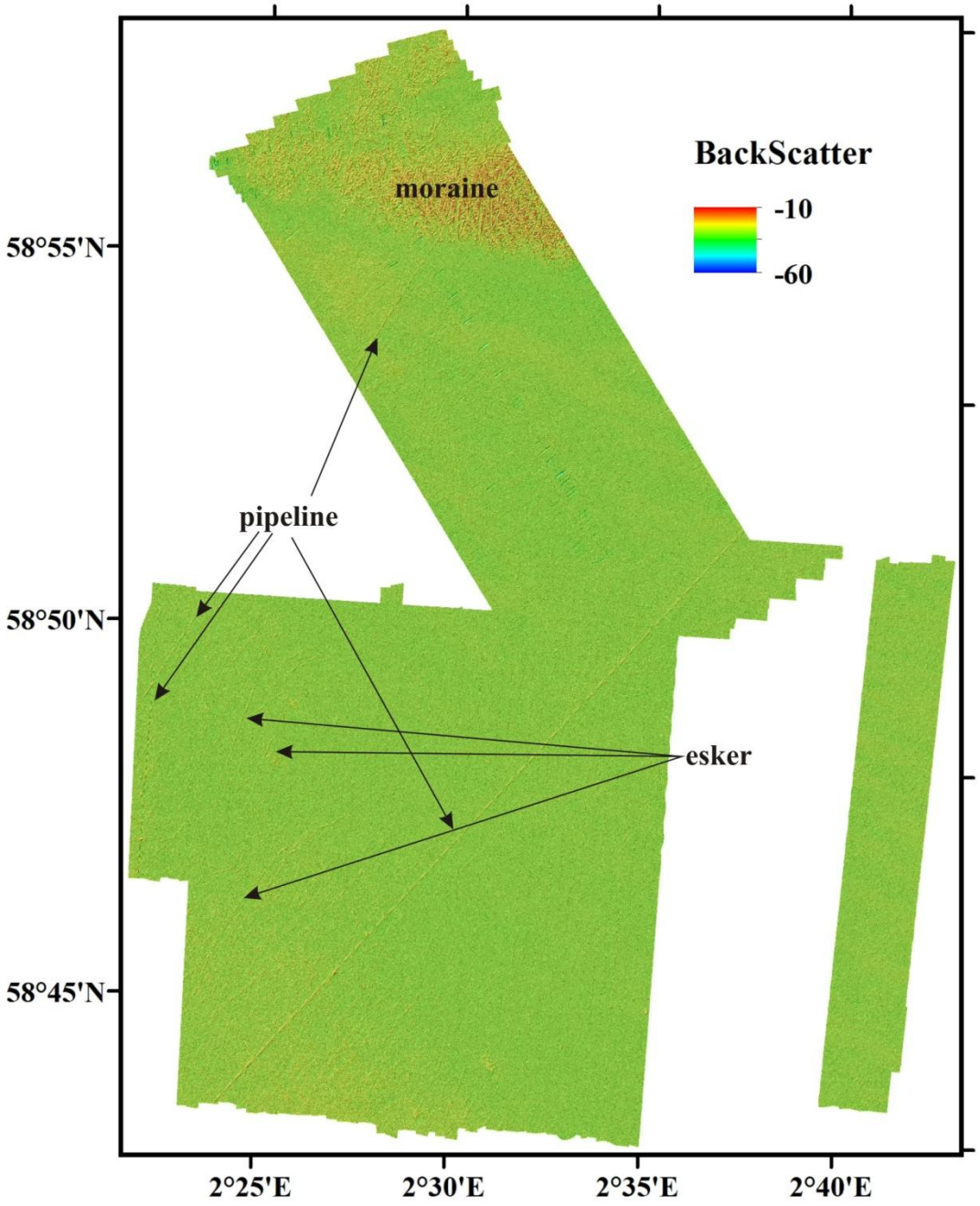

Figure 11b. Multibeam backscatter from the Utsira High study area.

The backscatter indicates high reflectivity along the E-W trending ridge and slightly higher reflectivity along the SW corner of the study area (Fig. 11b). The pipe lines can be seen with high reflectivity as linear features going across the study area (Fig. 11b). A closer investigation of the high backscatter (Fig. 12b) along the SW corner of the study area indicates arcuate highs in NW-SE direction visible both in the bathymetry and the backscatter (Fig. 12a &b). Linear features crossing these arcuate highs are also clearly visible on the backscatter data (Fig. 12b). The linear highs in NE-SW direction could be eskers. They are not clearly visible in bathymetry data, mainly due to high noise levels, but also because they are partly covered by soft sediments. They are however clearly visible in backscatter data since the backscatter gives an average of sediment properties in the upper decimeters of the seabed (Fig. 12a & b). The high backscatter corresponding to the pipeline can be easily seen

(Fig. 12b). The seafloor of Utsira High area appears to be sandy (Fig. 13a). The seafloor close to the wells indicates spills of drilling mud (Fig. 13b).

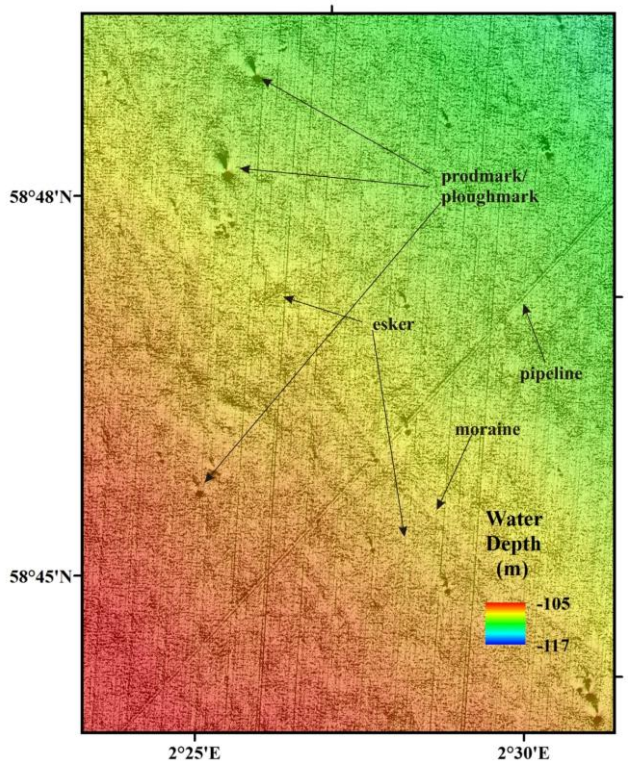

Figure12a. Multibeam bathymetry from the southern part of the Utsira High study area.

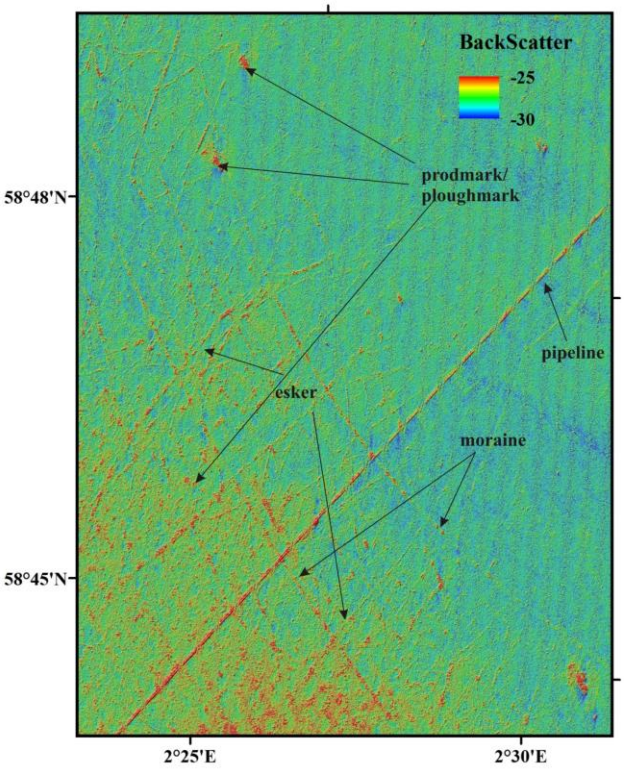

Figure12b. Multibeam backscatter from the southern part of the Utsira High study area. Notice the high backscatter along the SW corner of the study area.

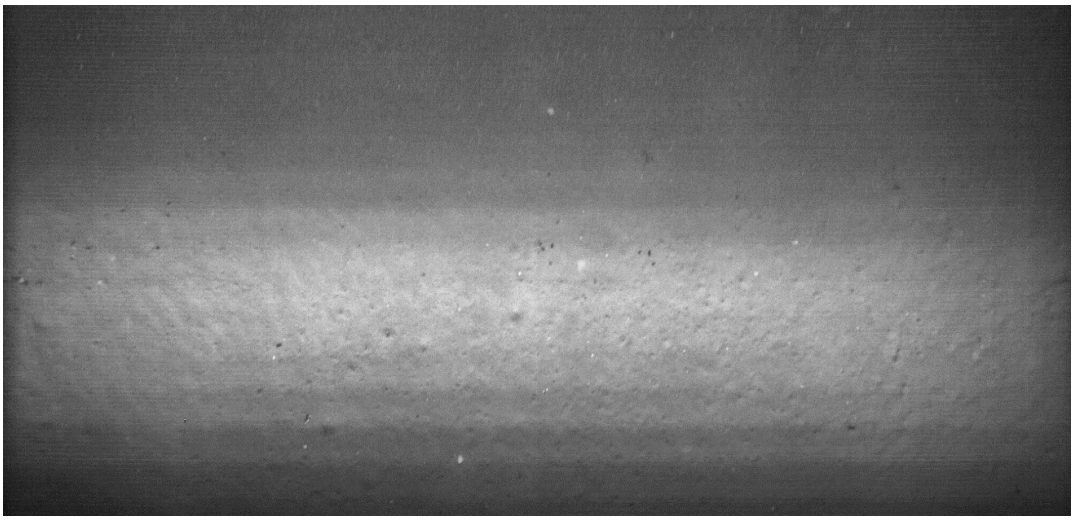

Figure 13a. HUGIN TFish photo of the seafloor from Utsira High showing sandy sediments with small ripples and barren seafloor indicating high current activity.

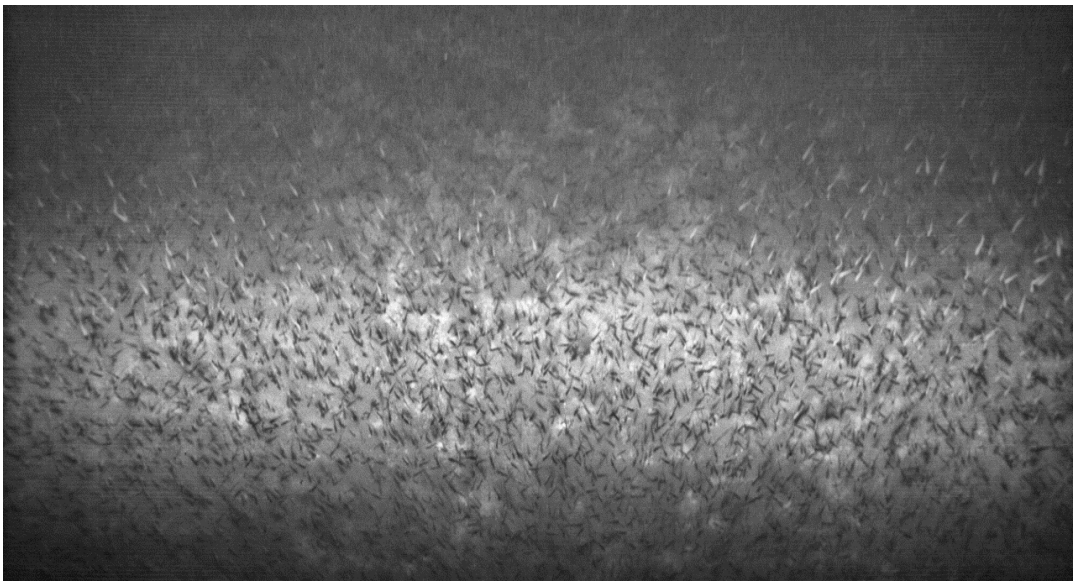

Figure 13b. HUGIN TFish photo of the seafloor location close to a well showing drilling mud spill (white patches) and school of fish.

4.1.3 Harstad Basin

The bathymetry in the Håkjerringdjupet/Harstad Basin area was acquired during various MAREANO cruises, but only parts of the study area have water column data. Hence, parts of the study area including IKU shallow borehole locations were remapped for water column data.

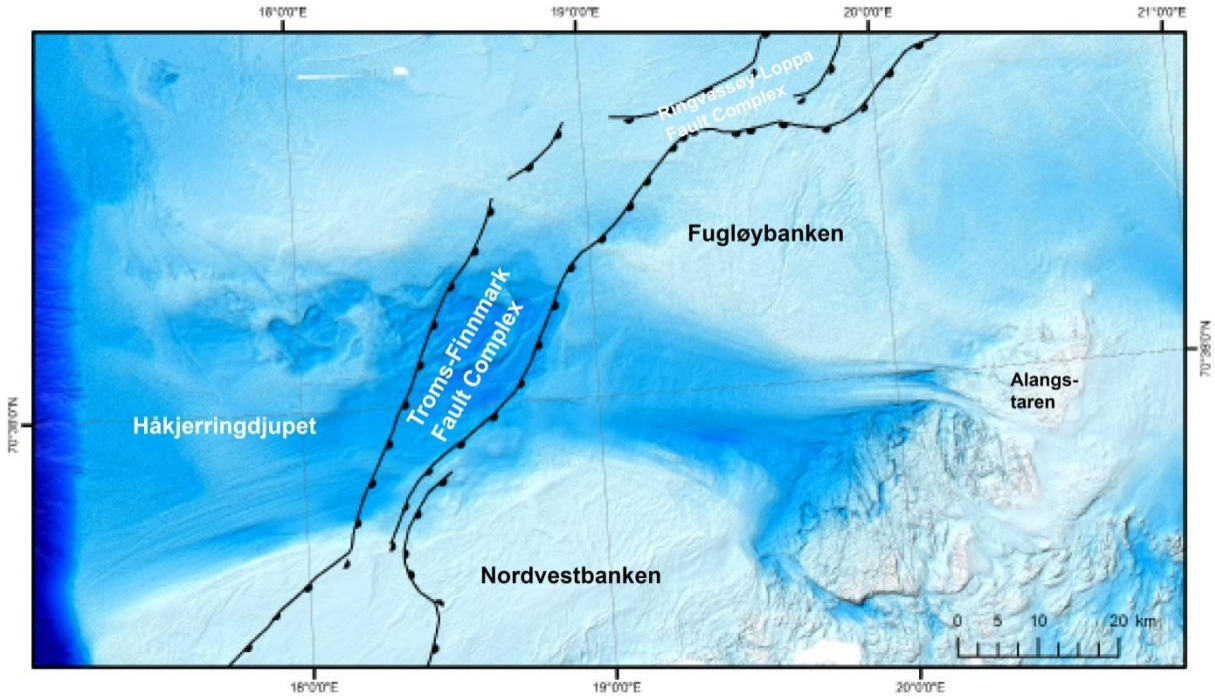

Figure 14a. Morphology and main structures of the Barents Sea study area (source www.mareano.no and www.npd.no).

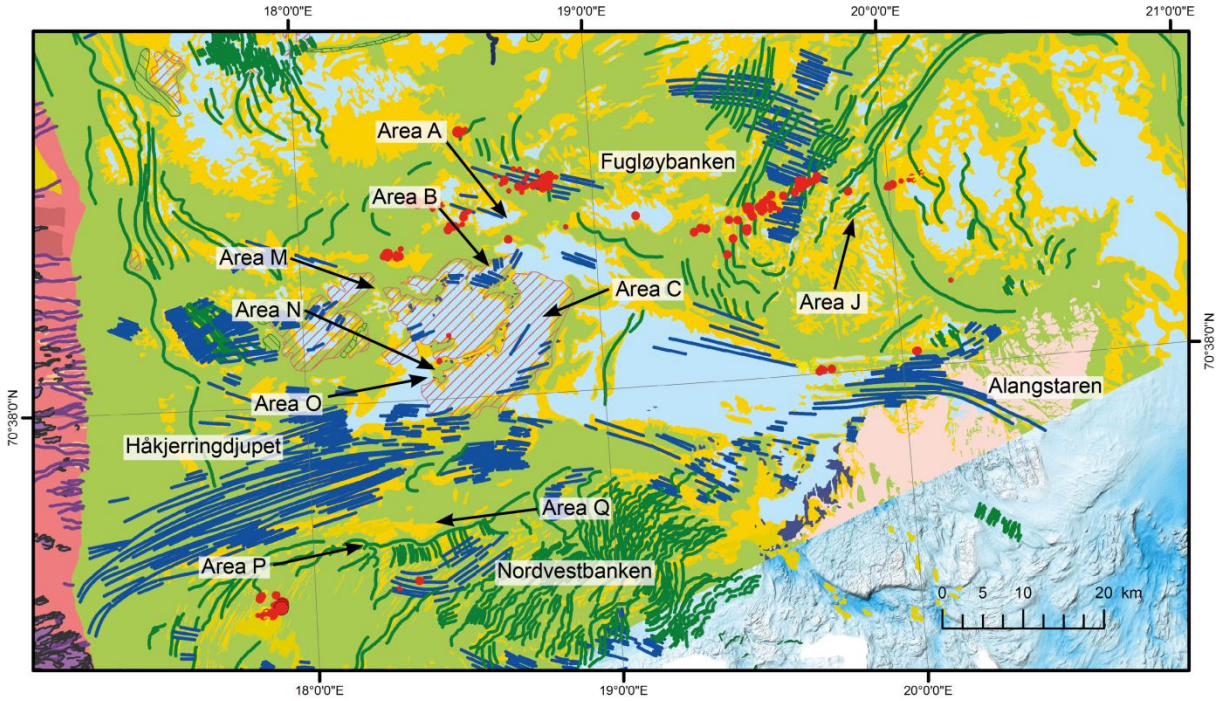

Figure 14b. Quaternary geology and landforms (from www.mareano.no). Green: till deposits; yellow: bedload (traction) deposits; blue: suspension deposits; pink: bedrock with thin or discontinuous sediment cover. Blue lines show glacial lineations, green lines show moraine ridges. Hatched areas show glaciotectonic holes (red) and hills (green). In the far west, mass movement deposits with channels and canyons are present (reddish to violet colours). Red dots show gas flares.

The morphology of the area (Fig. 14 a) is dominated by the 20-40 km wide Håkjerringdjupet glacial trough, extending c. 100 km E-W from the exposed basement rocks of Alangstaren (Fig. 14a) to the shelf edge in the west. Mega scale glacial lineations are very prominent on the northern part of Alangstaren, and in the southwestern part of Håkjerringdjupet (Figs 14a & b). Major banks occur to the north (Fugløybanken) and south (Nordvestbanken). Hill-hole glaciotectonic features are prominent in the central-western parts of Håkjerringdjupet (Fig. 14b), with the largest erosional structure ("hole") being close to 90 km^2. The eastern boundary of the hole coincides broadly with the eastern margin of the Troms-Finnmark Fault Complex (Fig. 14a).

Fine grained suspension deposits are found in the central and eastern parts of Håkjerringdjupet. Complex moraines are very prominent on the banks north and south of this glacial trough (Fig. 14b). Gas flares occur mainly at the till covered banks, with very few flares in Håkjerringdjupet (Fig. 14b). The backscatter data (Fig. 14c) show low reflectivity areas in the trough, and a complex pattern of moraines, particularly on Nordvestbanken to the south of Håkjerringdjupet, is evident. This is reflected in the seabed sediment grain-size map (Fig. 14d) showing predominantly fine-grained deposits in the central and eastern parts of Håkjerringdjupet, and a complex pattern of gravel/sand alternations.

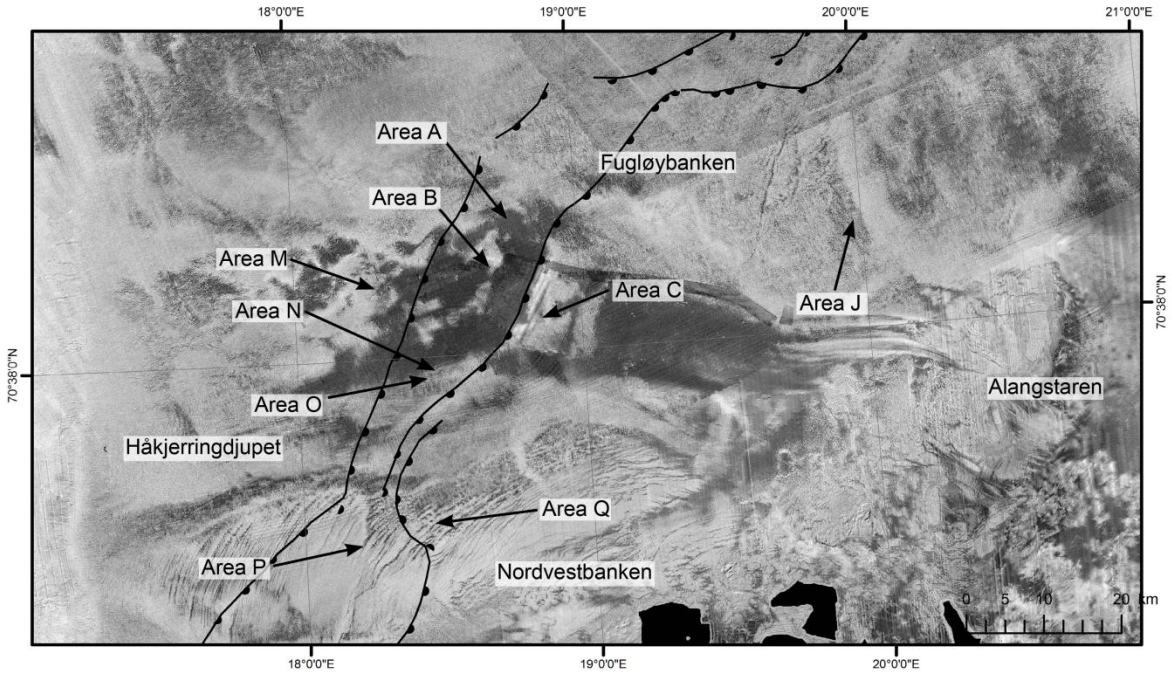

Figure 14c. Backscatter map from the Harstad Basin study area showing the Håkjerringdjupet trough with low backscatter (dark grey) indicating soft, fine grained sediments, and regional faults. Source www.mareano.no and www.npd.no.

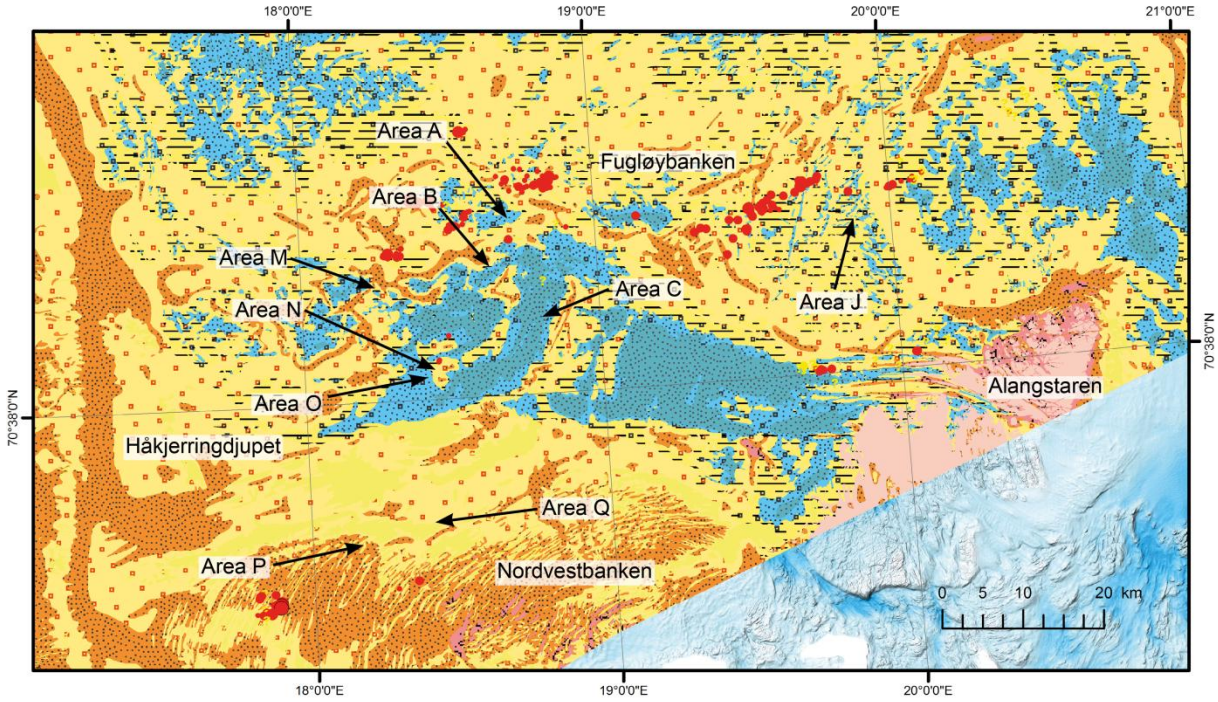

Figure 14d. Seabed sediment (grain size) map from Harstad Basin study area (source www.mareano.no). Orange: gravelly deposits; yellow: sandy deposits; blue: fine grained deposits; pink: bedrock; red dots: gas flares.

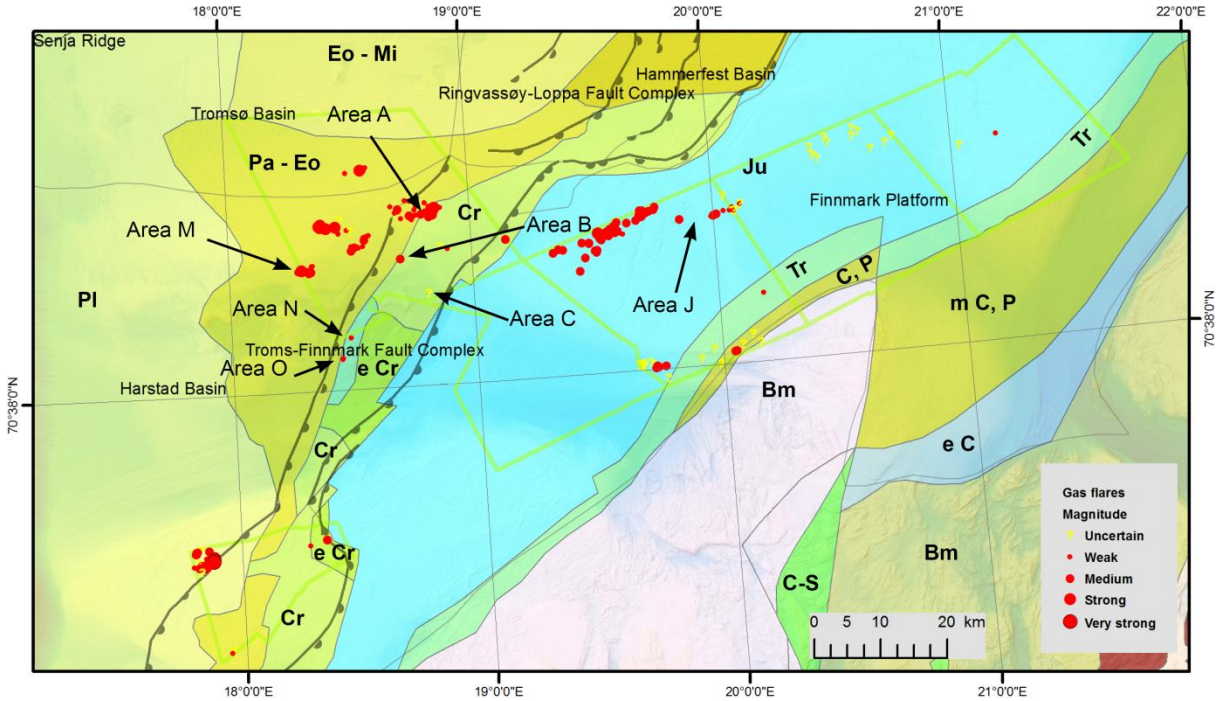

Figure 14e. Gas flares in the Harstad Basin study area. Green polygons show areas where water column data are available. Structural map from www.npd.no. Stratigraphic units: Bm: basement; C-S: Cambro-Silurian; e C: early Cretaceous; m C, P: mid Carboniferous, Permian; C, P: Carboniferous, Permian; Tr: Triassic; Ju: Jurassic; e Cr: early Cretaceous; Cr: Cretaceous; Pa-Eo: Paleocene-Eocene; Eo-Mi: Eocene-Miocene; Pl: Pliocene (from Sigmond 1992).

Detailed sediment characterization for the study areas covered by HUGIN and ROV data give similar results. Area A (Figs. 14d, 15) is dominated by gravelly sand and gravelly muddy sand with cobbles and blocks (high backscatter), alternating with iceberg ploughmarks filled with sandy to muddy sediments. The NE part of Area B (Figs. 14d, 16) has sediments dominated by sandy gravel and gravelly sand, with gravelly sandy mud in the NE part. Iceberg ploughmarks filled with more fine-grained material show up as randomly oriented, up to 130 m wide linear to curvilinear areas of low backscatter. Area C (Figs. 14d, 17a) has sediments dominated by sandy mud and sandy gravelly mud. In Area C, no iceberg plough marks are present, while pockmarks occur over the entire area. Some anthropogenic features such as a torpedo and trawl marks were found on the seafloor (Fig. 17b).

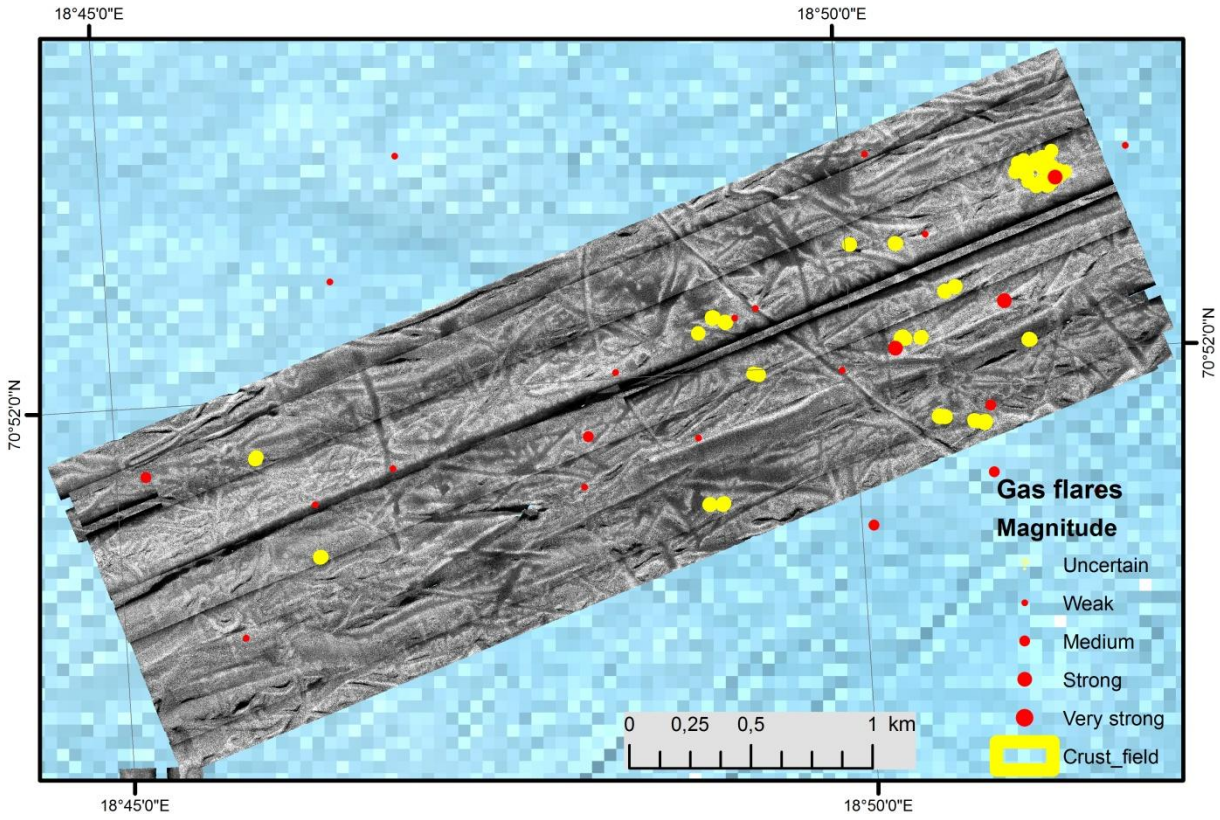

Figure 15. HISAS imagery from Area A.

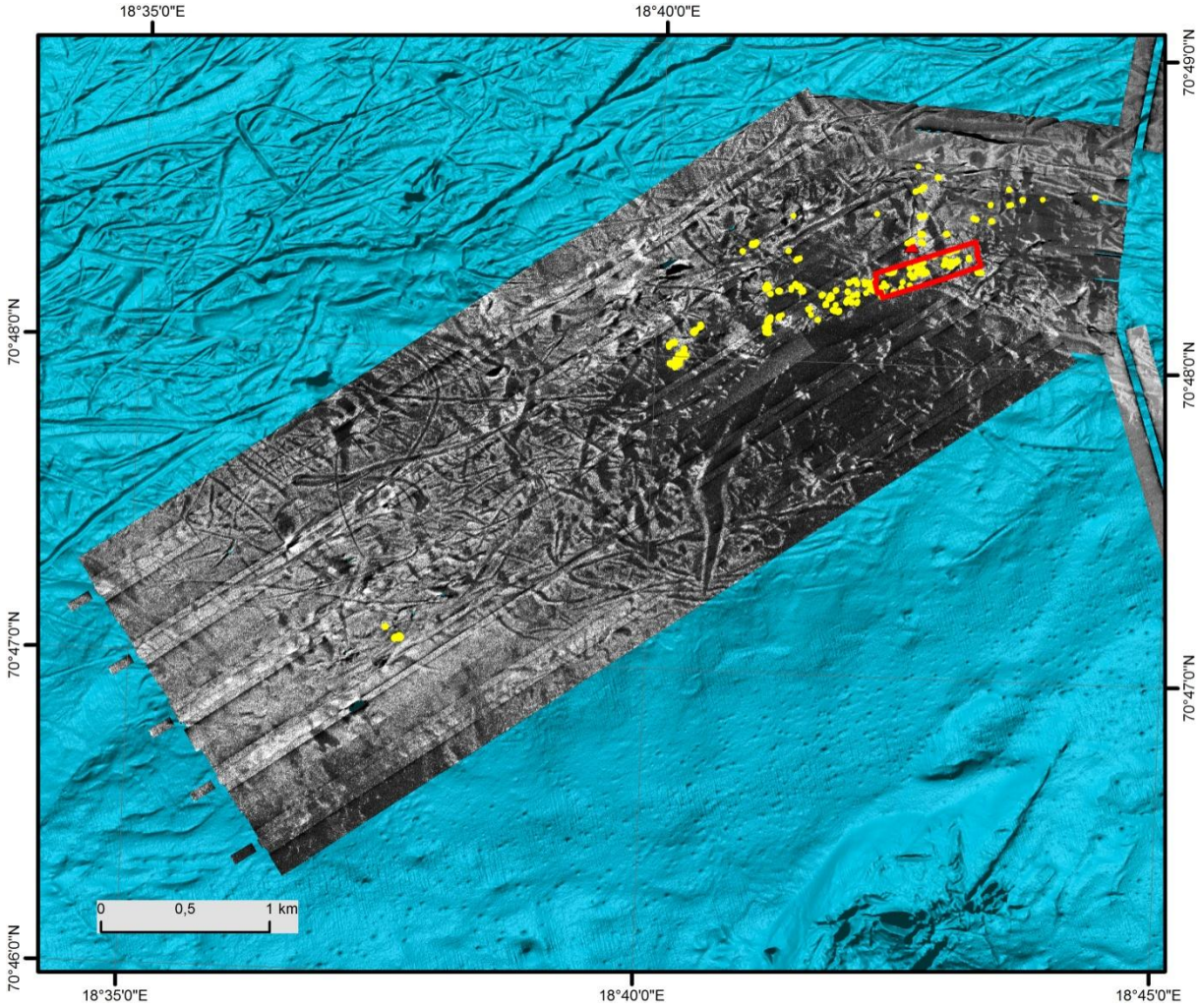

Figure 16. HISAS imagery of Area B showing one gas flare (red dot), carbonate crust fields (yellow polygons) and ROV multibeam bathymetry outline (red polygon).

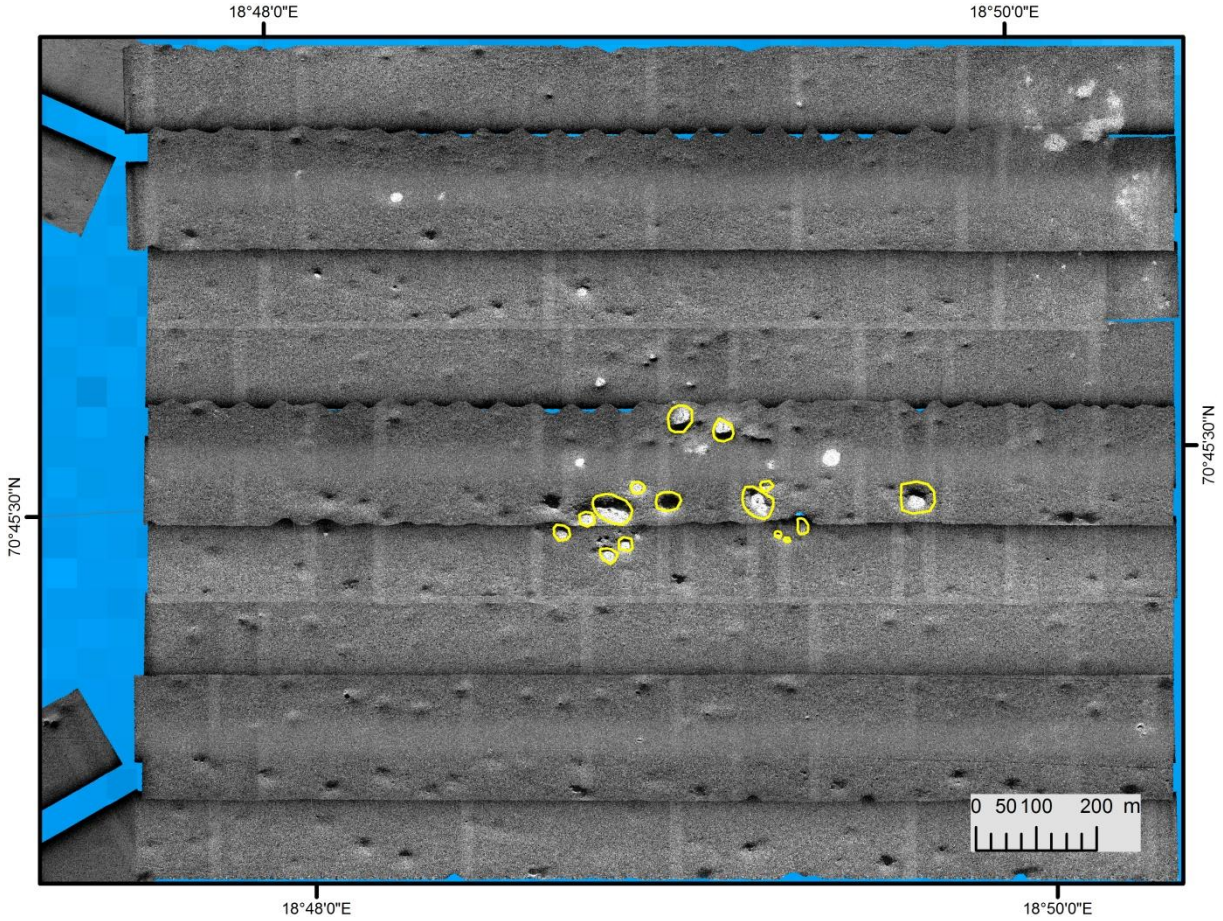

Figure 17a. HISAS imagery showing pockmarks with high backscatter (light grey patches) in Area C. Pockmarks with carbonate crusts are indicated by yellow outline.

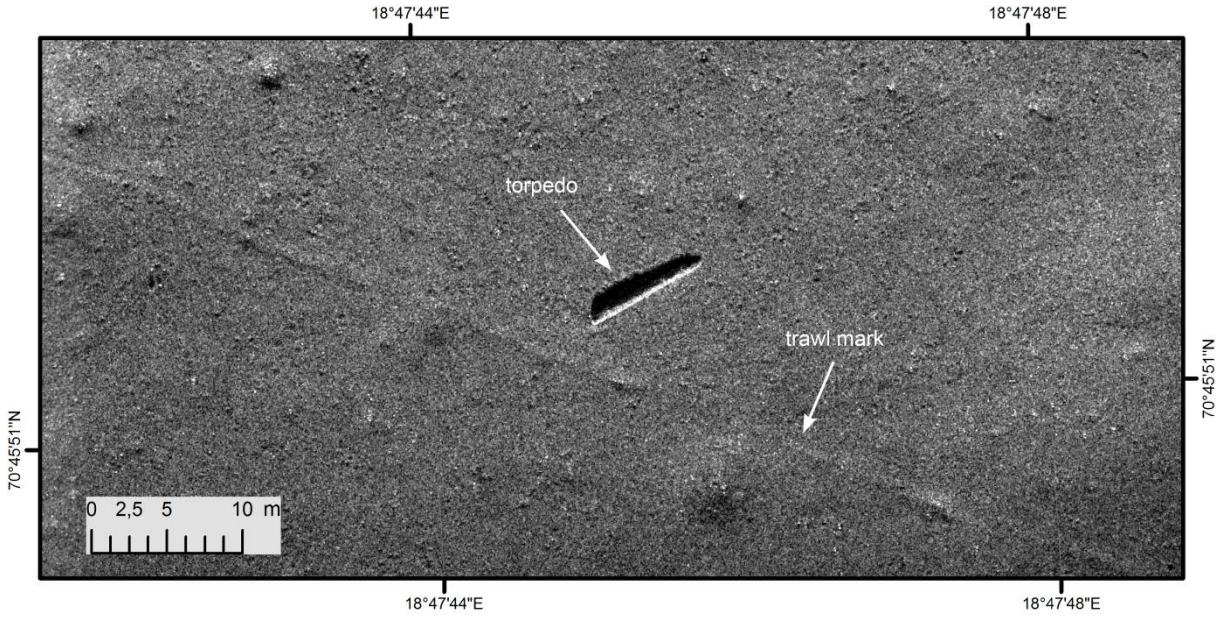

Figure 17b. HISAS imagery showing torpedo and trawl mark in Area C.

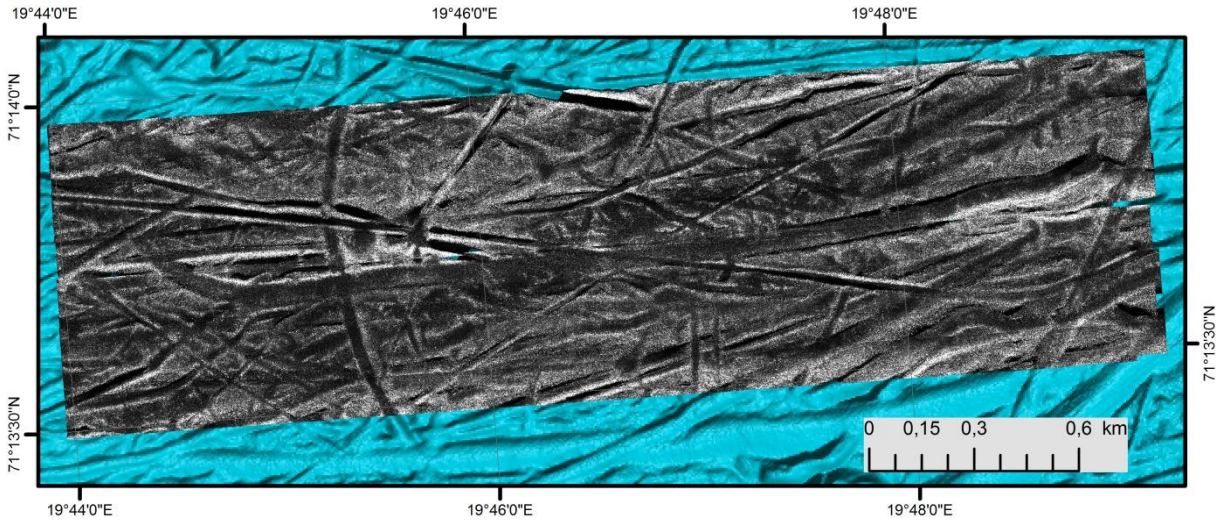

Figure 18a. HISAS imagery from Area F showing iceberg ploughmarks.

Area F (Figs. 14d, 18a) has gravelly sandy mud and gravelly muddy sand. Randomly oriented iceberg ploughmarks are prominent features, forming areas of low backscatter (Fig. 18a). Sand waves have formed in some of the ploughmarks, indicating that sand constitutes an important part of the ploughmark infill (Fig. 18b).

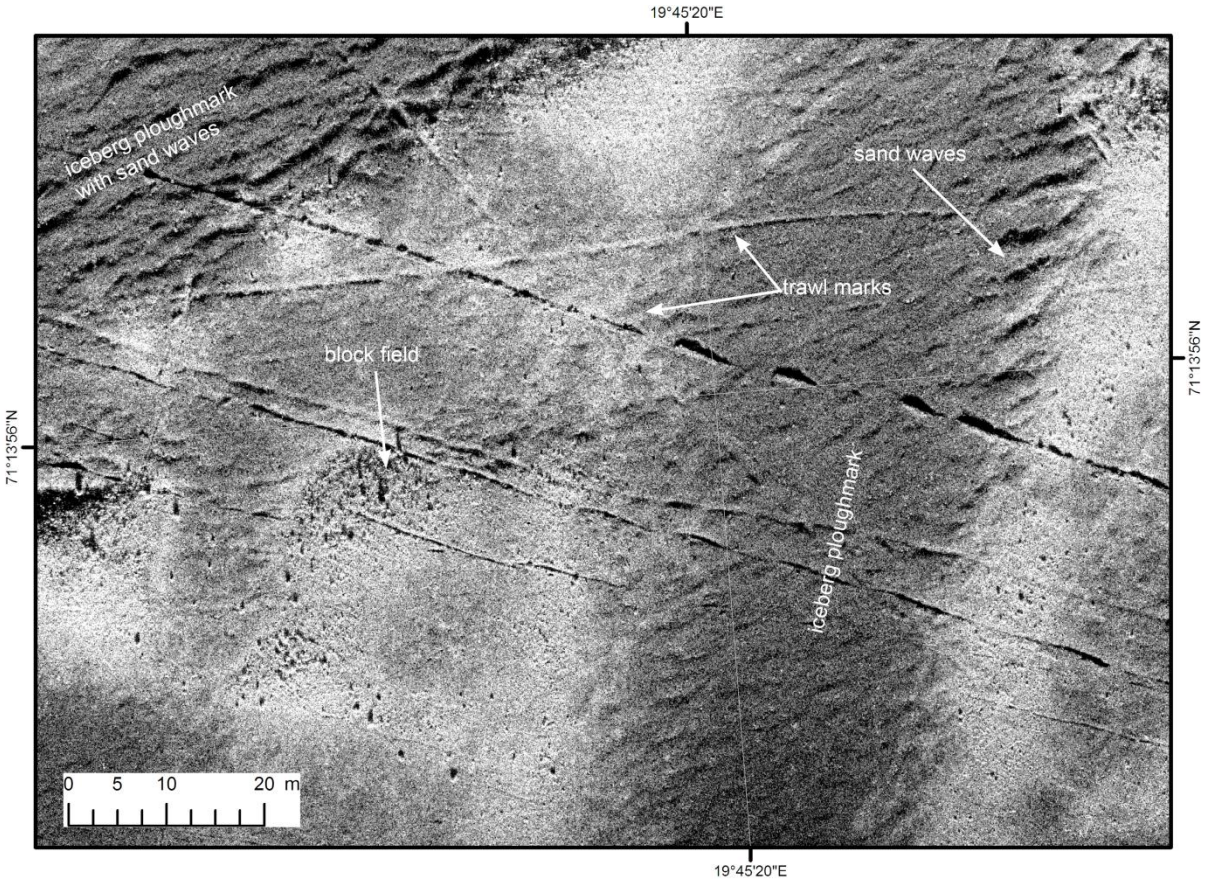

Figure 18b. HISAS imagery from Area F showing sand waves in iceberg plough marks (dark areas).

Area G and H are located (Fig. 14d) within an area of gravelly sand and gravelly muddy sand. Iceberg ploughmarks with sand waves are prominent features (Figs. 19 & 20). A few pockmarks, less than 5 m in diameter, are present. No carbonate crust fields have been observed. A small area (36 000 m^2) was covered with ROV bathymetry and video observations (Fig. 19).

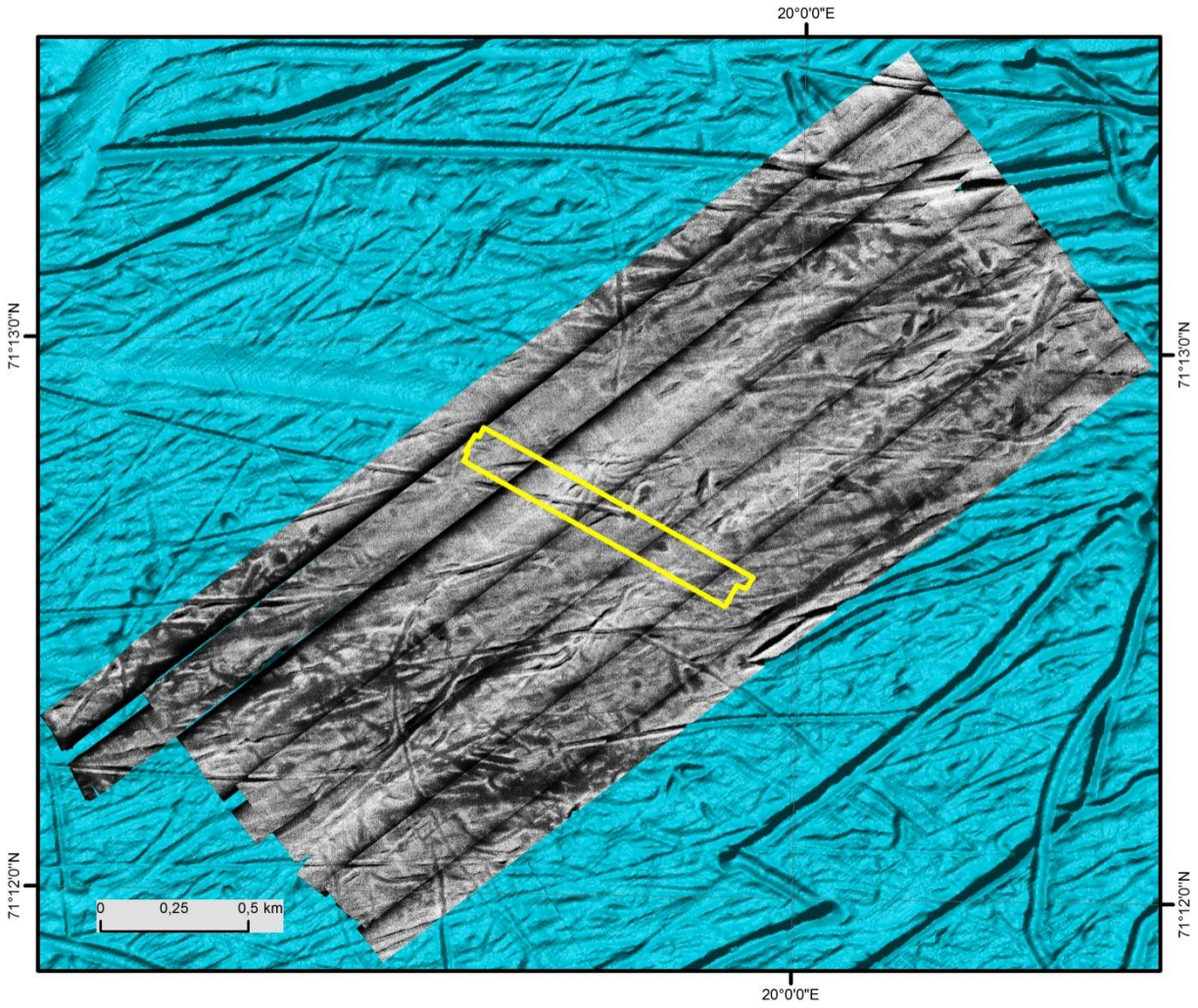

Figure 19. Shaded relief bathymetry from Area G with HISAS imagery and outline of ROV bathymetry (yellow polygon).

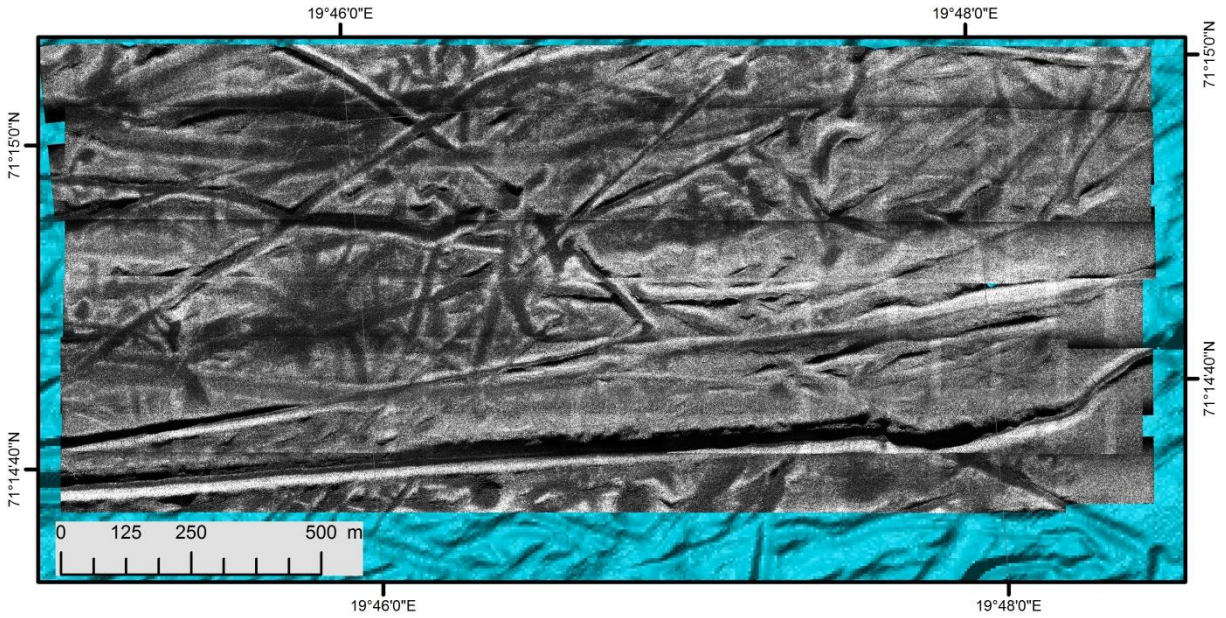

Figure 20. HISAS imagery from Area H.

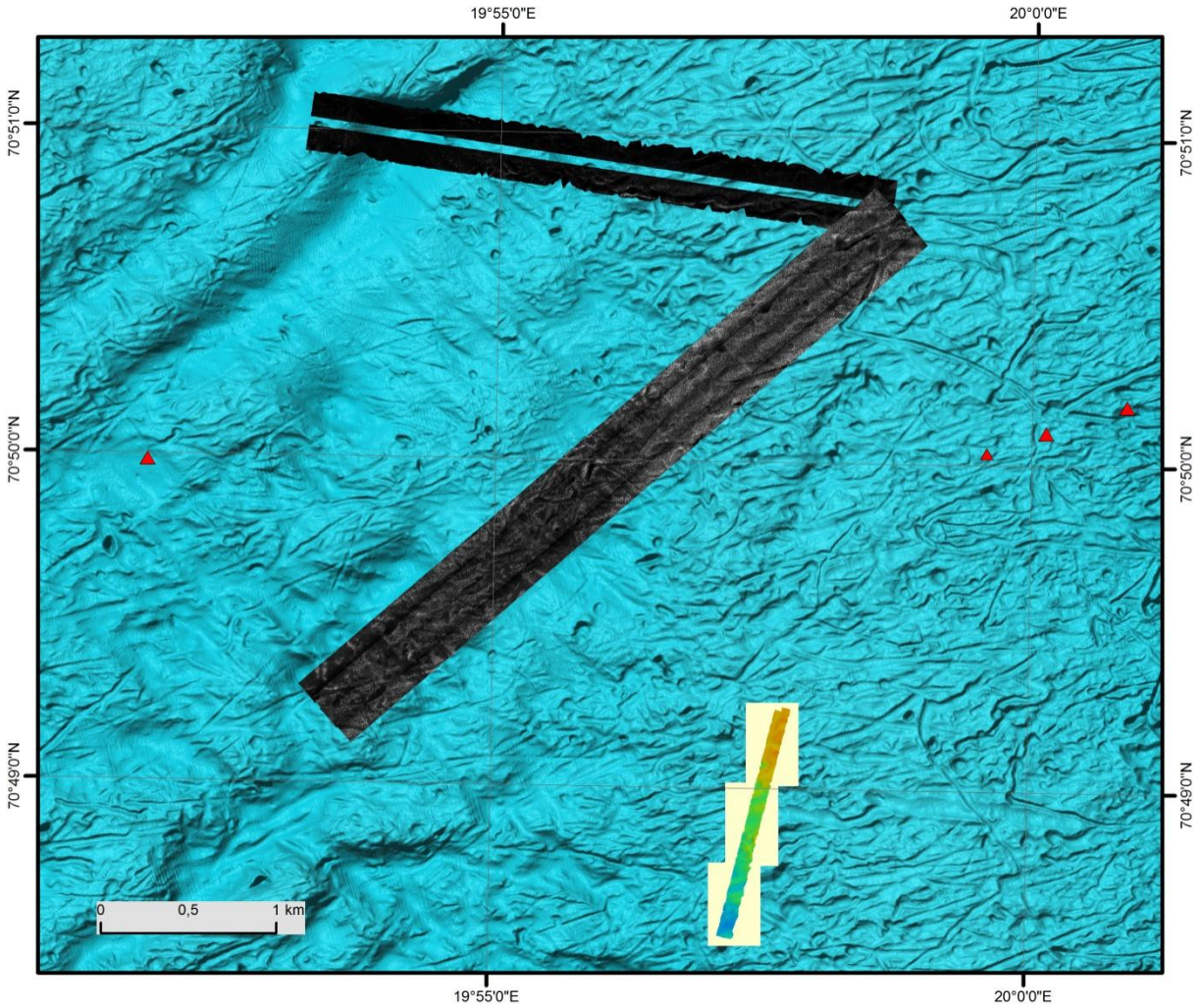

Figure 21. Shaded relief bathymetry showing HISAS imagery, ROV based multibeam bathymetry (in colours) and gas flares (red triangles) in Area J.

Area J in PL764 is located on the Finnmark Platform (Fig. 14d), in an area of gravelly sandy mud to gravelly sand, with a number of iceberg ploughmarks with low backscatter (Fig. 21).

Area M is dominated by sediments with high backscatter, alternating with 20-50 m wide, elongated zones of medium to low backscatter (Figs. 14d & 22). The latter are iceberg ploughmarks, infilled by sandy to muddy sediments, while the high backscatter areas are dominated by gravelly sand locally with cobbles and blocks (Fig. 14d). An SBP line (Fig. 22) shows that the sediment surface is irregular and the sediments are acoustically opaque, indicating that they are diamictites.

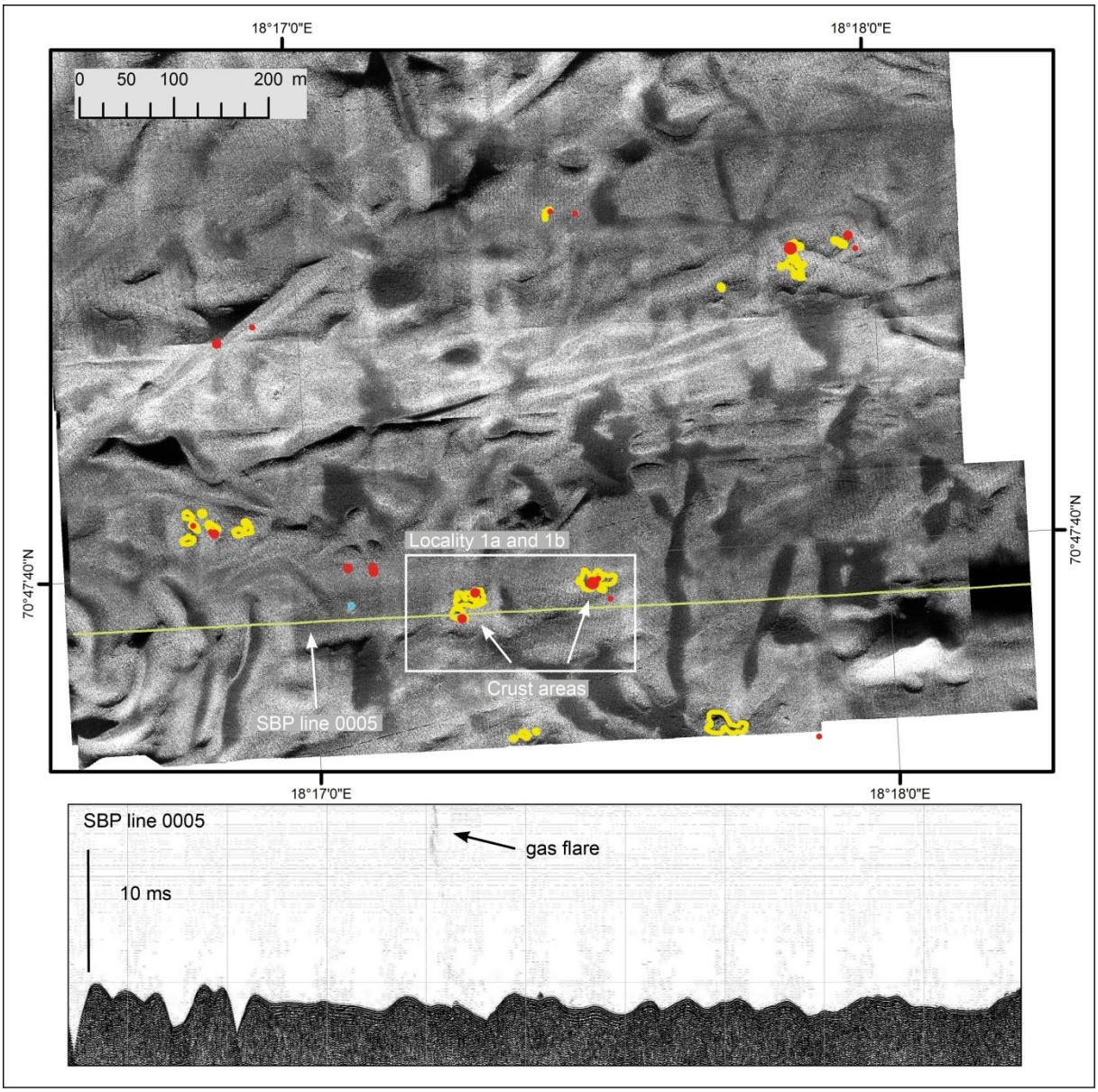

Figure 22. HISAS imagery (above) showing location of crusts (yellow polygons), gas flares (red dots) and location of SBP line (below) from Area M. Notice the gas flare indicated in the SBP section.

Area N (Figs. 14d, 23) have sediments varying from gravelly sand to gravelly mud. In Area N, several coral mounds occur on top of a glacially sculptured ridge incised by iceberg plough marks (Fig. 23). The SAS imagery reveals that there are c. 15 coral mounds ranging in size from 15 m to 100 m, partly forming complexes with several mounds having grown together.

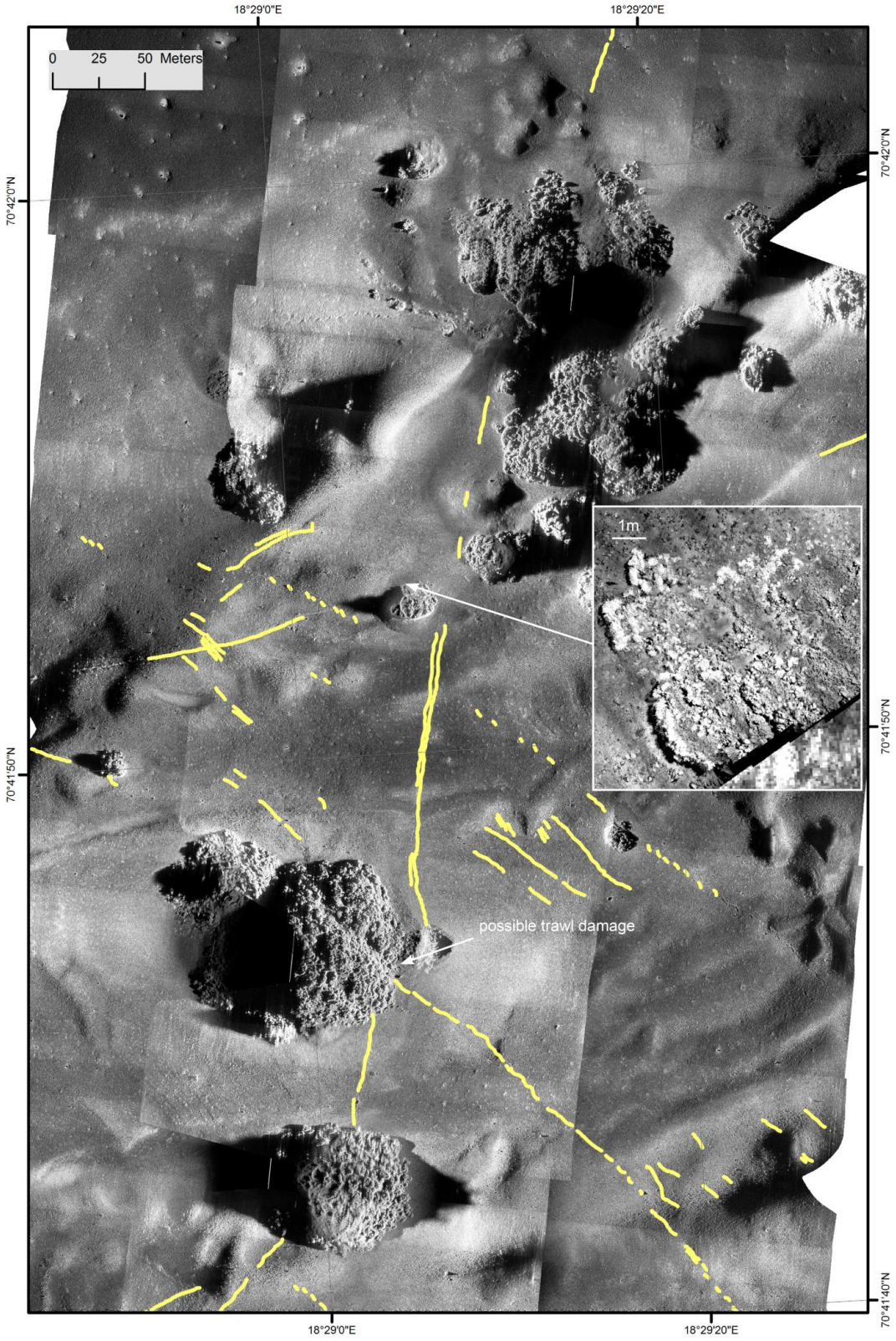

Figure 23. HISAS imagery from Area N showing trawl marks (yellow lines) and inset photo of TFish mosaic showing probable carbonate crusts at the flank of a coral mound.

TFish imagery reveals a diverse fauna, including *Lophelia pertusa and Paragorgia*. On the northern flank of one of the coral mounds (Fig. 23, inset photo), which measures c. 15 m x 20 m, a 10 m x 3.5 m area is covered by sea anemones and bivalves, apparently covering carbonate crusts. It seems likely that the rocks extend beneath the coral mound. ROV investigations are needed to confirm this interpretation. Similar crust-like features are also found in the northernmost part of the area. A prominent feature in this area is the relatively high number of trawl marks. The majority of the trawl marks avoid the mounds, but a few can be seen crossing and possibly causing damage by ripping off parts of the mounds.

Area O is dominated by gravelly muddy sand (Fig. 14d). Iceberg ploughmarks and pockmarks up to 20 m wide are present (Fig. 24). A 125 m wide coral mound is present, and has a "cauliflower" structure possibly reflecting a high number of *Lophelia* colonies. Trawl marks are abundant, and at least one of them crosses the mound, apparently causing some damage. Most of the pockmarks in Area O have a single block in their centers, pointing towards a link between the blocks and the pockmarks. We interpret this to be a result of current focusing around the blocks, causing erosion.

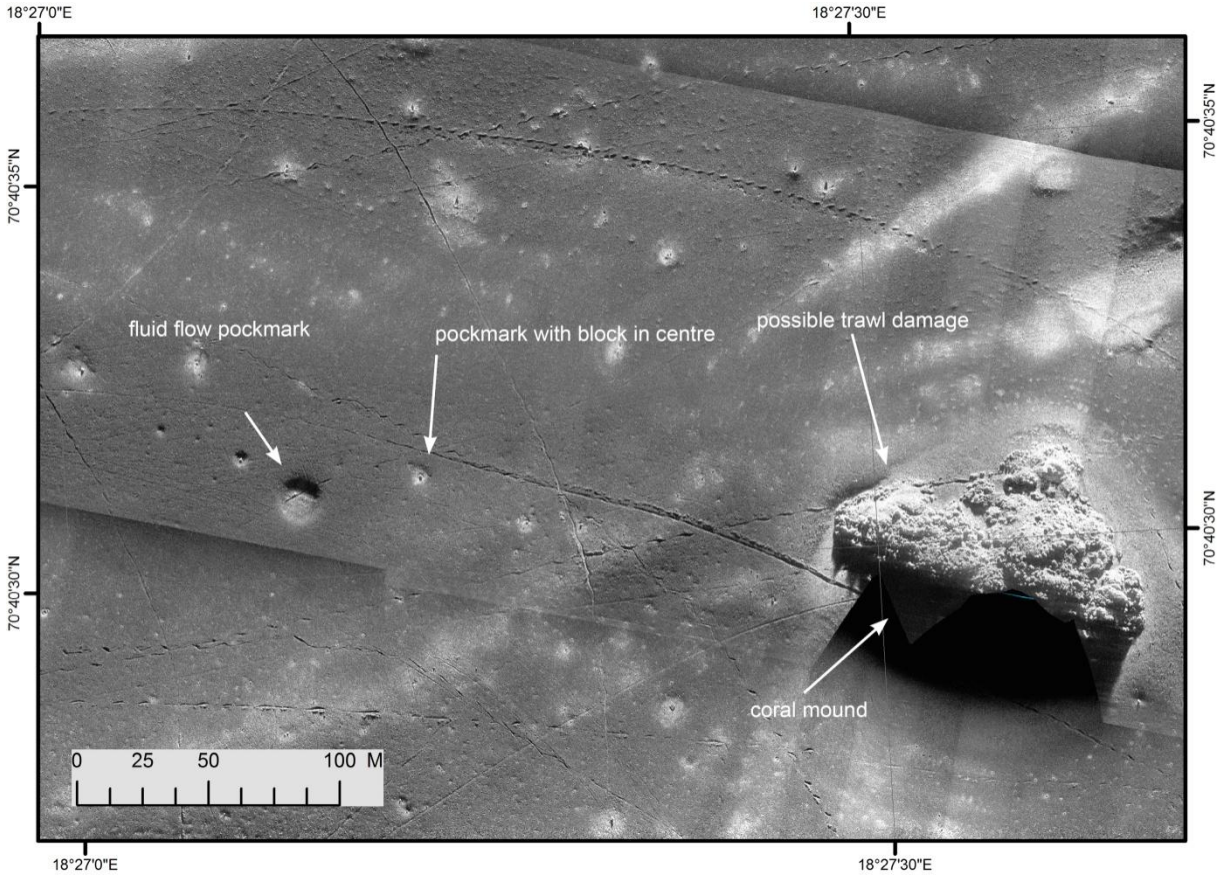

Figure 24. HISAS imagery from Area O showing coral mound, pockmarks and trawl marks.

Areas P and Q (Figs. 25, 26) are located within an area of sand, gravelly sand and sandy gravel (Fig. 14d), at the southern margin of the Håkjerringdjupet glacial trough. Apart from a

very high density of trawl marks, no features or structures of interest have been observed in Area P or Area Q (Figs. 25, 26).

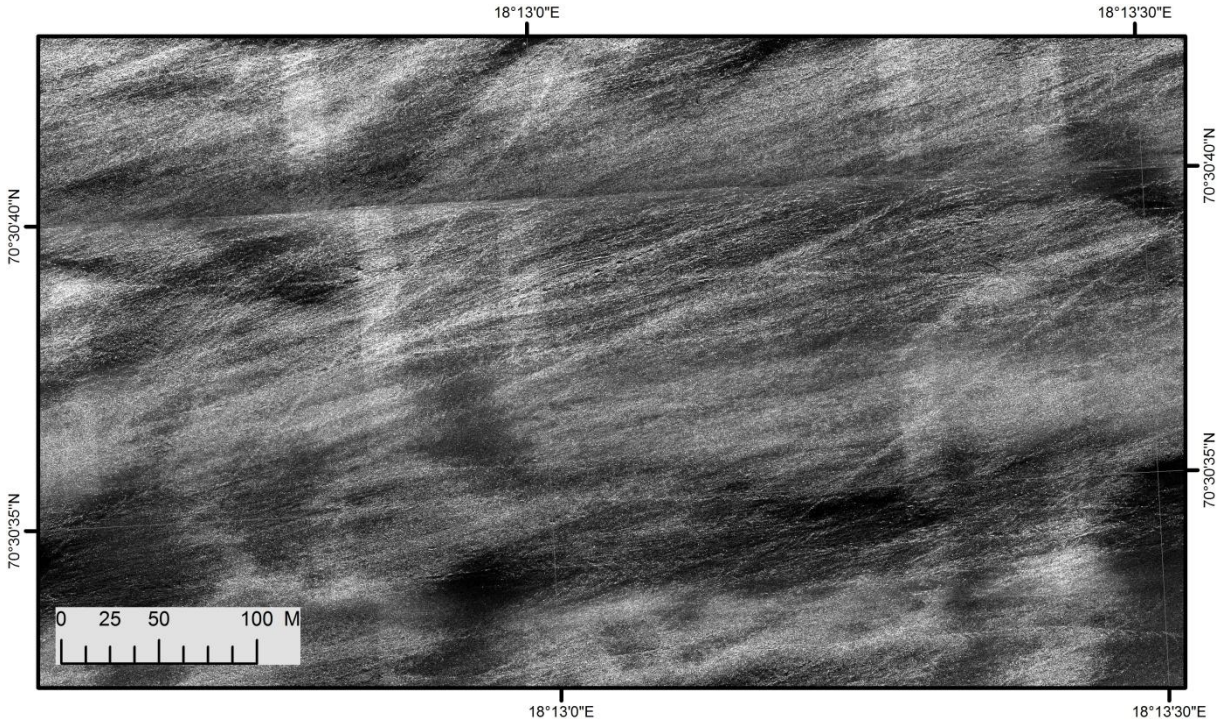

Figure 25. HISAS imagery from Area P showing dense coverage of trawl marks.

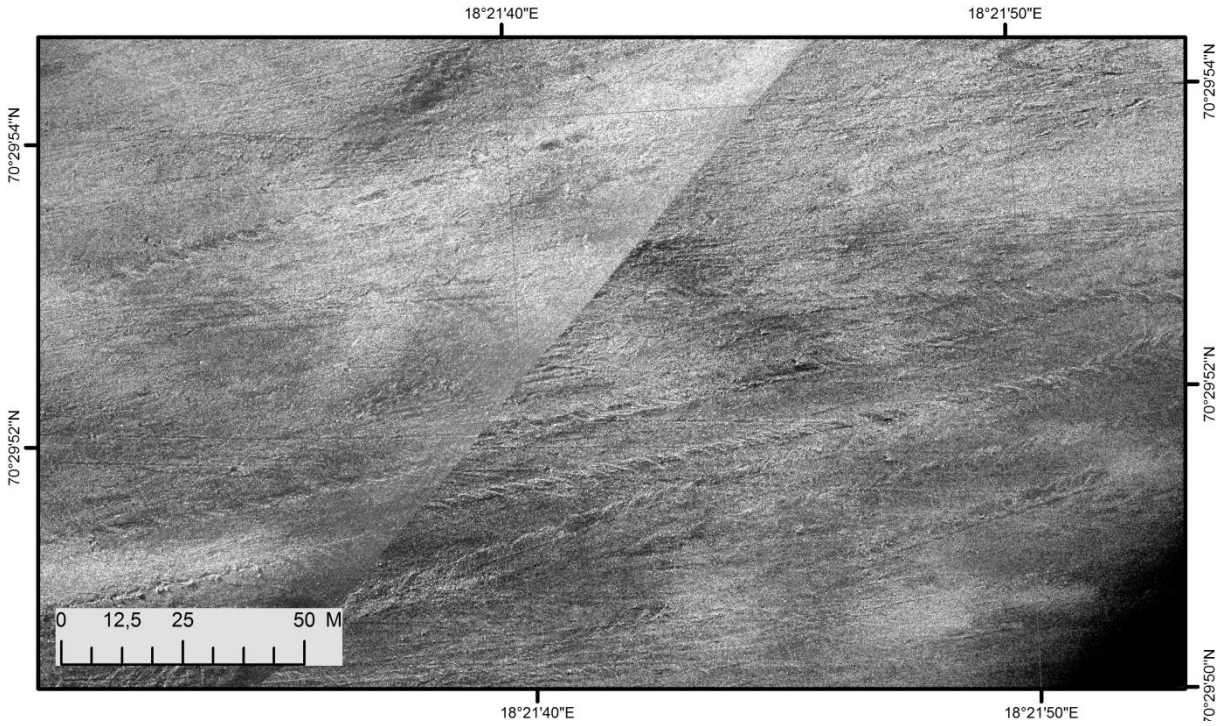

Figure 26. HISAS imagery from Area Q showing dense coverage of trawl marks.

4.2 Pockmarks

4.2.1 Alvheim

Pockmarks have been mapped in the Alvheim study area, especially in the channel and along the channel boundary. They occur randomly as isolated depressions and in limited numbers. They are not correlated to iceberg ploughmarks or any other regional geologic features. The pockmark (P2) structure with the acoustic gas flare indicates that it formed recently (Fig. 27). A nearby pockmark (P1) which is inactive has indications of subsurface pockmarks (Fig. 27). The paleo pockmark shows similar depressions with sediment infill indicating that the pockmarks were active for some time and there after filled by sediments. This also indicates that the fluid flow processes were affecting only the seafloor at the time of fluid escape since the pockmarks are differently filled and the depression is not open all the way to the base of the first pockmark. The latest channel infill pinches out towards the margin of the melt water channel indicating that only the base of the channel acted as deposition area during the post glacial period (Fig. 27).

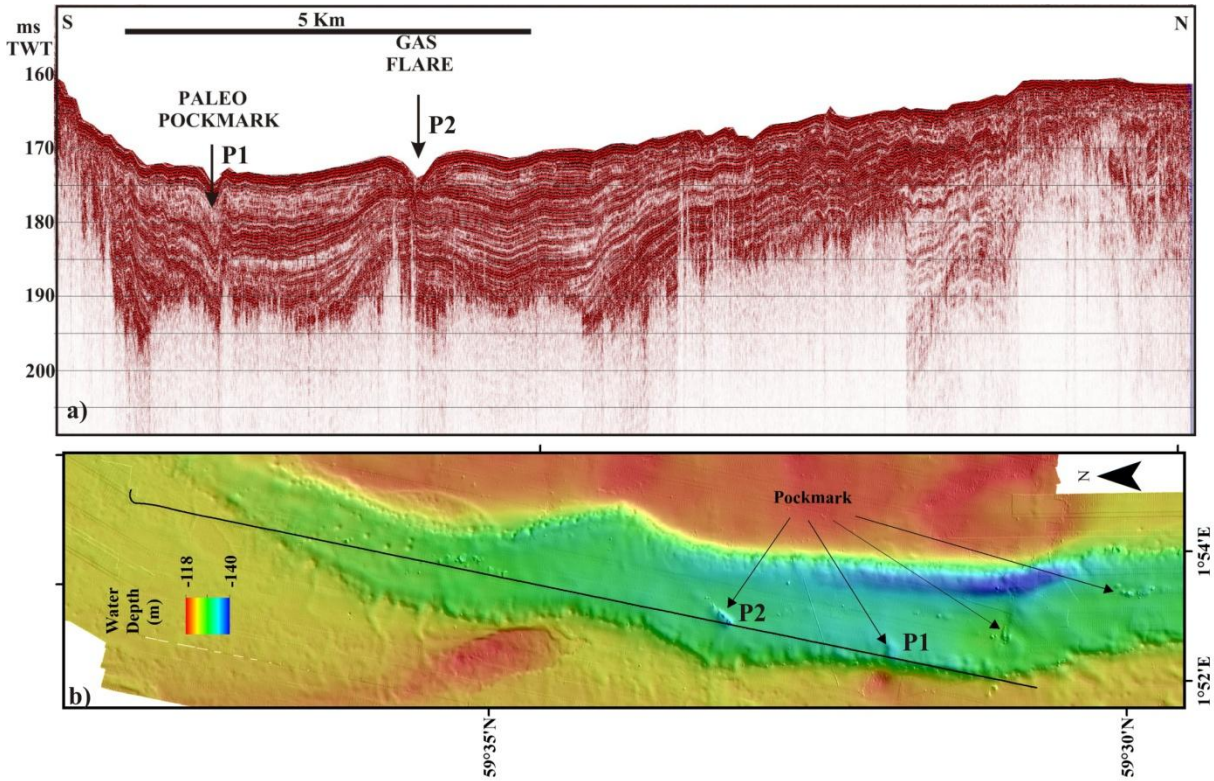

Figure 27. a) Topas line across the location of large pockmarks, b) Shaded relief bathymetry showing the location of seismic line and two pockmarks it is crossing.

4.2.2 Utsira High

No pockmarks were observed in the Utsira High study area.

4.2.3 Harstad Basin

A large number of pockmarks were observed in the deepest parts of the study area, Håkjerringdjupet. The pockmarks range in size, and an increase in size and depth is observed with increasing water depth (Fig. 28a). Some of the pockmarks indicate high backscatter (Fig. 28b) at their centres which can be correlated to their bases reaching the underlying till/glaciomarine deposits (Fig. 28c).

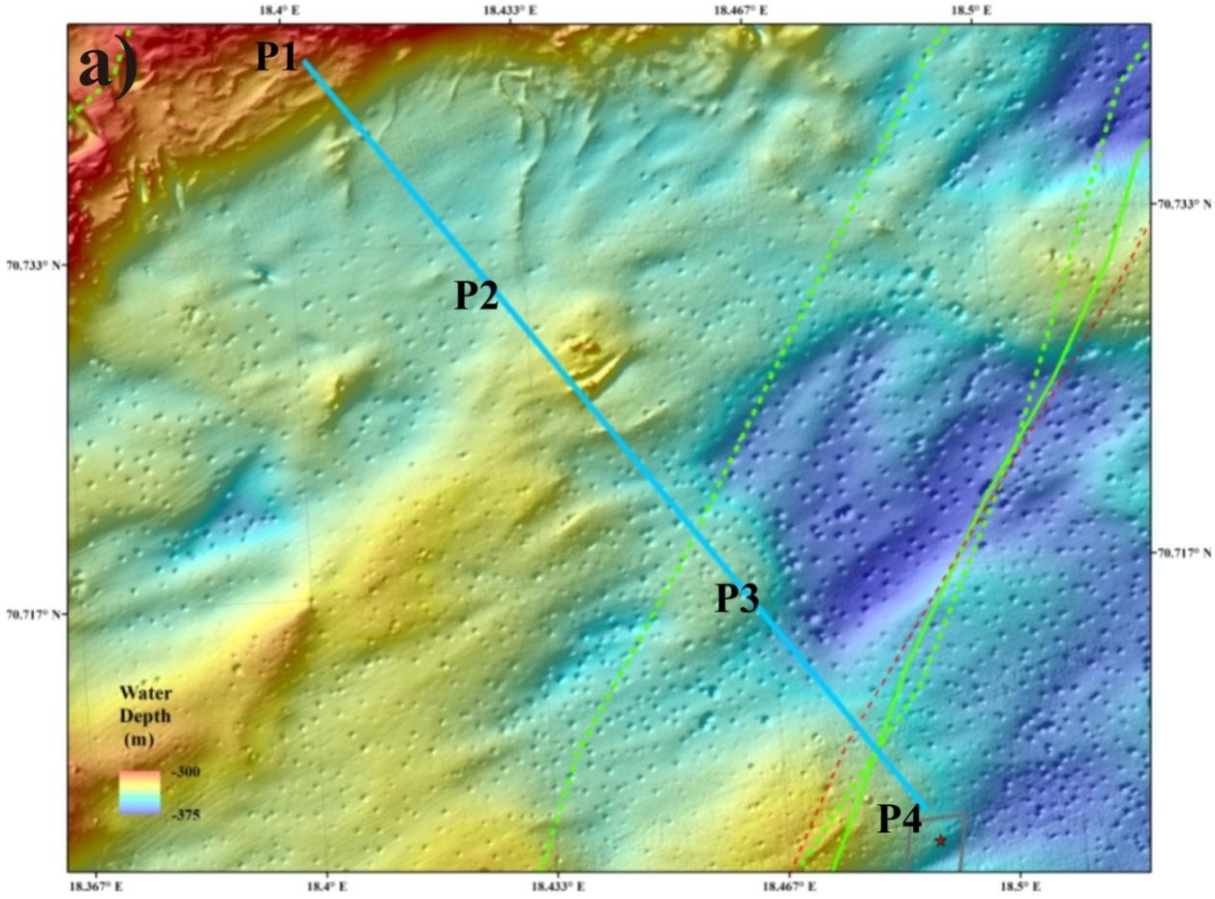

Figure 28a. Shaded relief bathymetry of seafloor with pockmarks in the deeper part of the Håkjerringdjupet. Notice the general increase in size and depth of the pockmarks towards the deepest part of the Håkjerringdjupet.

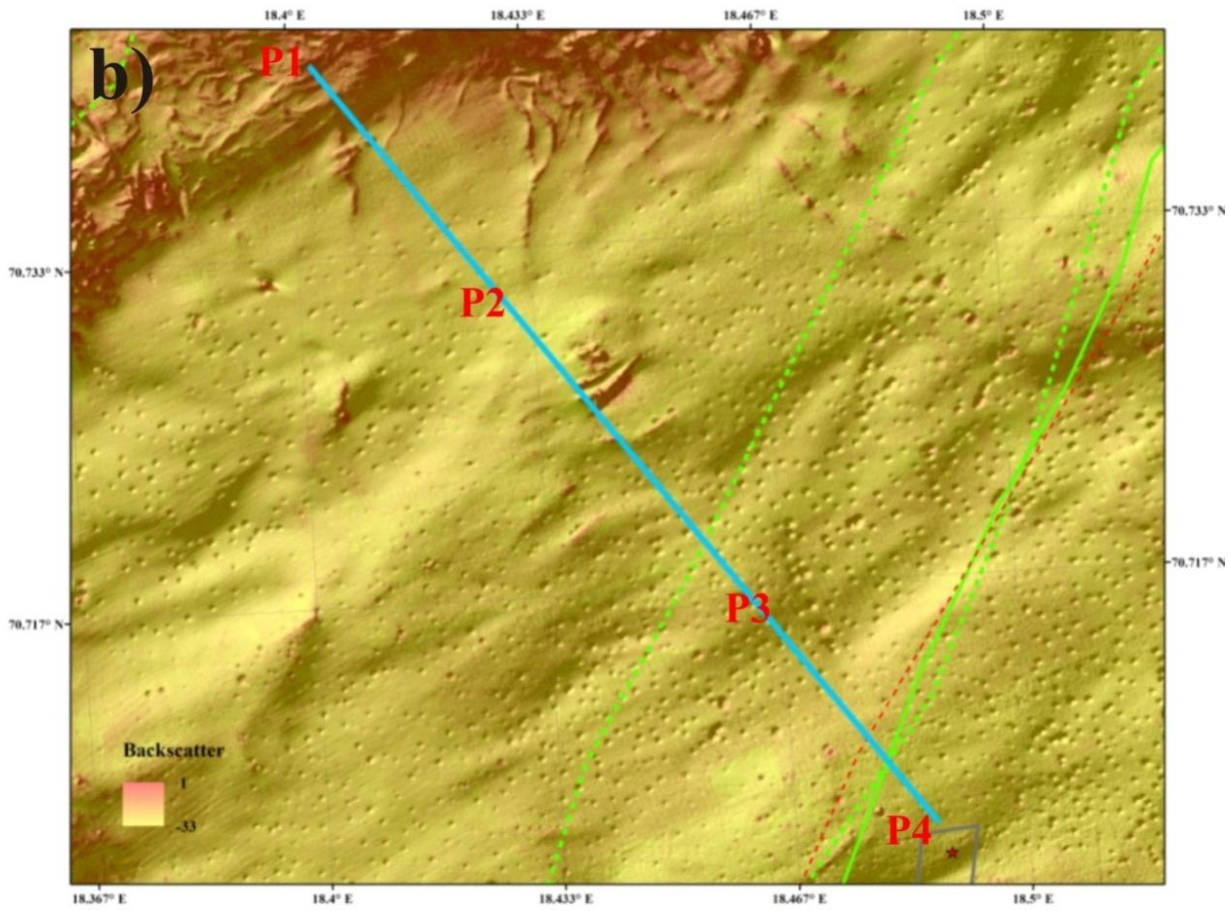

Figure 28b. Backscatter draped on shaded relief bathymetry of seafloor with pockmarks in the deeper part of the Håkjerringdjupet. Notice the higher backscatter in deeper pockmarks towards the deepest part of the Håkjerringdjupet.

The pockmarks above the Harstad Basin can be grouped into three categories. Category 1 occur over the entire area, are sub-circular, up to 40-50 m wide and with little backscatter contrast compared to the surrounding seabed. Category 2 pockmarks (Fig. 29a) are mainly found in the central part of the area. They are sub-circular to elongated, 15 to 70 m wide, have high backscatter in the central part and irregular structures with low relief in their central parts. ROV inspection of the structures reveals that they are carbonate crusts, forming the habitat for spectacular sea trees, anemones and sponges (Fig. 29b). Category 3 pockmarks are smaller, generally up to 5 m in diameter, and occur with highest density around the category 2 pockmarks (Fig. 29a). The reason for the high backscatter in the central parts of the category 2 pockmarks is suggested to be exposure of harder sediments below the muddy sediments in which the pockmarks are developed. This is similar to pockmarks with high reflectivity centres at the Loppa High (Chand et al. 2012a).

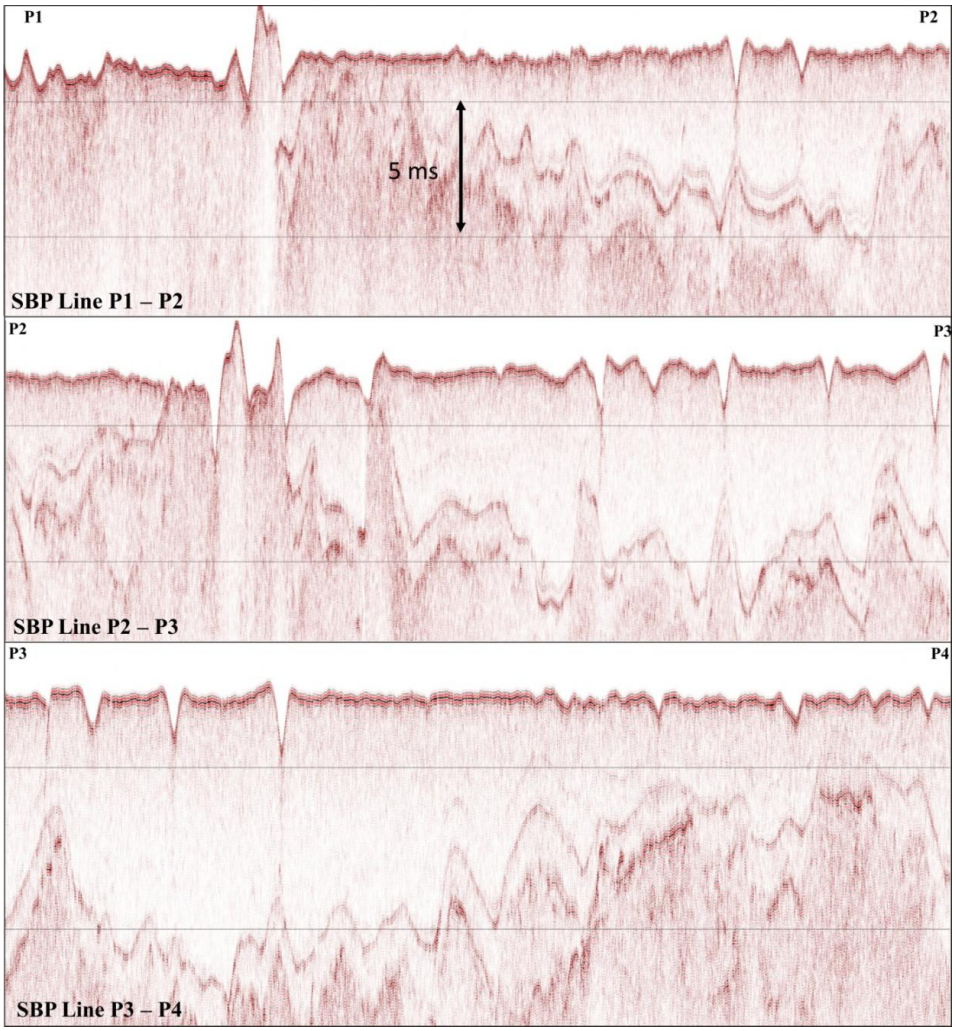

Figure 28c. Sub bottom profiler data across the pockmarks in Håkjerringdjupet. Location of the profiles are shown in Fig. 28a.

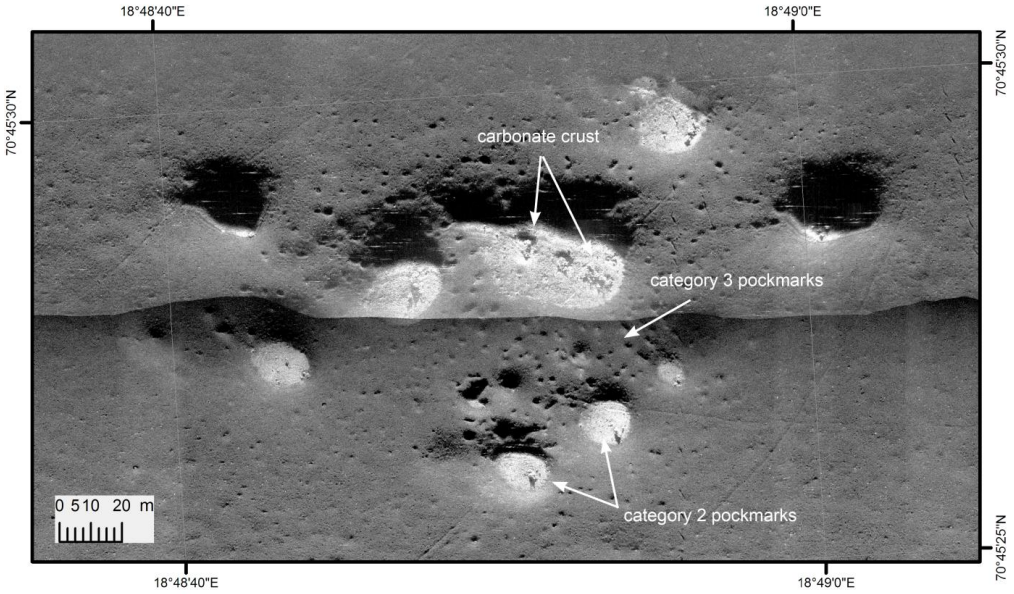

Figure 29a. HISAS imagery from Area C showing Category 2 pockmarks (20-70 m diameter) with high reflectivity due to carbonate crust/angular blocks in their central parts, and angular blocks. Category 2 pockmarks are surrounded by smaller Category 3 pockmarks.

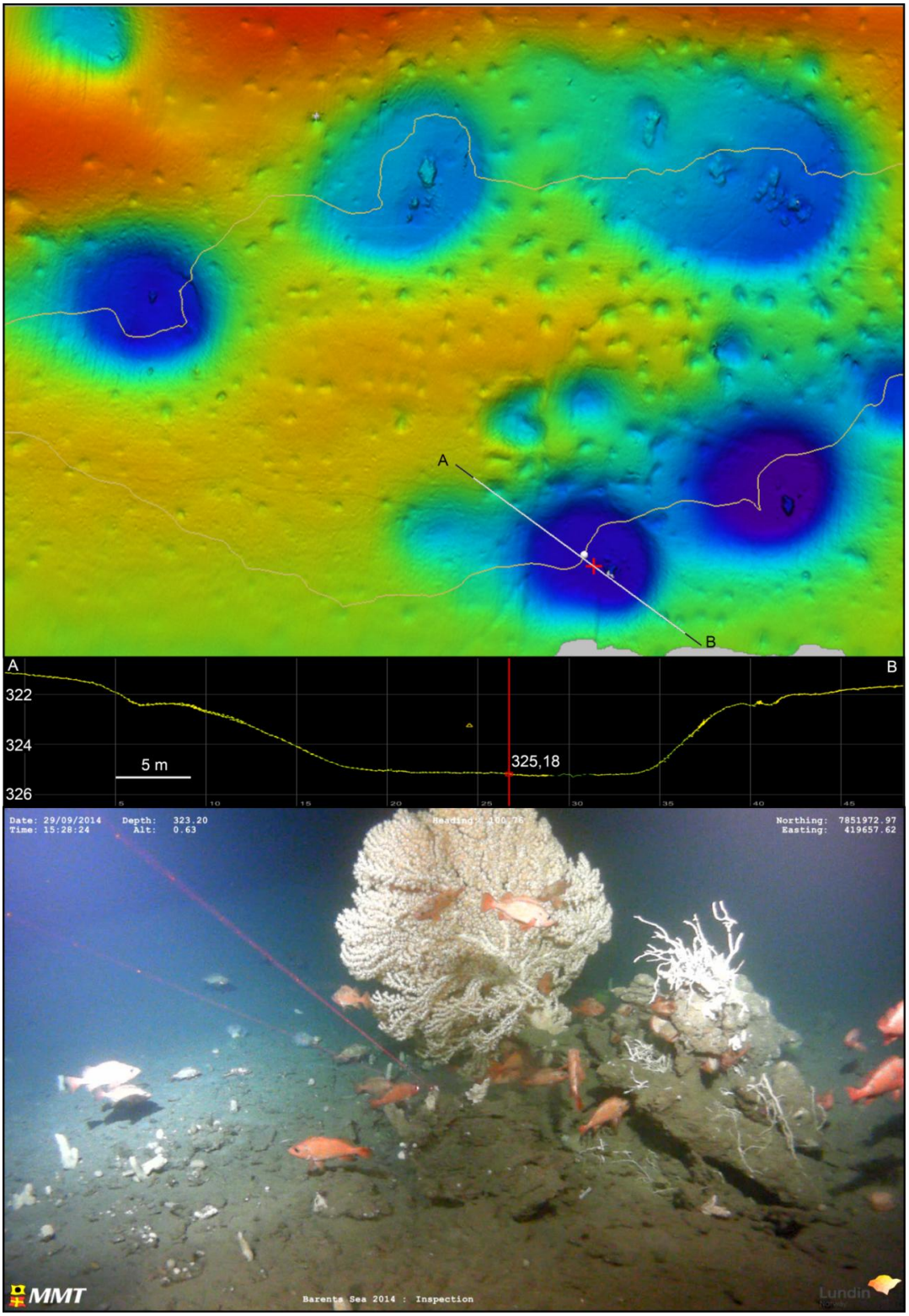

Figure 29b. Upper panel shows shaded relief bathymetry from Area C using ROV data (~ same area as upper panel in Fig. 29a). Water depths range from 318 to 326 m. Middle panel shows topographic profile A-B. Lower panel shows a photo of carbonate crust with sea trees.

4.3 Gas flares, carbonate crusts and methane anomalies

Several gas flares and gas anomalies in the near subsurface have been reported from the North Sea (von Deimling, 2001; Hovland and Sommerville, 1985; Hovland, 2007). Carbonate crusts and gas in sediments were also reported from the Utsira High study area (Hovland et al., 1987; Karstens and Berndt, 2015) and gas in sediments from the Alvheim study area (Brekke et al., 1997).

4.3.1 Alvheim gas flares, gas anomalies, carbonate crusts and shallow gas

Water column data from the Alvheim study area analysed using the FlederMaus Midwater package indicate 25 acoustic gas flares in the area covered by the multibeam data (Figs. 30a & b). Most of the flares are located along the shoulder of the channel (Figs. 30a & b). There are some flares located within the channel which are associated with the large pockmarks (Fig. 30a). ROV inspection of the seafloor revealed only limited bubbling at a few sites, but at many sites with carbonate crusts (Fig. 31) and microbial mats, the sediments are very gas-rich as indicated by active bubbling during push-in coring.

The immediate subsurface of the study area indicates presence of shallow gas and chimney structures bringing gas from the deeper sub-surface to shallow levels and also to the seafloor (Figs. 32 a, b, c & d). The gas appears to be concentrating about 20 ms TWT below the seafloor indicated by a total loss of reflections (Fig. 32a). Shallower wipe out zones due to loss of energy at shallow gas pockets can be seen close to a pockmark (Fig. 32a). Small pockets of gas occur at shallower levels indicated by high amplitude anomaly/chimney pairs (Fig. 32a). The chimneys can be real features produced by the gas flow, but can also be artifacts created by loss of energy due to the gas in the sediments. A similar large gas chamber can be observed close to the shoulder of the channel (Figs. 32b & c) indicating focusing of gas close to this boundary where infill of the channel pinches out against older sediments outside the channel probably due to difference in character between older and younger sediments (Figs. 32b & c). One of the flares reported along the shoulder of the channel does not give any indication of shallow gas, implying that the gas anomalies could be very small as well, producing no effect on the seismic data (Fig. 32d).

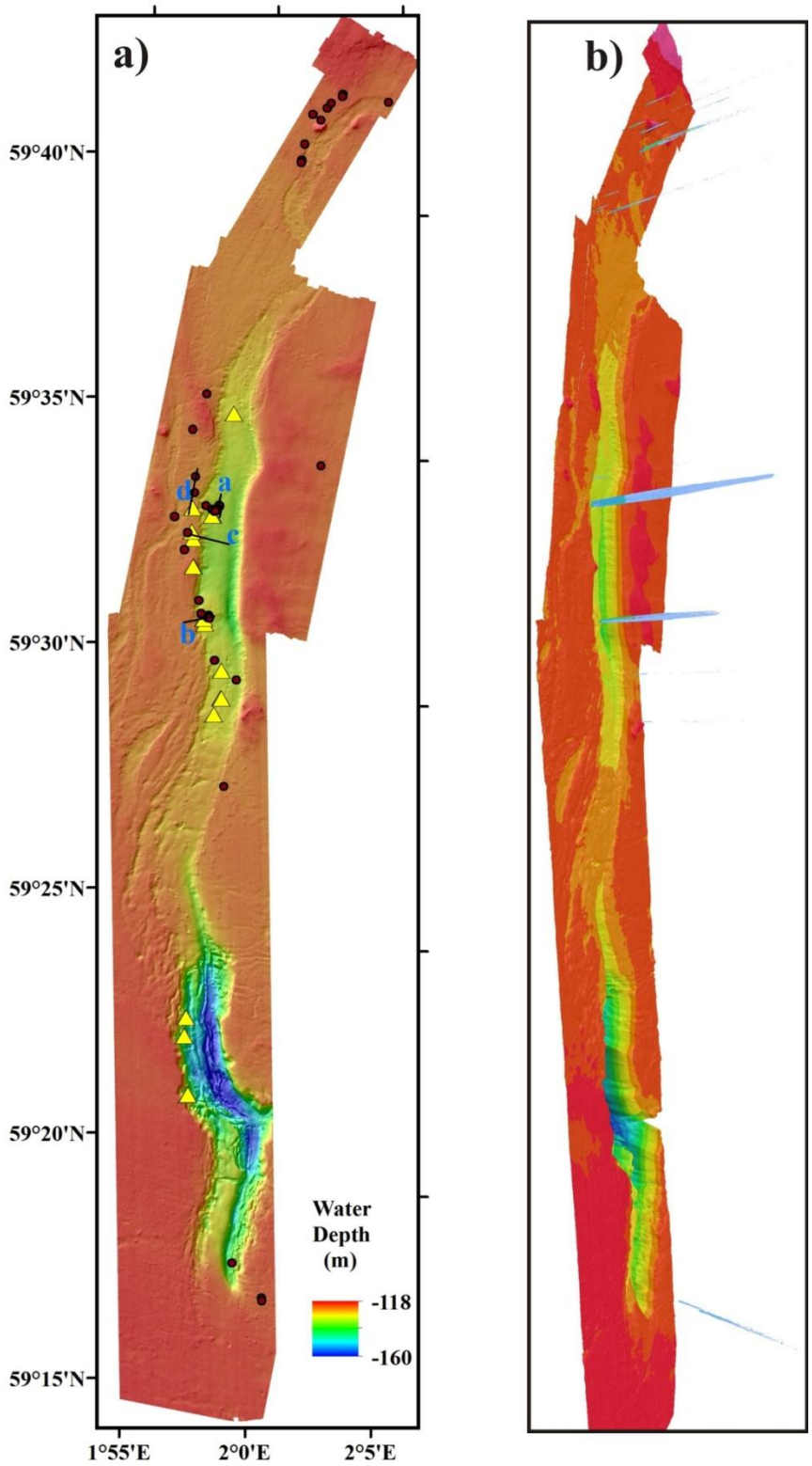

Figure 30. a) Shaded relief bathymetry of the Alvheim study area showing the location of flares, carbonate crusts (yellow triangles) and sub bottom profiler seismic lines. b) Three-dimensional relief of bathymetry from the Alvheim study area showing some of the flares.

Figure 31. Carbonate crust sampling by ROV in the Alvheim study area during the September 2013 cruise.

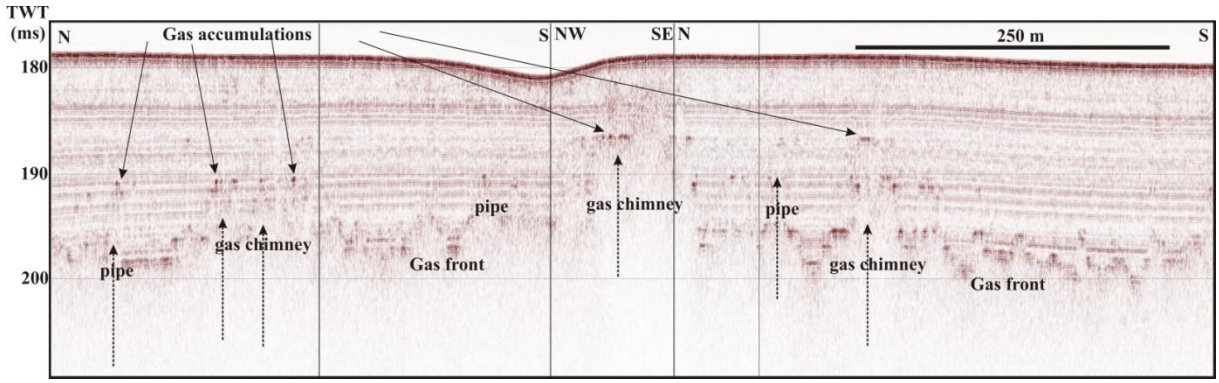

Figure 32a. HUGIN subbottom profiler (SBP) seismic line (a in Fig. 30a) across a pockmark showing a gas front and chimney and pipe structures.

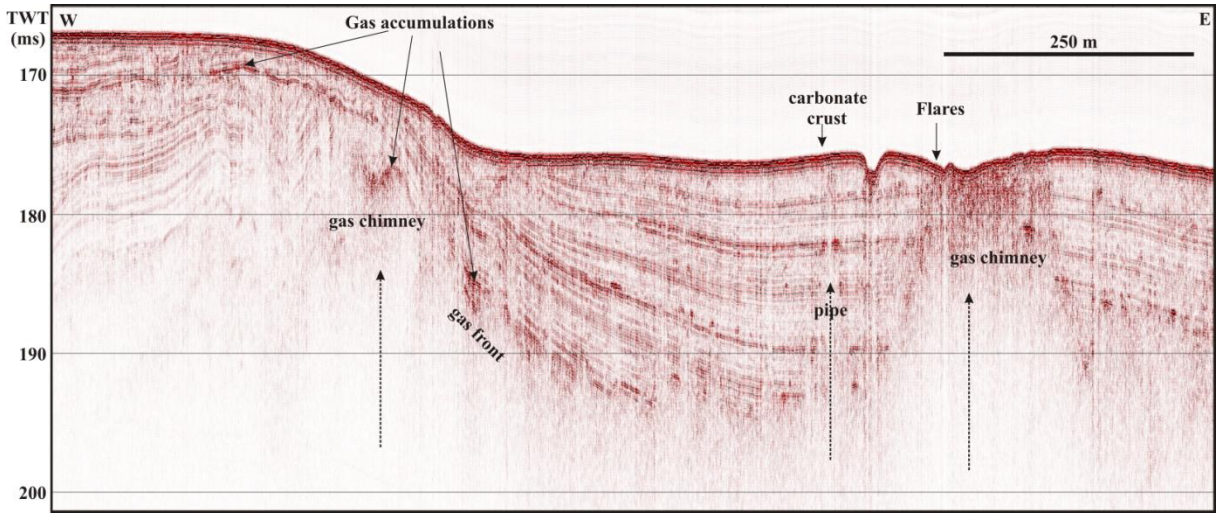

Figure 32b. HUGIN Subbottom profiler seismic line (b in Fig. 30a) starting from the shoulder of the channel (left) across the side of a pockmark and showing the buildup of a gas front and chimney structures towards the seafloor. Also shown are the locations of carbonate crust and gas flares.

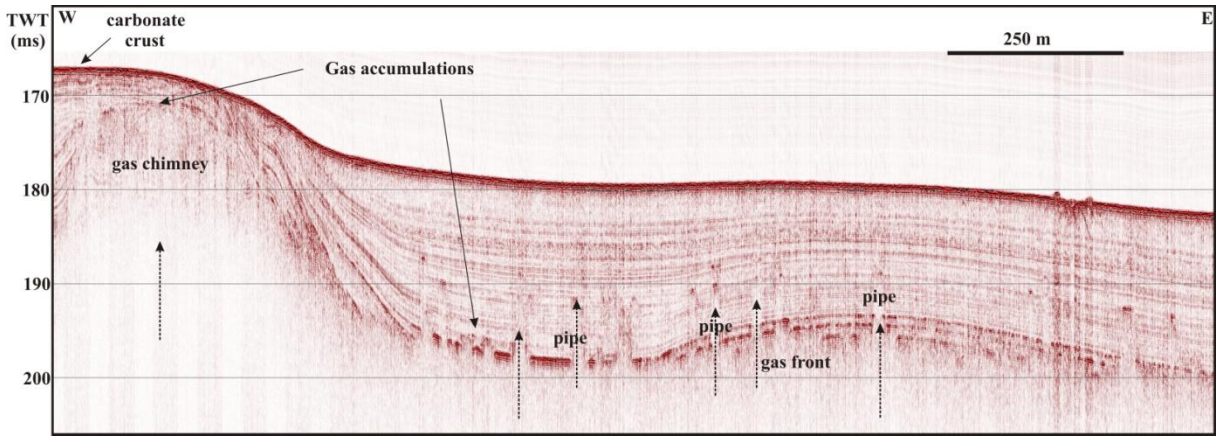

Figure 32c. HUGIN Subbottom profiler seismic line (c in Fig. 30a) from the shoulder of the channel (left) to the middle of the channel (right) showing a gas front and chimney structures.

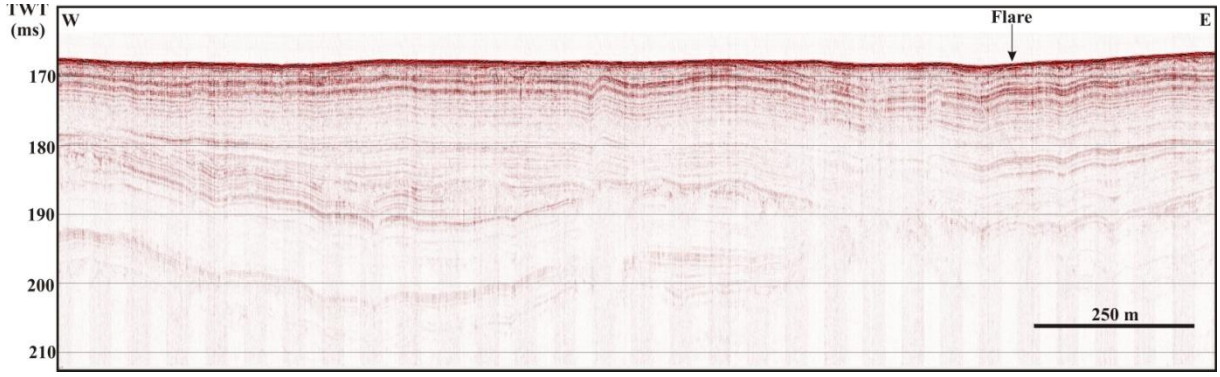

Figure 32d. HUGIN Subbottom profiler seismic line (d in Fig. 30a) on the shoulder of the channel across a gas flare. There is no clear gas anomaly in the subsurface associated with this gas flare.

4.3.2 Utsira High gas flares/anomalies, carbonate crusts and shallow gas

Initial analysis of multibeam water column data from January 2013 data indicated flare like anomalies (Fig. 33). A revisit to these areas during the cruise in March 2013 did not show any water column anomalies at the same locations. The January 2013 data were collected in very rough weather. This could have triggered the release of gas into the water column whereas very calm weather in March 2013 probably didn't result in gas release through the seafloor. Similar water column acoustic anomalies were observed in the new multibeam areas (the northern bathymetric rectangle) collected during the March 2013 cruise (Fig. 34). A Topas seismic line across four of the flares observed in the January 2013 data indicate gas related blanking or wipe out zones in the subsurface (Fig. 35). Similar anomalies can be observed on the sub bottom profiler seismic data as well (Figs. 36a & b). The sub bottom profiler data clearly indicated zones of gas accumulation in the shallow sub surface associated with high amplitude anomalies followed by blanking or wipe outs, typical of gas (Figs. 36 a & b). Even

though no active seepage sites with carbonate crusts were seen in this area, the gas flares appear as real and their release could be driven by changes in weather.

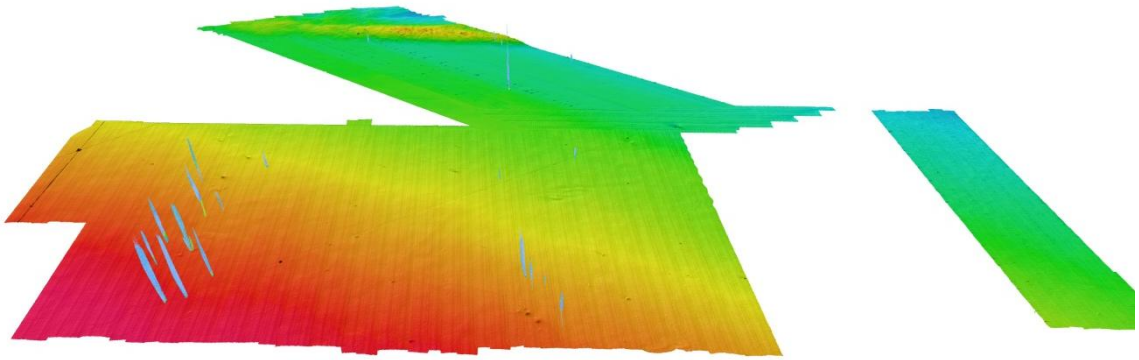

Figure 33. 3D bathymetry of the Utsira High study showing water column gas flares observed in the January 2013 data.

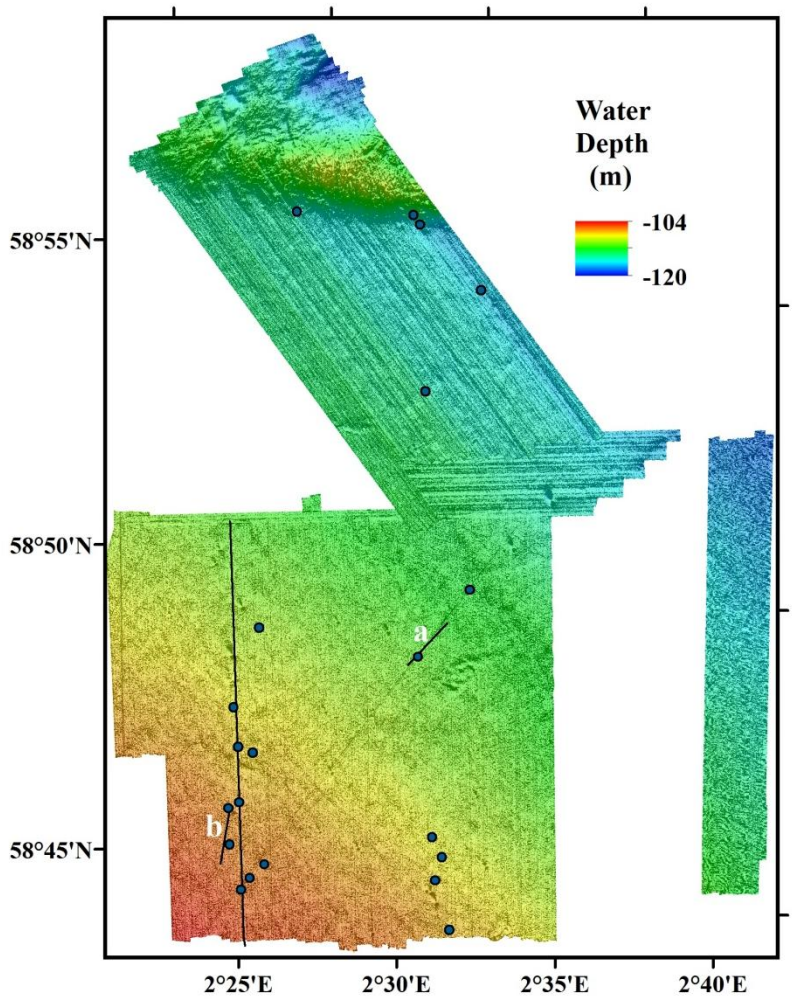

Figure 34. Shaded relief bathymetry of the Utsira High study area showing the location of flares (blue dots).

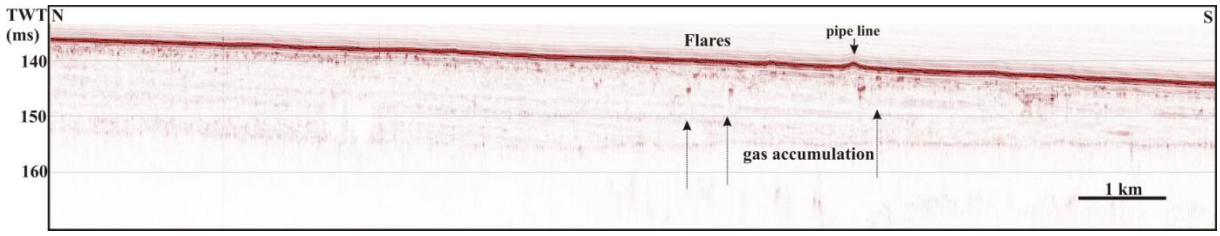

Figure 35. Topas seismic line across four flares and a pipeline showing the immediate sub-surface. Location is given in Fig. 34.

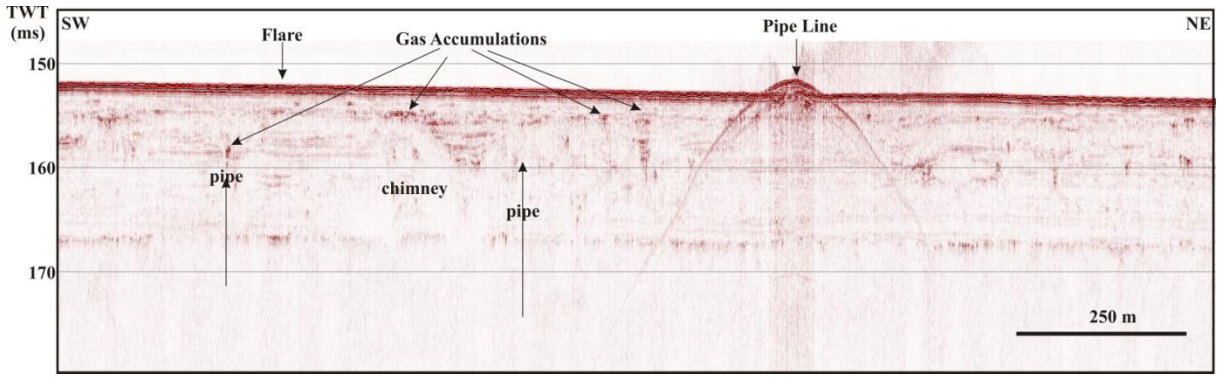

Figure 36a. HUGIN subbottom profiler seismic line (a in Fig. 34) across a flare and pipe line showing the immediate subsurface and gas accumulations and chimney/pipe structures.

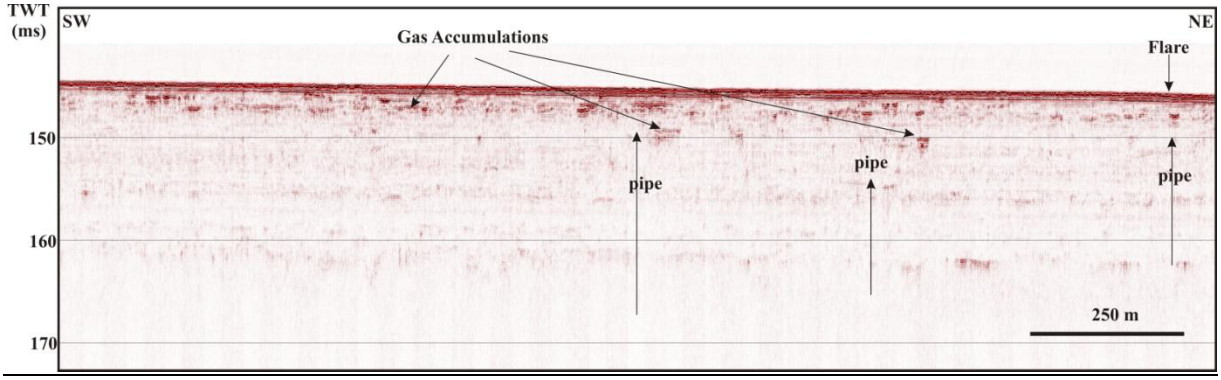

Figure 36b. HUGIN sub-bottom profiler seismic line (b in Fig. 34) across a flare showing the immediate subsurface, gas accumulations and pipe structures.

4.3.3 Sources of gas for acoustic flares in North Sea.

2D industrial seismic data from the study area were interpreted to study the structure and stratigraphy of the subsurface. Three main horizons were interpreted based on a stratigraphic tie from the exploration wells 24/6-1, 24/6-2 and 24/6-4 (Fig. 37). These include the base Quaternary, top Oligocene and top Paleocene covering the study areas and the surrounding (Figs. 37, 38 & 39). The base Quaternary varies in depth from 200 ms two way time (TWT) at the north eastern part of the study area to 675 ms TWT along the southern part of the study area (Fig. 37).

The top Oligocene varies in depth from 550 ms TWT along the eastern part of the study area to 1350 ms TWT along southern and central part of the study area. The top Oligocene deepens from the west and east towards the central part of the study area with localized depressions within the central part (Fig. 38). The top Paleocene also shows a similar structure with the shallowest part occurring along the eastern part of the study area and deepening towards centre and shallowing again towards the western part of the study area (Fig. 39). The deepest part of the top Paleocene occurs along the southernmost part of the study area.

Interpretation of subsurface stratigraphic boundaries indicates a deep linkage to the acoustic gas flares occurring at the seafloor. The Alvheim and Utsira High study areas are located where the top Paleocene shallows from the deepest part in the south indicating a possibility of fluid focusing towards these two locations from the deepest part of the basin (Fig. 39). A seismic section across the Alvheim study area shows the subsurface structure of the melt water channel where the large pockmarks and main flares are located (Figs. 40a & b). The channel is filled with Quaternary glacial and post glacial sediments probably. Gas accumulation at the base of the channel sediments can be seen as a high amplitude acoustic anomaly (Figs. 40a & b). The gas anomaly is connected to the top Paleocene through faults which could also be the pathways for fluid flow towards the base of the channel sediments (Fig. 40b).

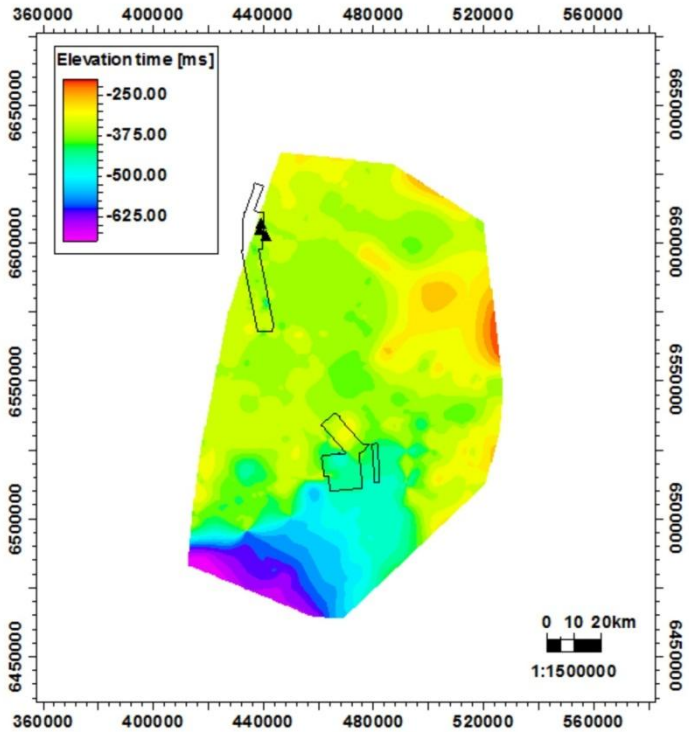

Figure 37. Two way time map of the base Quaternary surface interpreted from 2D seismic data (UTM zone 32 ED50). The polygons show the locations of the detailed study areas with multibeam bathymetry data.

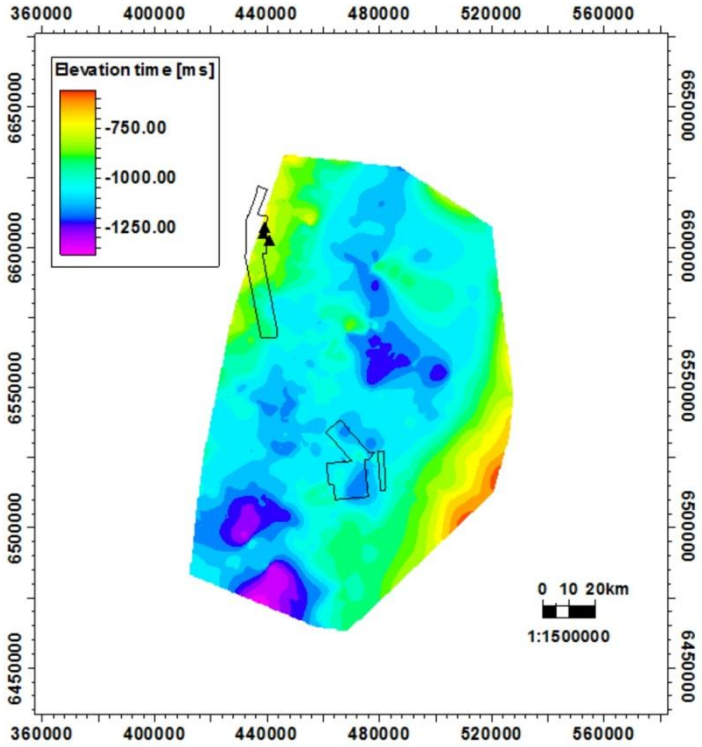

Figure 38. Two way time map of the Top Oligocene surface from 2D seismic data (UTM zone 32 ED50). The polygons show the locations of the detailed study areas with multibeam bathymetry data.

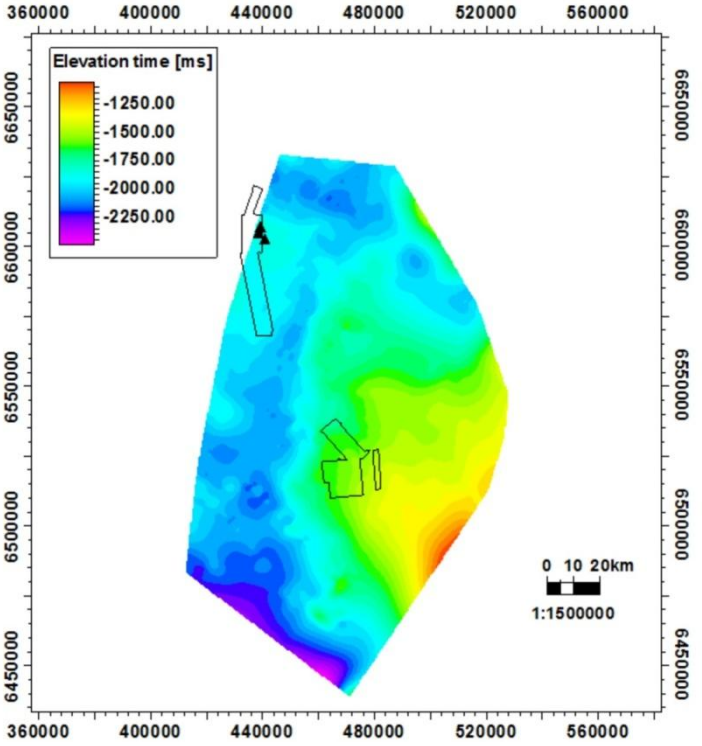

Figure 39. Two way time map of the Top Paleocene surface from 2D seismic data (UTM zone 32 ED50). The polygons show the locations of the detailed study areas with multibeam bathymetry data.

It remains to be shown whether faults have had control on the formation of the channel. The fluid flow observed presently within the channel through the pockmarks and along the side walls suggests that the faults were activated and leaking during glacial times causing ice-sheet fracturing and formation of sub-glacial gullies which probably facilitated the formation of the channel.

The subsurface of the Utsira High indicates a different story where gas anomaly pockets can be observed at shallower levels compared to the Alvheim study area. The gas anomalies are quite concentrated (Figs. 40c & d). There is no high amplitude anomaly close to the seafloor thus gas probably leak through the seafloor (Figs. 40 c & d). Analysis of gas samples from the Alvheim study area shows geochemical signatures typical of microbial origin (Fig. 41).

Fluid flow and shallow gas anomalies from different parts of the North Sea have been investigated in detail earlier by many geophysical and geochemical studies (Karstens and Berndt, 2015; Haavik and Landrø, 2014; von Deimling et al., 2011; Andresen et al., 2008; Hovland, 2007; Schroot et al., 2005; Mazzini et al., 2003; Haas et al., 1997; Clayton et al., 1997; Brekke et al., 1997; Hovland 1991; Hovland and Sommerville, 1985; Hovland, 1982a, 1982b; Hubscher, C. & Borowski, C., 2006; Rise et al., 1999; Fichler et al., 2005; Hovland et al., 1987). A geophysical study using 3D seismic data from the Viking Graben indicated focused fluid flow structures in the shallow subsurface (Karstens and Berndt, 2015). A large number of chimney structures were mapped in the Utsira High study area in which they related the fluid flow model to seal weakening, formation pressure and presence of free gas as essential pre-requisites for initiating these vertical fluid conduits (Karstens and Berndt, 2015) (Fig. 42). They suggested possible presence of gas flares in the water column as observed in our study. von Deimling et al. (2011) quantified the gas expelled from the flares in the Tommeliten area of the North Sea and estimated that only 4% of the gas reaches the sea surface. Shallow gas is suggested to be concentrating along palaeo-iceberg ploughmarks in the deep sub-surface as well (Haavik and Landrø, 2014; Fichler et al., 2005). These could be also palaeo-melt water channels formed during previous glaciations containing accumulations of sand.

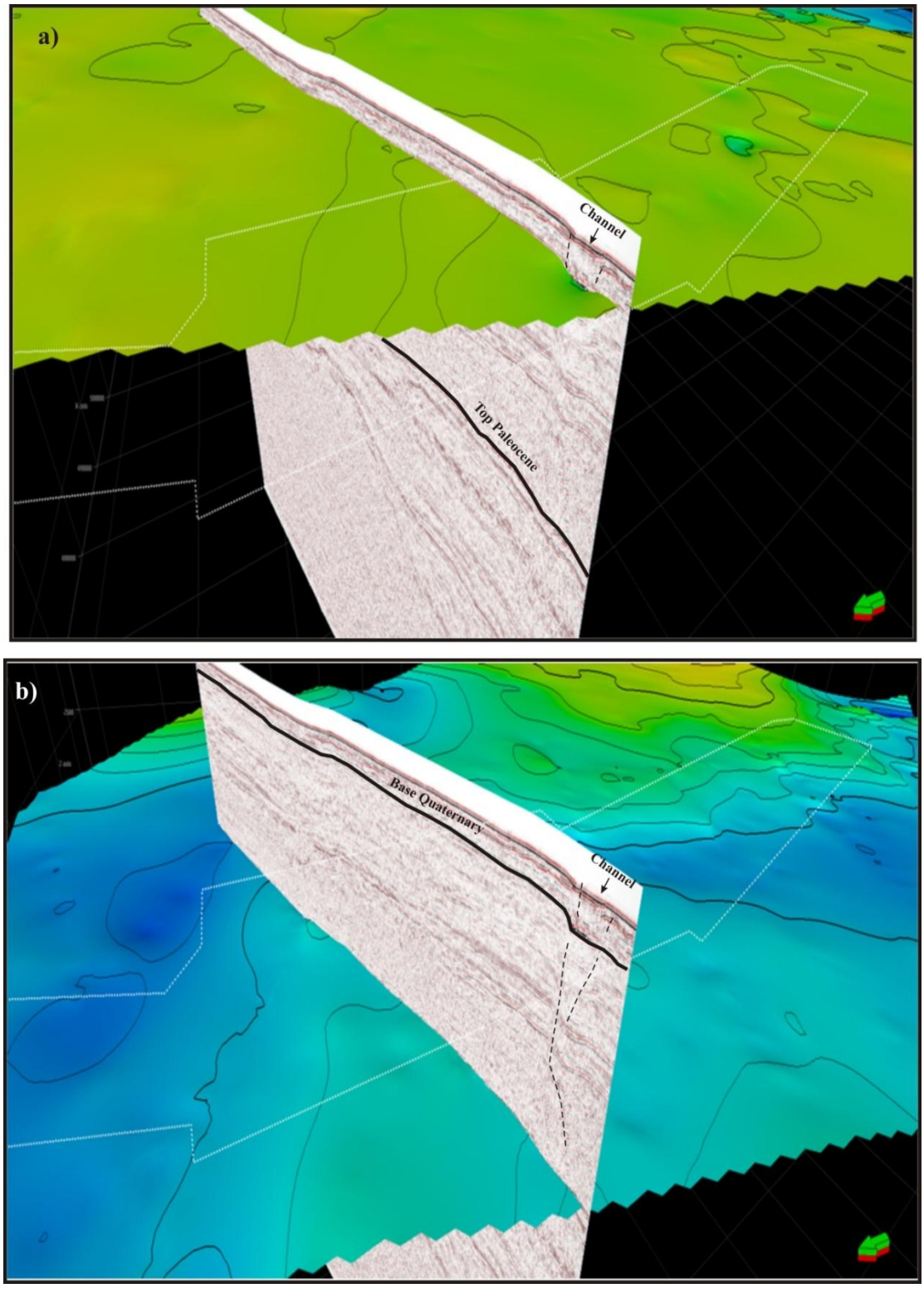

Figure 40. a) E-W 2D seismic line across the melt water channel in the Alvheim study area with 3D base Quaternary surface. b) E-W 2D seismic line across the melt water channel in the Alvheim study area with 3D base top Paleocene surface. The white polygon indicates the boundary of the multibeam data set.

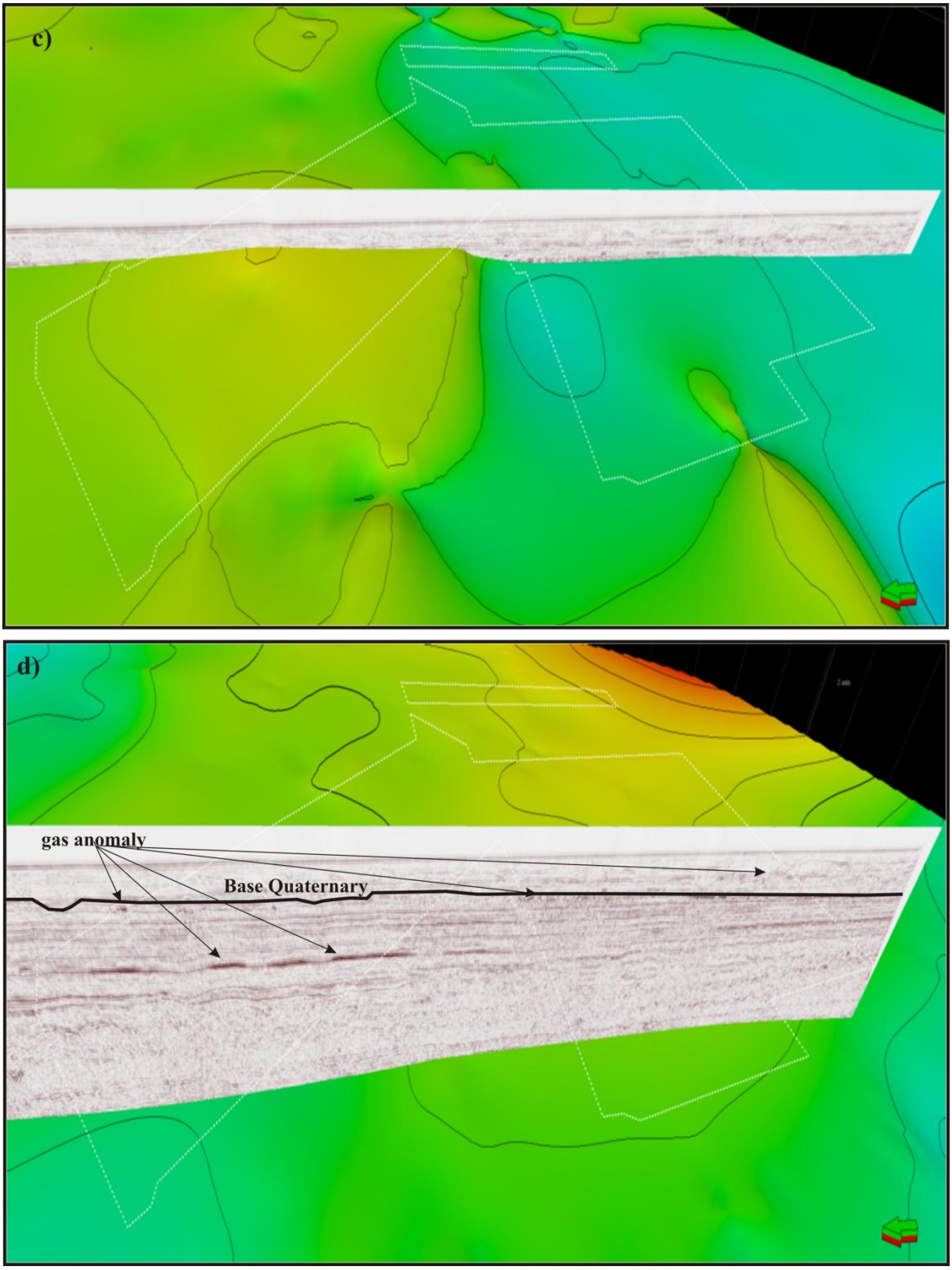

Figure 40. c) N-S 2D seismic line across the Utsira High study area with 3D base Quaternary surface. d) N-S 2D seismic line across the Utsira High study area with 3D top Paleocene surface. The white polygon indicates the boundary of the multibeam data set.

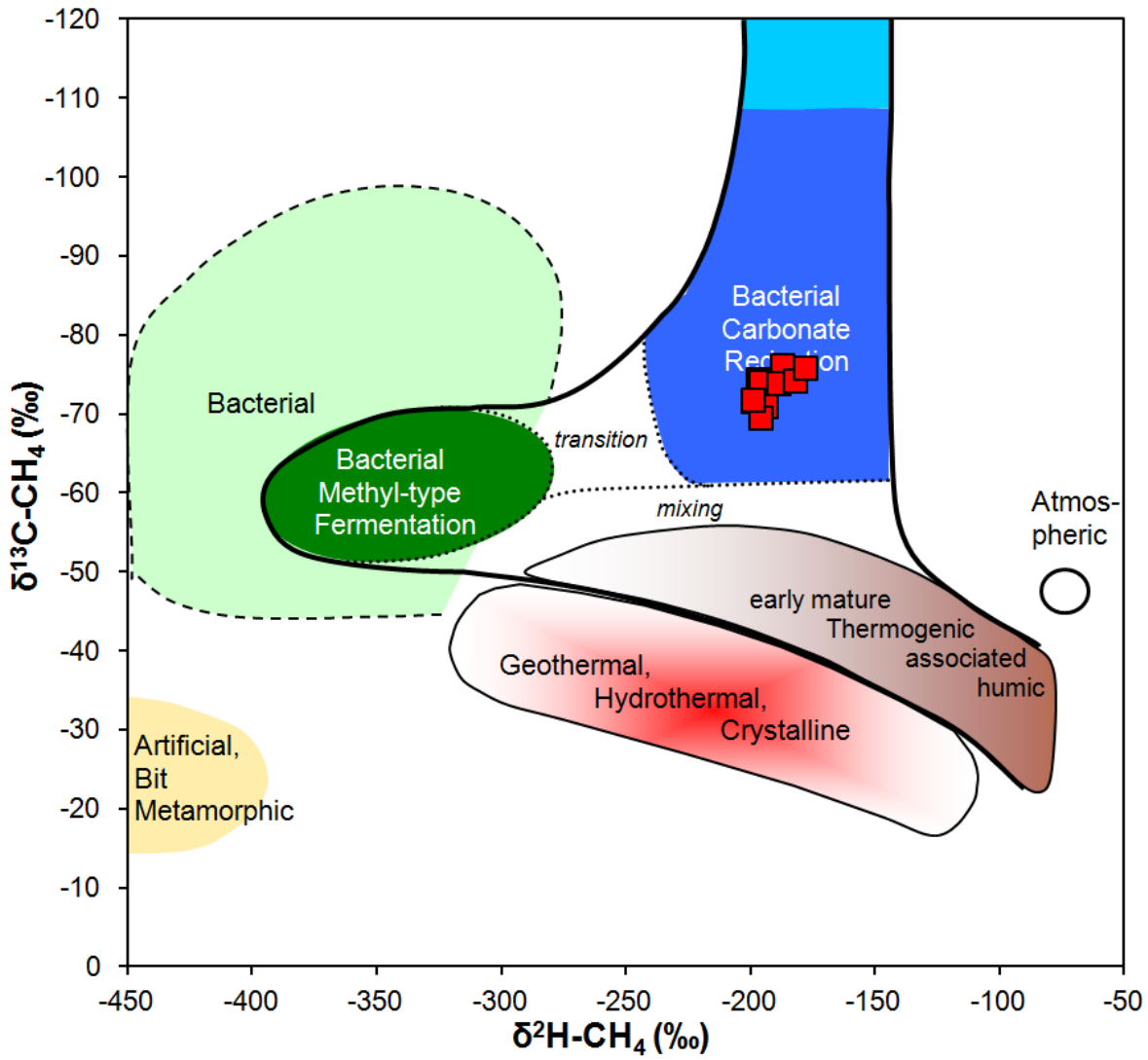

Figure 41. Isotopic composition of 12 gas samples collected with ROV from the Alvheim study area in September 2013.

Analysis of head space gases indicates that the leaking gas in most cases is of shallow origin (Brekke et al., 1997) whereas isotope values of gas collected at active seeps indicate that they originate from deep seated thermogenic sources (Hovland and Sommerville, 1985). The sub-surface of our study areas also indicates chimney like features both in the Utsira High and Alvheim study areas (Figs. 32a, b, c, d, 35, 36a & b). Similar observations are made from other areas of the North Sea where gas is observed to be routed from deep sources but giving a signature of microbial origin (Clayton et al., 1997; Brekke et al., 1997).

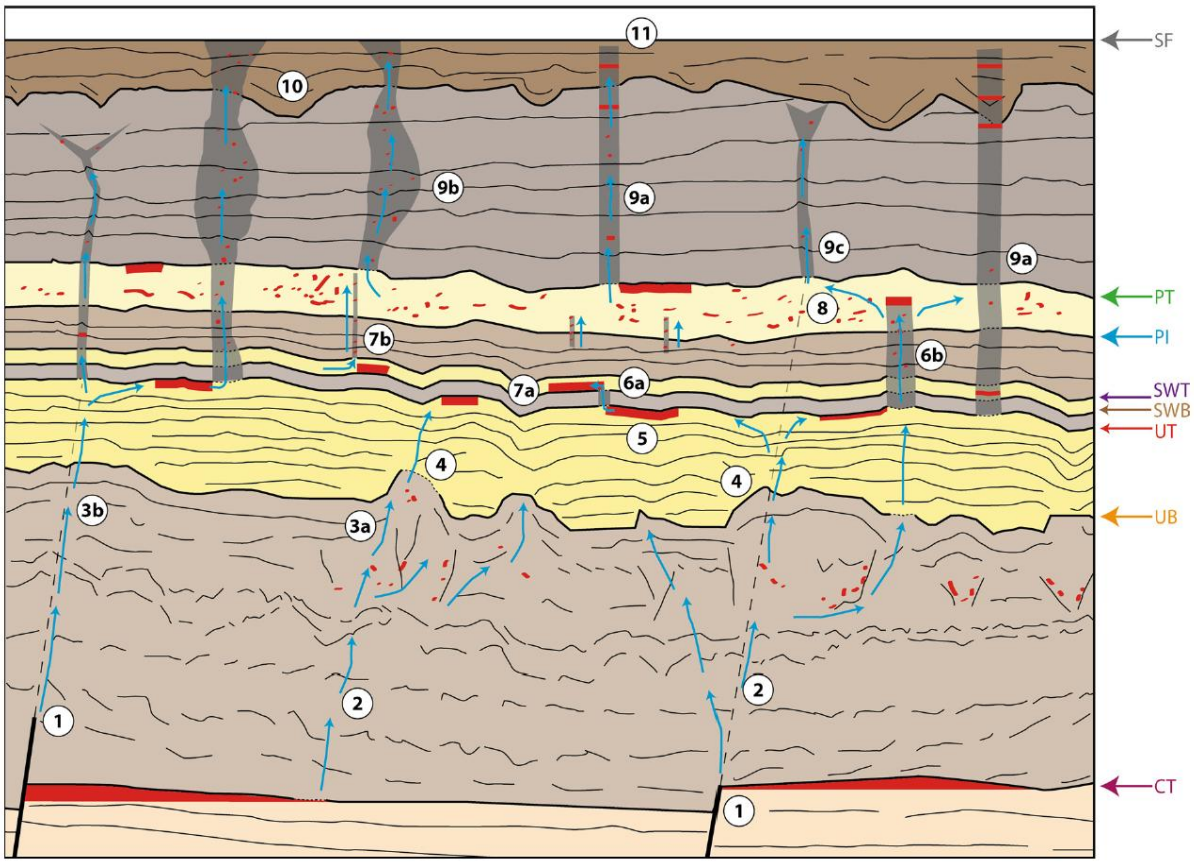

Figure 42. Sketch of fluid flow system illustrating the different stages of fluid migration: 1) Fluids leaking from deep hydrocarbon reservoirs; 2) fluids pass through the Hordaland mudstones via polygonal faults; 3a) fluids cause mud liquefaction forming mud diapirs and 3b) widespread mobilizations; 4) fluids enter the Utsira formation and 5) accumulate at its top; 6a) gas migrates from the Utsira formation towards shallower depth sand wedge and 6b) Upper Pliocene section using hydro-fracturing related pipes; 7a) gas accumulates within the sand wedge or 7b) creates pipes and migrates into the Upper Pliocene section; 8) fluids accumulate within and at the top of the Pliocene section; 9) high overpressure leads to the formation of hydrofracturing related 9a) type-A-chimneys, 9b) type-B-chimneys and 9c) type-C-chimneys at the top of the Upper Utsira formation and at the top Pliocene, which continue to shallower depth; 10) chimneys cross-cut buried tunnel-valleys; 11) in some cases chimneys reach the seafloor causing the release of fluids to the water column. Coloured arrows mark seismic reflections corresponding to important stratigraphic boundaries (SF- seafloor, PT- Pliocene Top, PI- Pliocene Intra, UT- Utsira Top, UB- Utsira Base, CT- Cretaceous Top) (Modified from Karstens and Berndt, 2015).

4.3.4 Harstad Basin gas flares/anomalies, carbonate crusts and shallow gas

Multibeam water column data collected by MAREANO (www.mareano.no) from the study area and surrounding areas have been analysed. There is only partial coverage within the Harstad Basin since water column data were not collected prior to 2010 by MAREANO. The analysis of available data indicates 190 locations with gas flares (Fig. 21). The number of individual gas flares is higher, because multiple closely spaced flares are recorded as a single flare in the database. The gas flares vary in strength, from "weak" to "very strong". Possible gas flares have been tagged "uncertain". These may be gas flares, but they are difficult to distinguish from fish shoals with sufficient confidence.

The gas flares occur above the Harstad Basin, the Troms-Finnmark Fault Complex, and the Finnmark Platform. The flares form two WSW-ENE trending linear clusters - one between Area A and Area M, and one close to Area J (Fig. 43). It should be stressed that water column data are available only from parts of the study area, and the apparent distribution could change significantly if a full coverage was available. Nonetheless, the clusters are considered to be real features, and not artifacts caused by the data availability.

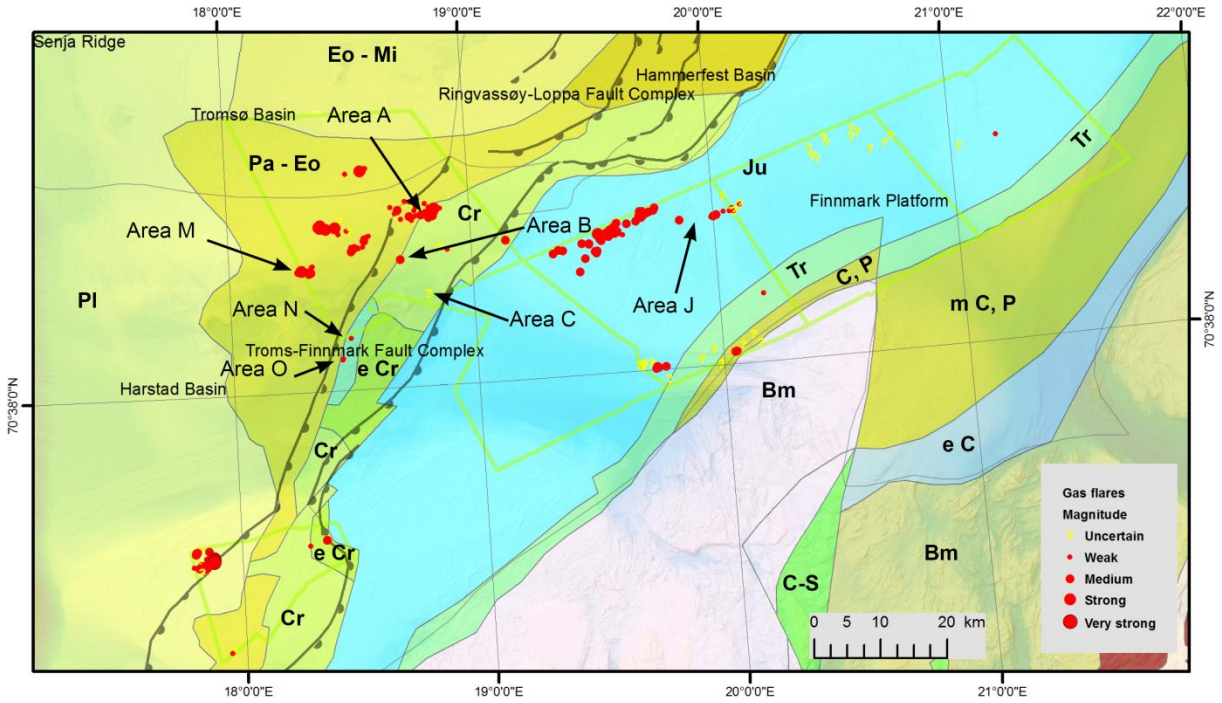

Figure 43. Structure and subcrop map (Sigmond, 1992) of the study area showing gas flares above the Harstad Basin, Troms-Finnmark Fault Complex and Finnmark Platform. Green polygons indicate the areas where water column data are available. Stratigraphic units: Bm: basement; C-S: Cambro-Silurian; e C: early Cretaceous; m C, P: mid Carboniferous, Permian; C, P: Carboniferous, Permian; Tr: Triassic; Ju: Jurassic; e Cr: early Cretaceous; Cr: Cretaceous; Pa-Eo: Paleocene-Eocene; Eo-Mi: Eocene-Miocene; Pl: Pliocene (from Sigmond 1992).

Most of the flares are associated with carbonate crust fields exposed at the seabed. Gas flares occur within the whole Area A (Figs. 43 & 44), but with highest concentration in the NE part. Carbonate crust fields also have the highest density in the NE part (Fig. 44). The interpreted distribution of carbonate crust fields based on HISAS imagery collected in November 2013 was verified by TFish imagery collected in June 2014. ROV videos collected in September 2014 confirmed the presence of carbonate crusts at all sites which were inspected.

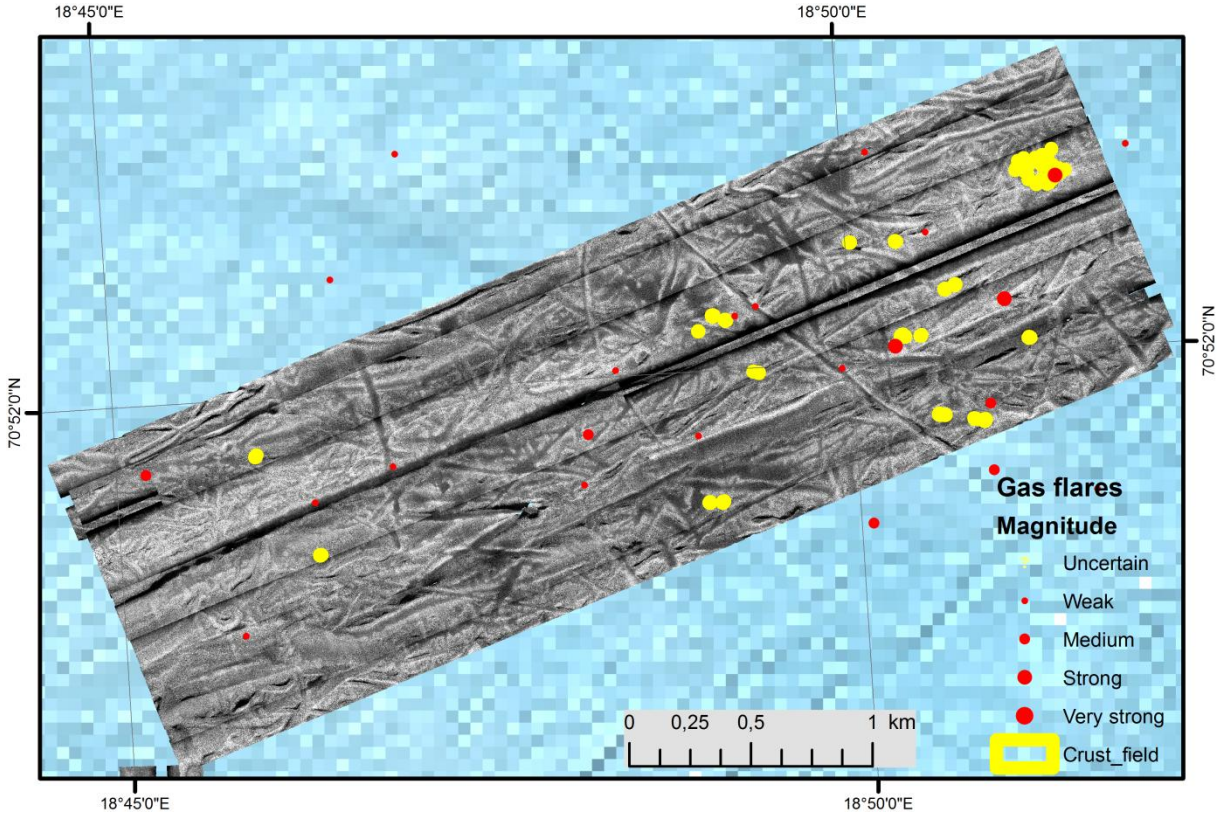

Figure 44. HISAS imagery from Area A.

The HISAS imagery from Area B show a number of carbonate crust fields occurring along a WNW-ENE linear trend. An ROV survey during the same cruise verified the presence of carbonate crusts. Based on this, a new HUGIN survey with HISAS and other instruments was conducted in June 2014, extending towards the WSW from the area surveyed in 2013 (NE corner). The new data show that there is a 1900 m long and 250 m wide WSW-ENE central belt with 116 interpreted occurrences of carbonate crust fields. The total number of carbonate crust fields in the area is 139, extending over a total distance of 2700 m. Part of the area was surveyed with TFish imagery in June 2014, verifying the interpretations of crust occurrences. An example of this is shown with SAS imagery and TFish imagery from the same area (Figs. 45, 46, 47 & 48). Further confirmation of the interpretation was given by ROV video inspection in September 2014. The high number of crust occurrences is in contrast to the fact that only one gas flare has been observed from the water column data. This means that the vast majority of crust sites can be regarded as records of extinct gas release. The area was

surveyed with ROV in September 2014 (Fig. 45), collecting multibeam bathymetry, video imagery, crust and gas samples. Carbonate crust drilling using the rock drill was attempted without success.

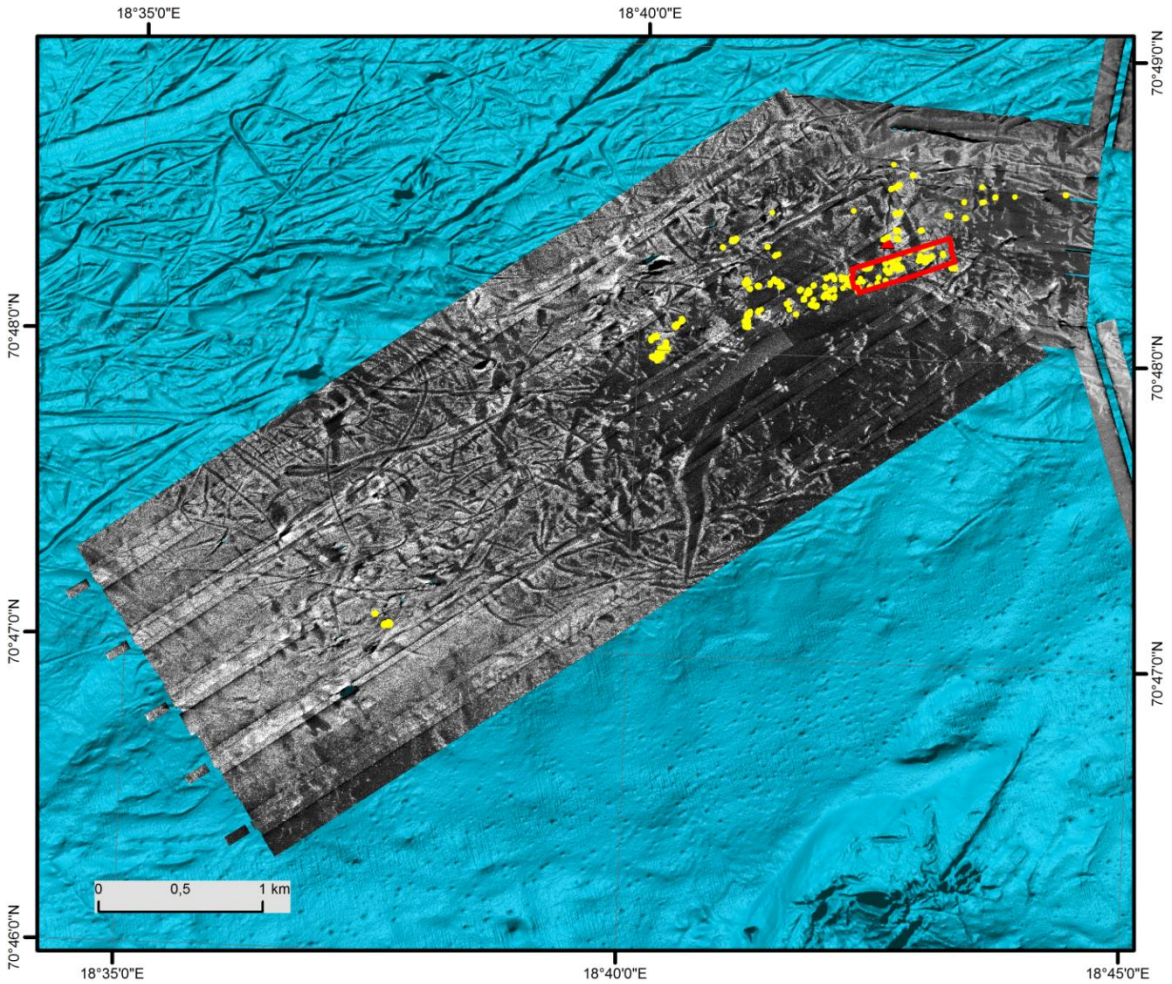

Figure 45. HISAS imagery of Area B showing a gas flare (red dot), carbonate crust fields (yellow polygons) and ROV multibeam bathymetry outline (red polygon).

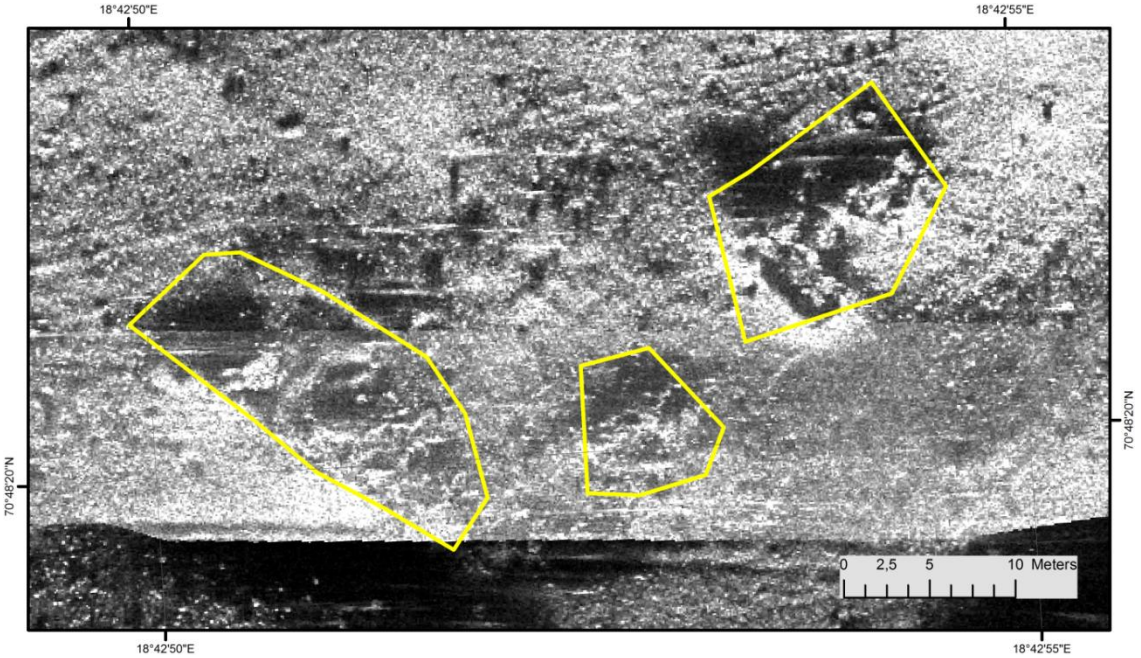

Figure. 46. HISAS imagery of the seafloor from Area B showing the location of carbonate crust fields (yellow polygons).

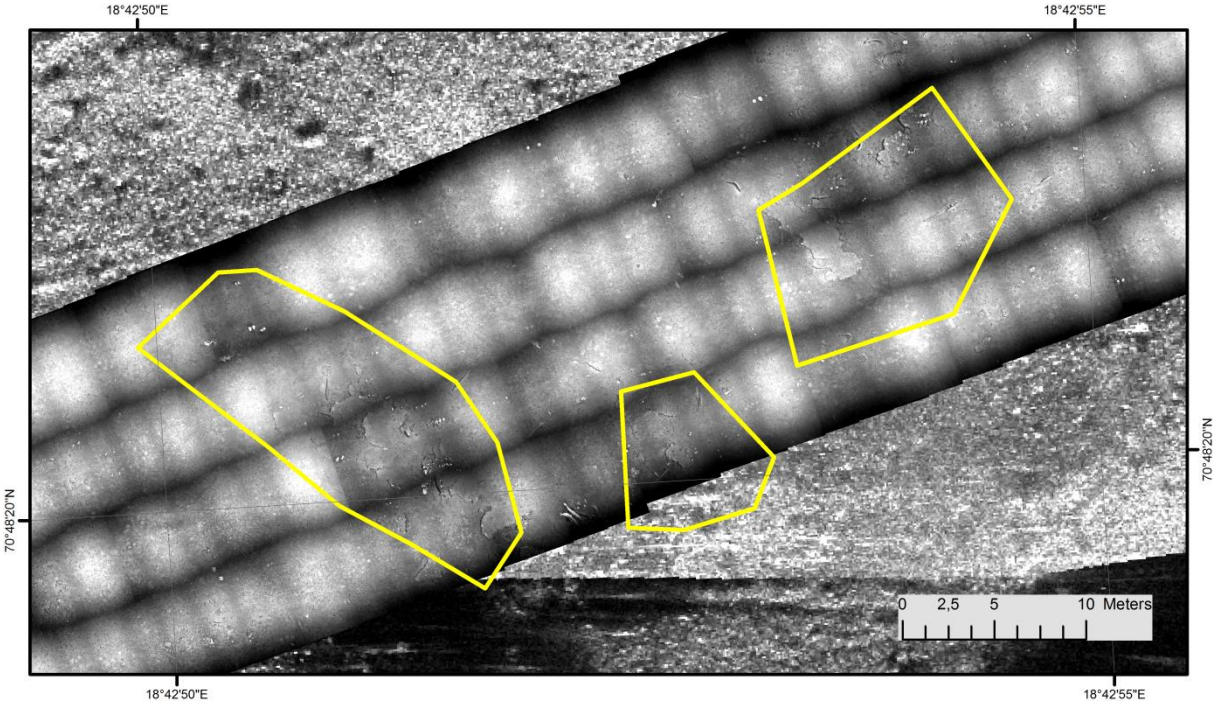

Figure 47. HISAS imagery overlain by TFish photo mosaic from Area B showing carbonate crusts (yellow polygons).

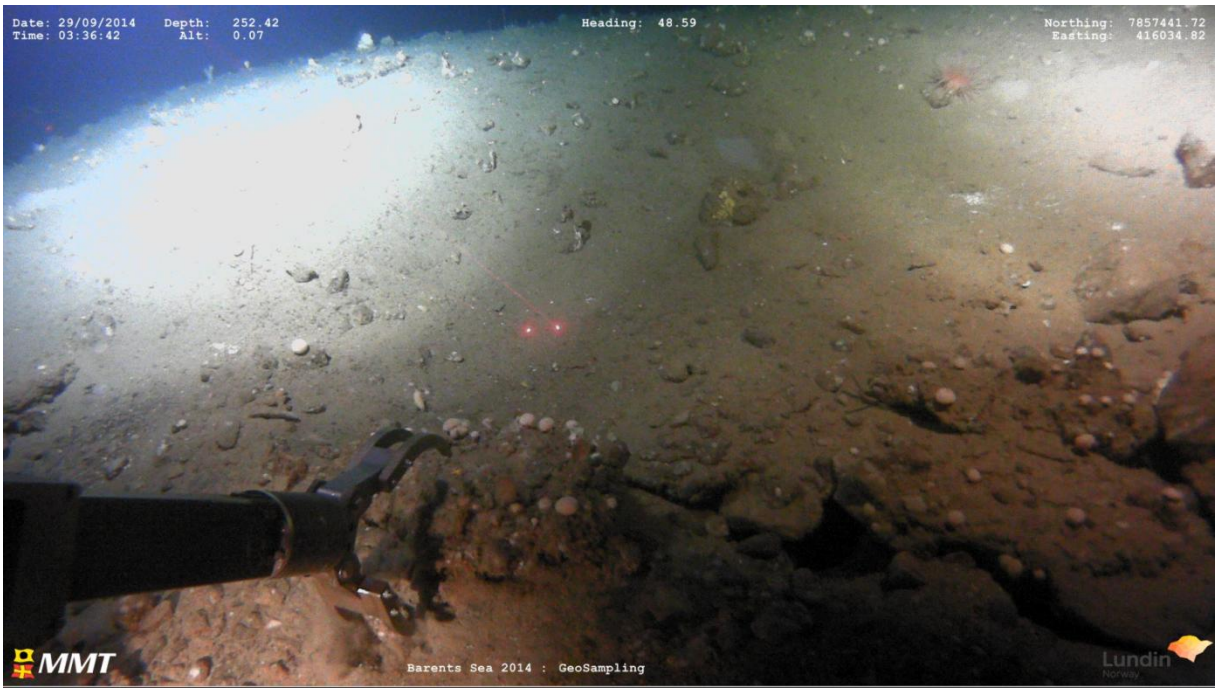

Figure 48. Photo from ROV showing the sampling of carbonate crust from Area B.

Area C consists of carbonate crusts and coral mounds associated with pockmarks (Fig. 49). ROV inspection of Area C revealed that the structures within the pockmarks are carbonate crusts. Nearby is a coral mound that has a dense cover of live corals, interpreted as *Lophelia pertusa*, together with a high number of mussels and sea anemones (Figs. 50 & 51). The corals grow on dark grey blocks of dead corals. Possible occurrences of white bacteria mats can be observed. The base of the mound is characterised by a transition from dark grey fine grained sediment with shells and coral fragments (bioclastic sediments) to dark grey coral blocks. The pockmark c. 50 WSW of the coral mound is c. 4 m deep, and has carbonate crust in its centre, which is c. 3.5 m below the projected seabed (Fig. 52). Carbonate crusts are normally formed at shallow levels below the seabed. A possible explanation for this is initial formation of a palaeo pockmark (see "palaeo seabed in Fig. 52), followed by crust formation, and finally erosion to expose the carbonate crust.

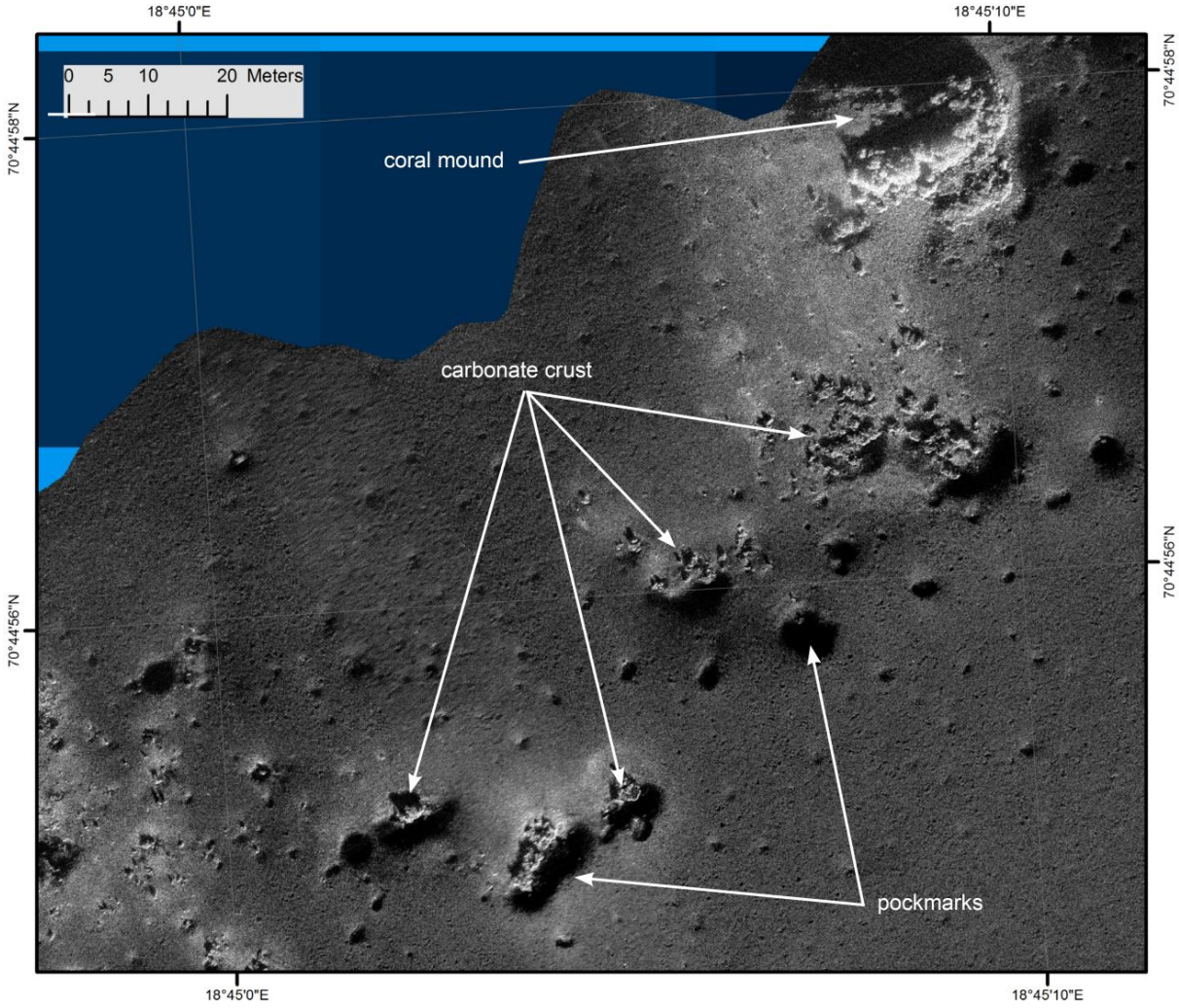

Figure 49. HISAS imagery from southwest of Area C showing coral mound, pockmarks and carbonate crusts.

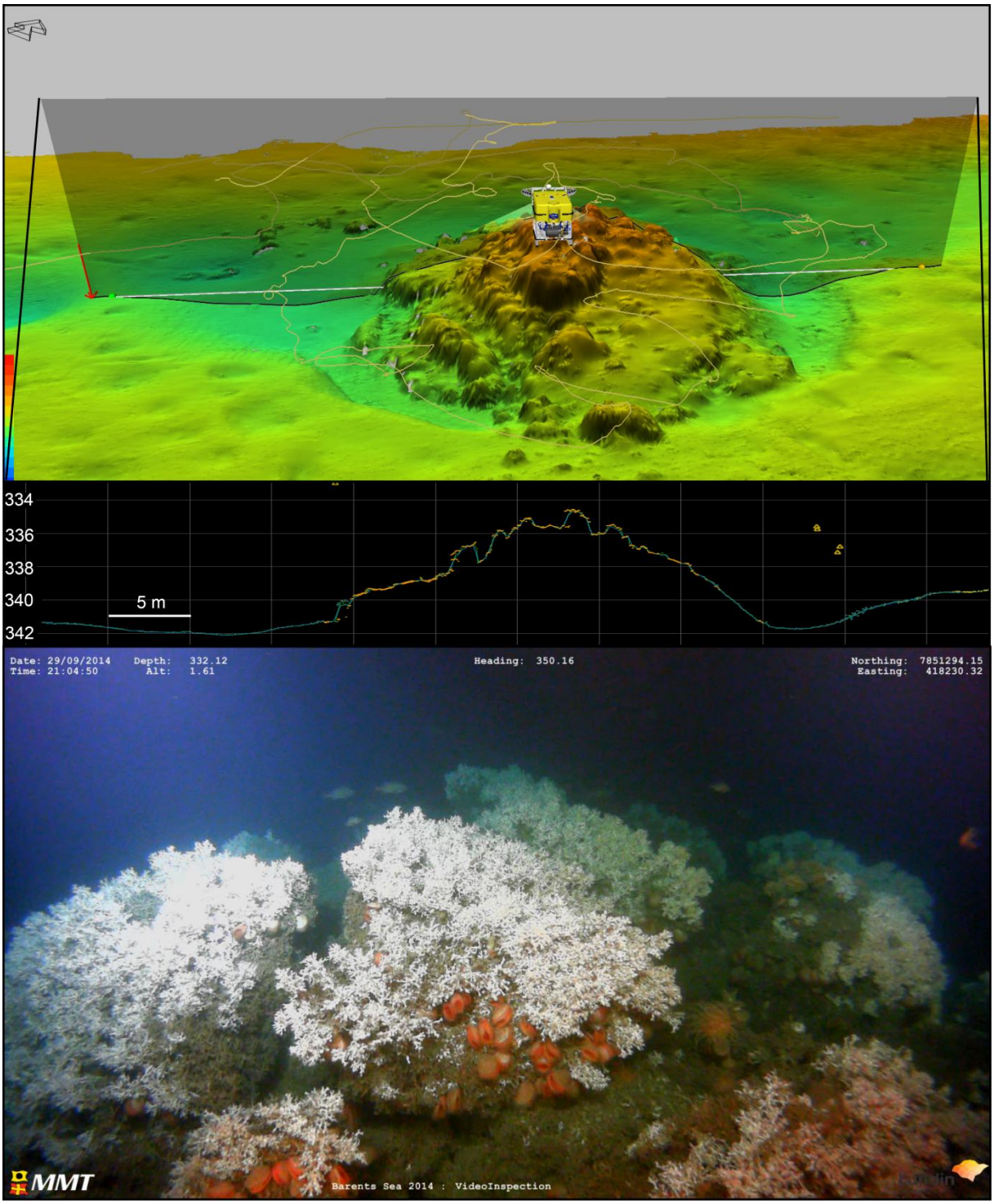

Figure 50. Shaded relief bathymetry map of Area C from ROV data (~ same area as in Fig. 31a) (water depths 334-342 m) (upper panel); Topographic profile (middle panel); Photo from ROV showing live corals and mussels on the top of the mound (lower panel).

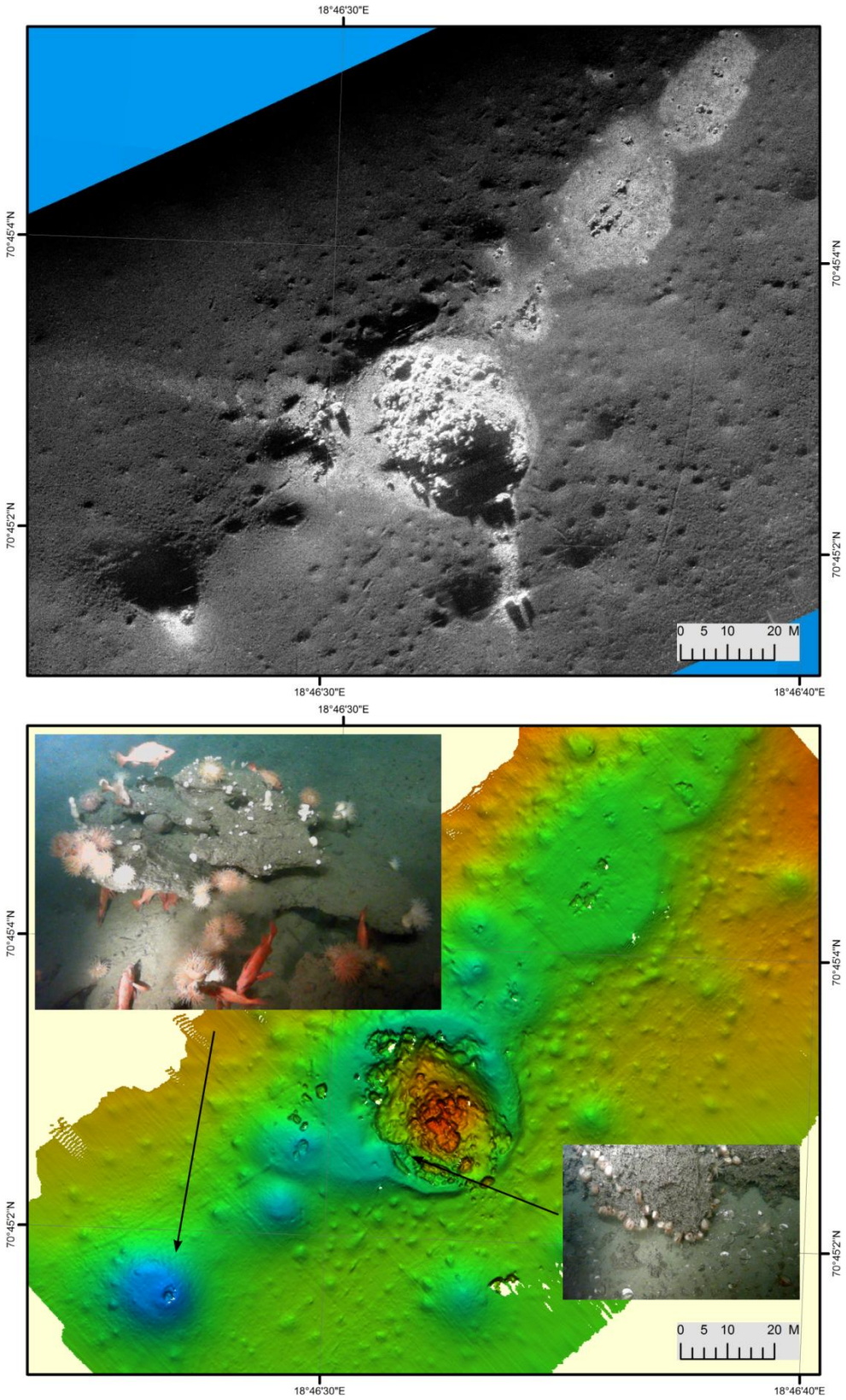

Figure 51. HISAS imagery showing coral mound and Category 2 and 3 pockmarks (top); Bathymetry from ROV data showing coral mound, and Category 2 and 3 pockmarks (bottom). Also shown are the images of carbonate crusts (inset).

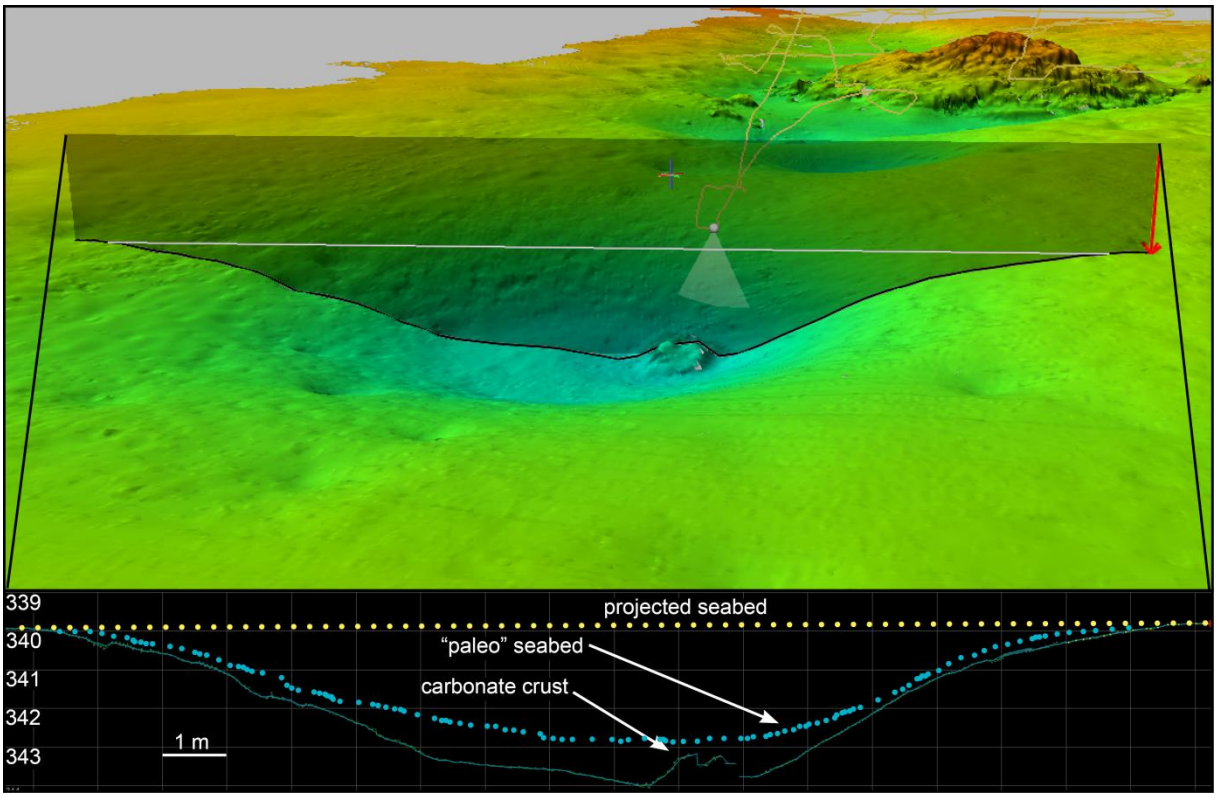

Figure 52. Shaded relief bathymetry from ROV data showing a pockmark with carbonate crust at its centre (top); Topographic profile over the pockmark (bottom).

The bathymetry and video observations from Area J revealed a small field with carbonate crust (Fig. 53) covering an area of 50 m^2. The carbonate crusts are located in a 50 cm deep depression. It was attempted to drill one of the carbonate crusts.

Area M (Figs. 54 & 55) is the most active location where several strong gas flares were identified from multibeam bathymetry water column data. These can be directly linked with carbonate crust fields identified by both HISAS imagery, TFish imagery and ROV video and still photo. Gas bubbling is also evident in TFish imagery and ROV photo/video (Fig. 56). The carbonate crusts are found in shallow depressions with the upper surface of the carbonate crusts at a lower level than the surrounding seabed. If the seabed is interpolated between the flanks of the depression, the top parts of the crusts are 10-20 cm lower than the interpolated seabed (Fig. 57). A good example of this is found in the easternmost part of Area M (Fig. 58). One exception is found in the middle part with a block sticking up, but ROV inspection shows that this is a block of crystalline bedrock lagging on top of the crusts. As carbonate crusts form in shallow sub-surface sediments due to anaerobic oxidation of methane, their occurrence on the seafloor must be a result of erosion subsequent to their formation. The two main crust fields have an area of c. 1500 m^2 (Fig. 59). Area M lies within the Harstad Basin, at the southwestern end of a WSW-ENE trending linear cluster of gas flares extending between Area A and Area N (Fig. 43).

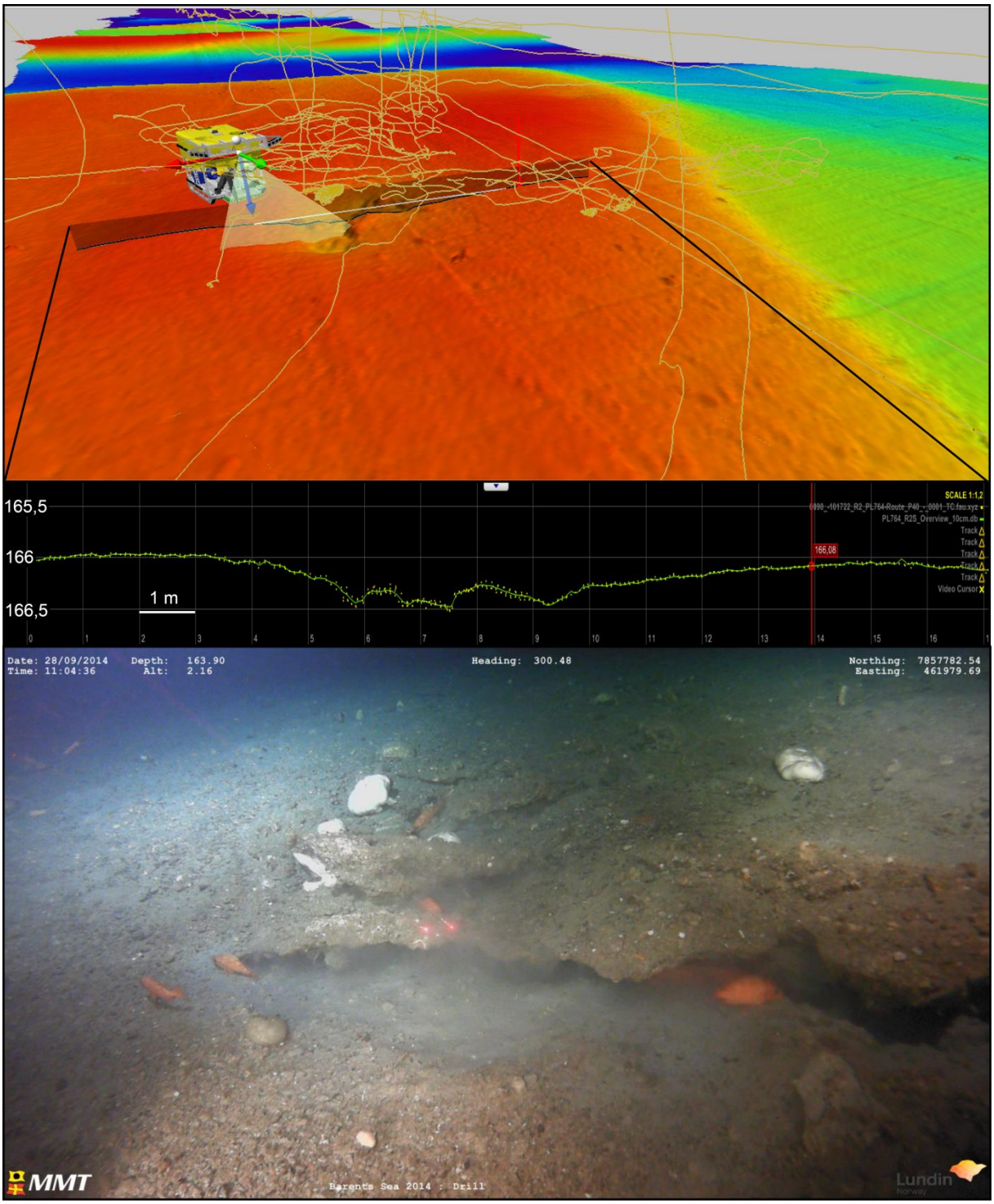

Figure 53. Shaded relief bathymetry of Area J from ROV data showing the carbonate crust field (upper panel); Topographic profile (middle panel); Photo from ROV showing carbonate crust on the seafloor (lower panel).

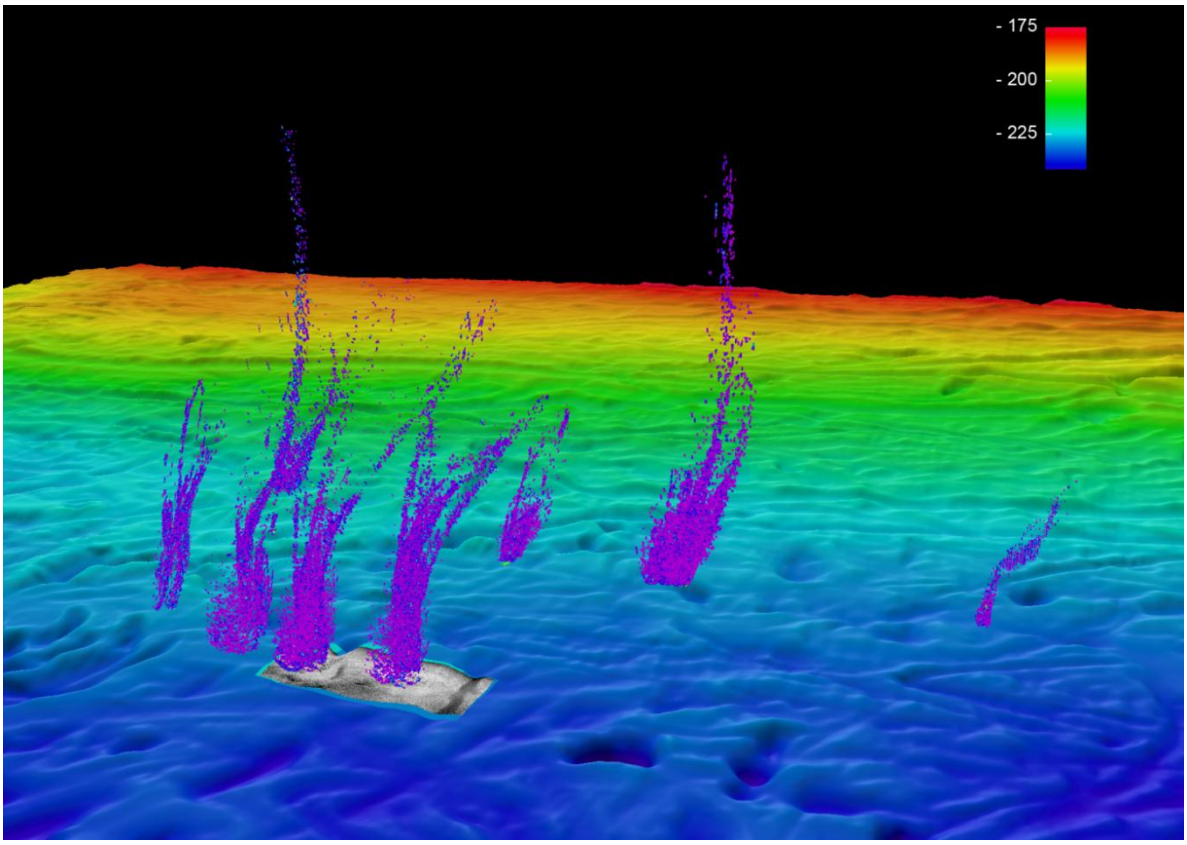

Figure 54. 3D shaded relief bathymetric view of Area M overlain by HISAS data (grey scale image) and gas flares (violet)

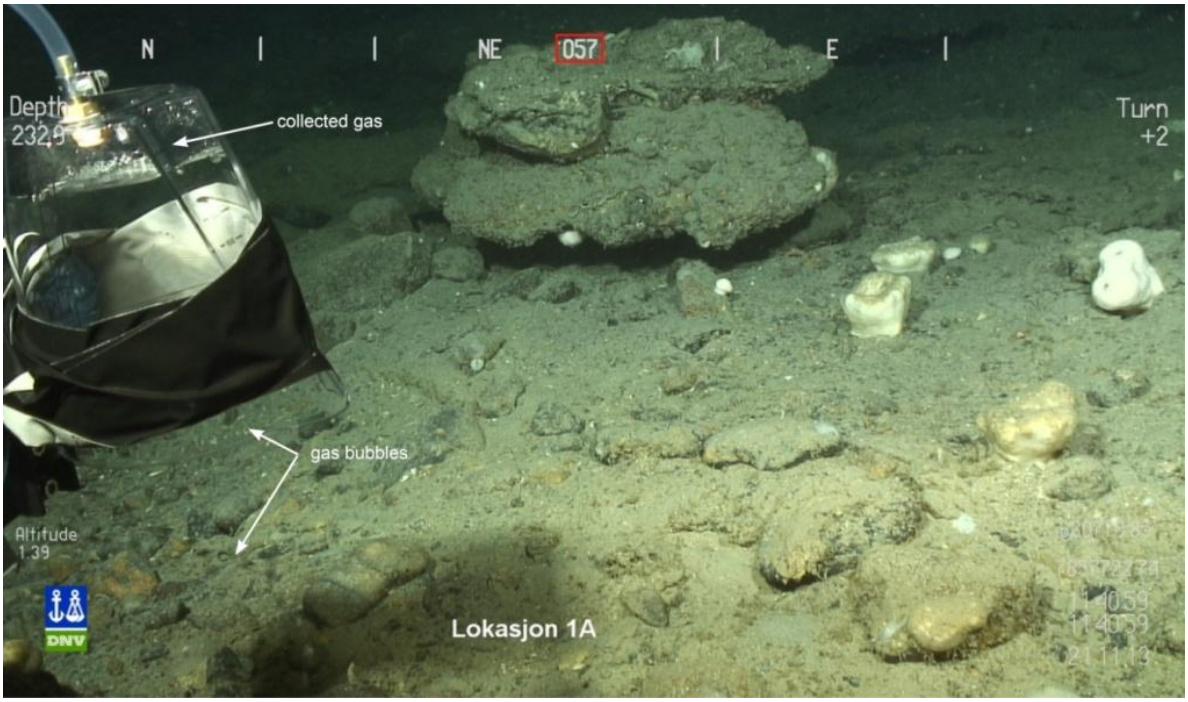

Figure 55. ROV photo of the seafloor with carbonate crusts and bubbling gas from Area M (November 2013 cruise). Notice the gas bubbles flowing upwards into the gas collection chamber. Photo: DNV GL.

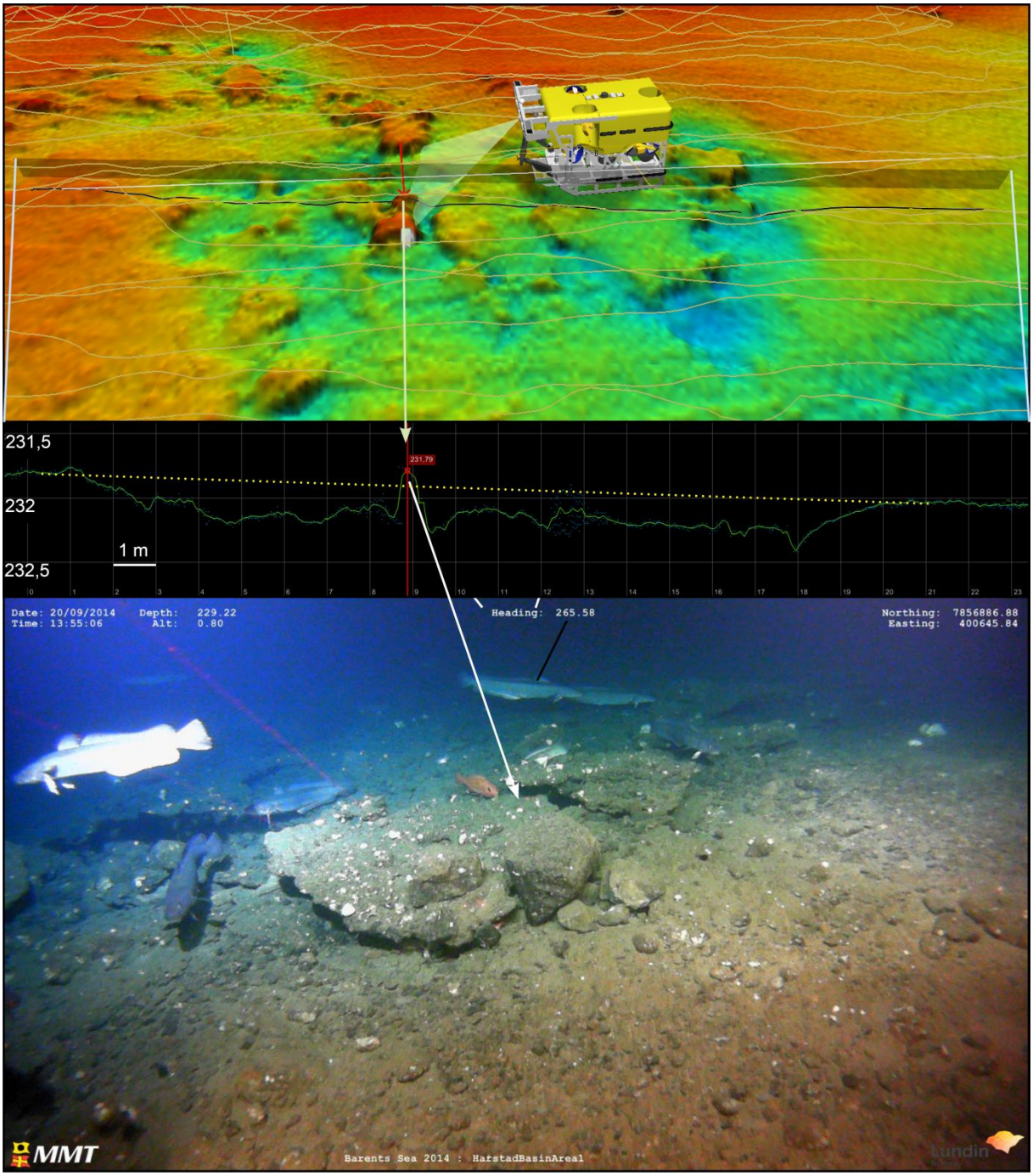

Figure 56. Shaded relief bathymetry from the eastern part of the crust field from Area M (upper panel) showing ROV track lines (light brown),topographic profile(grey),view field of ROV(light grey); Topographic profile (middle panel) showing interpolated seabed surface (yellow dotted line) as it was prior to erosion; Erratic cobble and boulders of glacial origin(till or ice dropped material) occur on top of carbonate crust (lower panel).

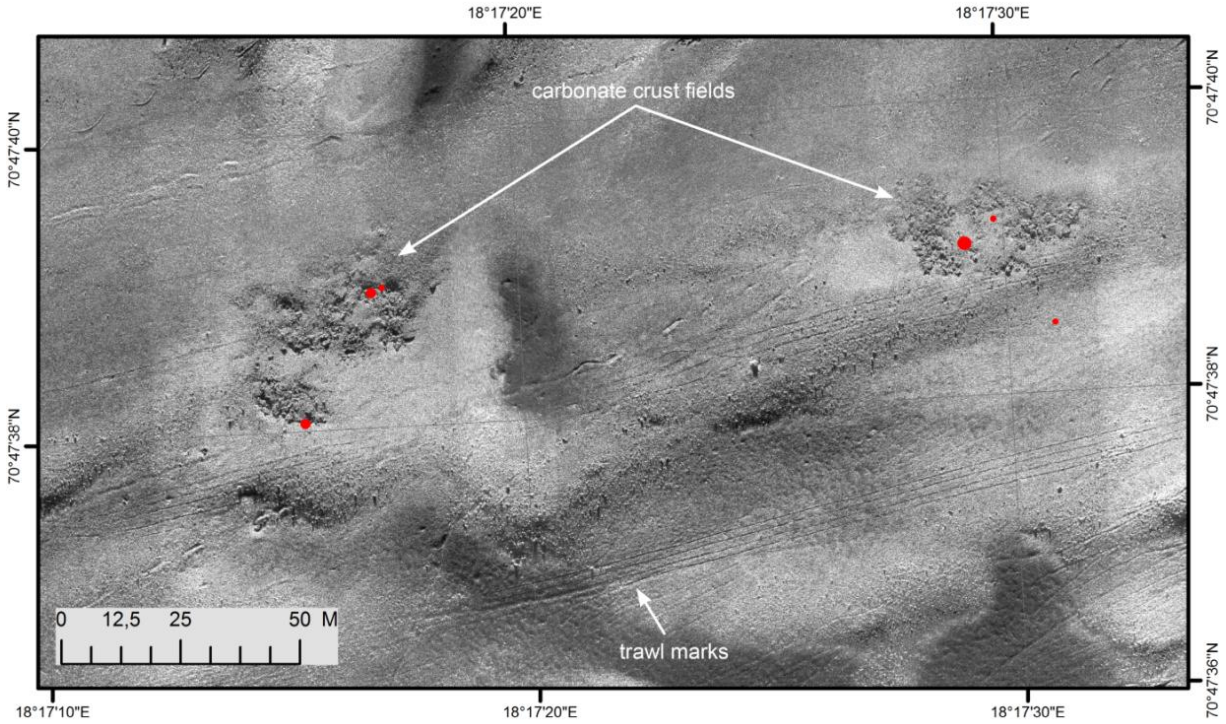

Figure 57. HISAS shaded relief imagery of the two main carbonate crust fields in Area M, locality 1a (left) and 1b (right) given in Fig. 22. Also shown are locations of gas flares (red dots).

The METS methane sniffer was used simultaneously with the recording of HISAS data on three lines in the Harstad Basin (Fig. 58a, b). The methane levels range from close to 0 to 0.43 micromole per litre. The first 500-1000 records have been filtered out, because they showed anomalously high levels (Fig. 59a). Visual inspection of XY plots of the three lines indicates a background level below 0.03. Weak, but distinct anomalies were found in both Mets_run_20131114 (Fig. 59b) and Mets_run_20131119 (Fig. 59c). The strongest anomalies were found in Area M (Fig. 59d and e). This is in good agreement with the observation of gas bubbles both from the water column data, the TFish system onboard HUGIN HUS, and direct observations from the ROV. The weak anomalies in Area C, N and O are similarly linked to gas flares observed on water column data. In addition, there are weak anomalies SW of Area C which do not correspond to water column data gas flares. In Area A, there is no anomaly despite the high number of flares observed in this area. This may indicate that the gas expulsion system has a highly episodic nature, or it may indicate that it is not methane, but other gases such as carbon dioxide which are leaking. The same argument can be applied for Area B, but note that only one gas flare has been observed in that area.

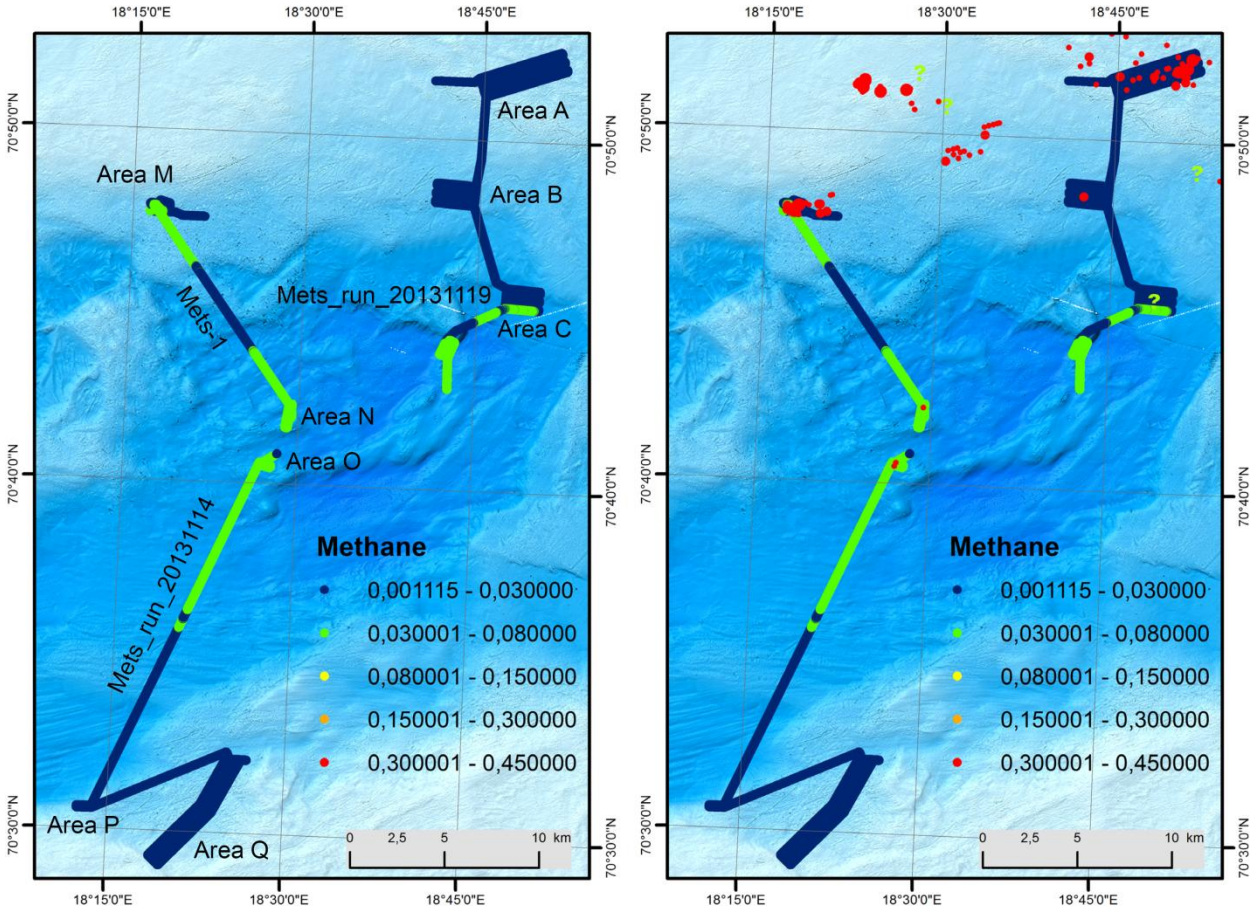

Figure 58. a) Overview of the three lines where gas sniffer data were collected. Lines are colour coded according to relative methane levels in micromole per litre. High levels in Area M are overprinted by low level recordings (green) at this map level because f the sequence of point plotting in ArcMap. Also see Fig. 59e. b) Methane levels and gas flares (red dots).

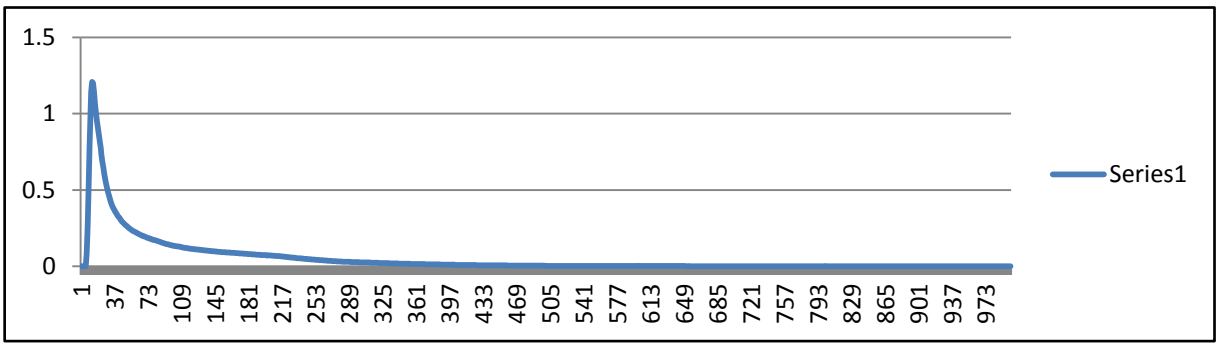

Figure 59a. XY plot of methane levels versus the first 1000 records for Mets_run_20131114.Unit concentrations are given in micromole per litre.

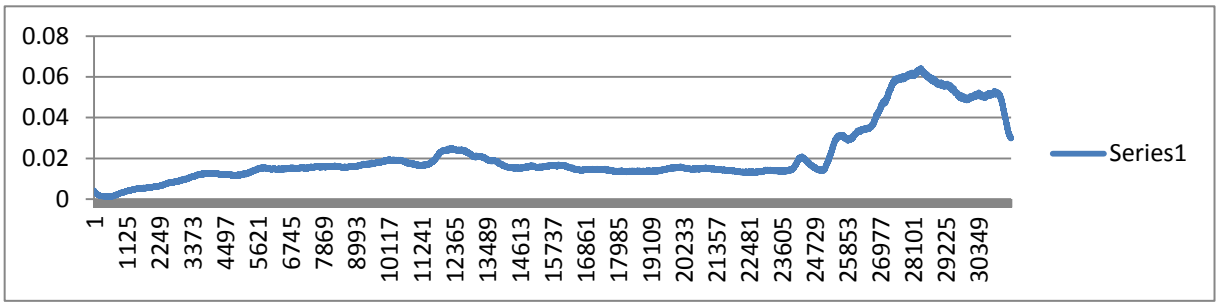

Figure 59b. XY plot of methane levels versus record number for Mets_run_20131114. The first 1000 records have been filtered out. Unit concentrations are given in micromole per litre.

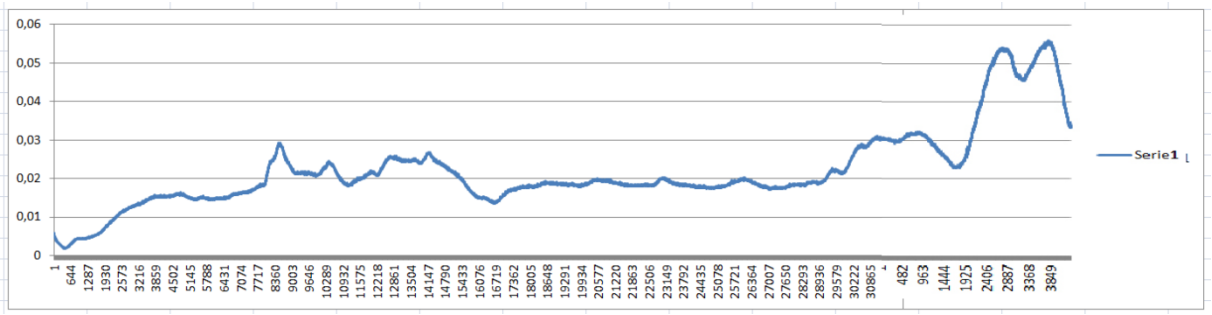

Figure 59c. XY plot of methane levels versus record number for Mets_run_20131119. The first 500 records have been filtered out. Unit concentrations are given in micromole per litre.

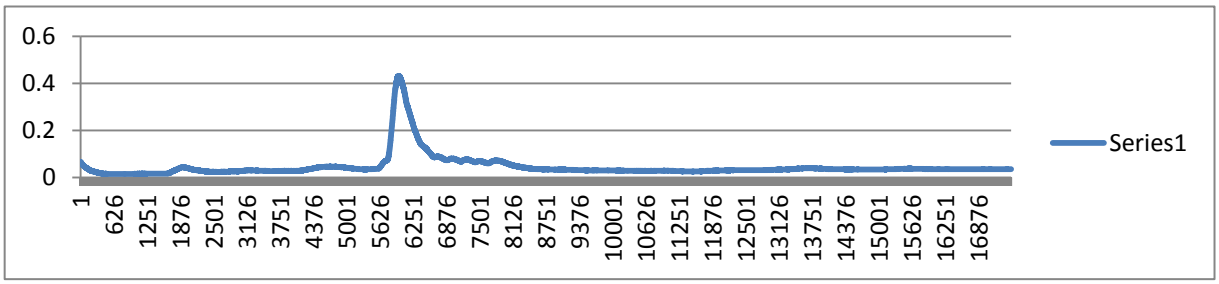

Figure 59d. XY plot of methane levels versus record number for Mets-1. The first 1000 records have been filtered out. Note different scale compared to d) and e). The peak is related to the gas flares in Area M. Unit concentrations are given in micromole pr. litre.

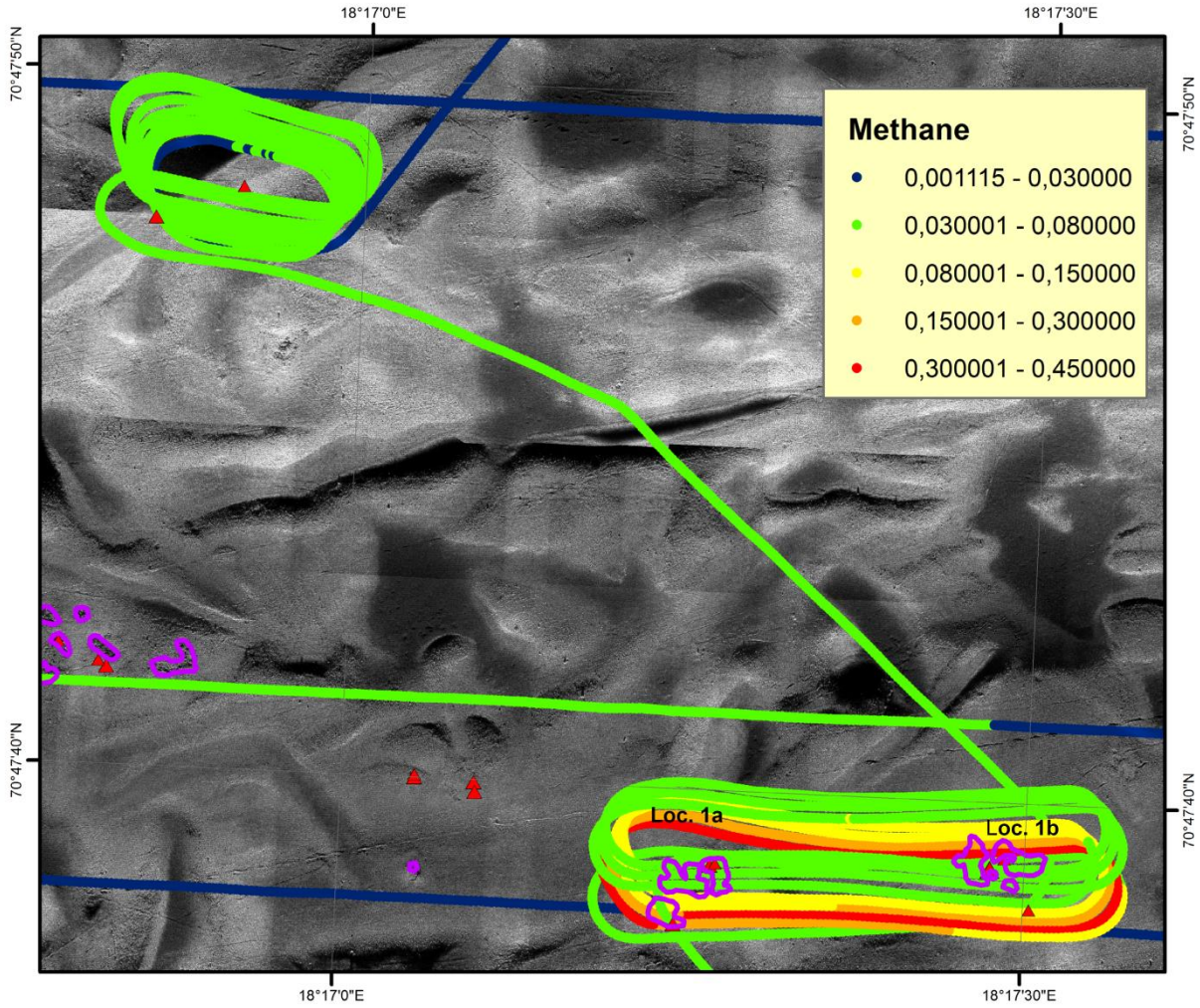

Figure 59e. Map showing methane levels as recorded by Hugin in Area M. Note gas flares (red triangles) and carbonate crust outlines (violet polygons). HISAS imagery in the background.

4.3.5 Sources of gas for acoustic flares in Harstad Basin

The source of the methane leaking in the Harstad Basin is similar to that at the Loppa High (Chand et al., 2012b). The study area in the Harstad Basin where the flares are observed is located where the dipping subsurface stratigraphic layers come close to the seafloor (Figs. 60, 61, 62 & 63). Also, the Troms Finnmark Faults Complex crosses the study area (Fig. 4a). Both these factors probably influence the fluid flow in the study area.

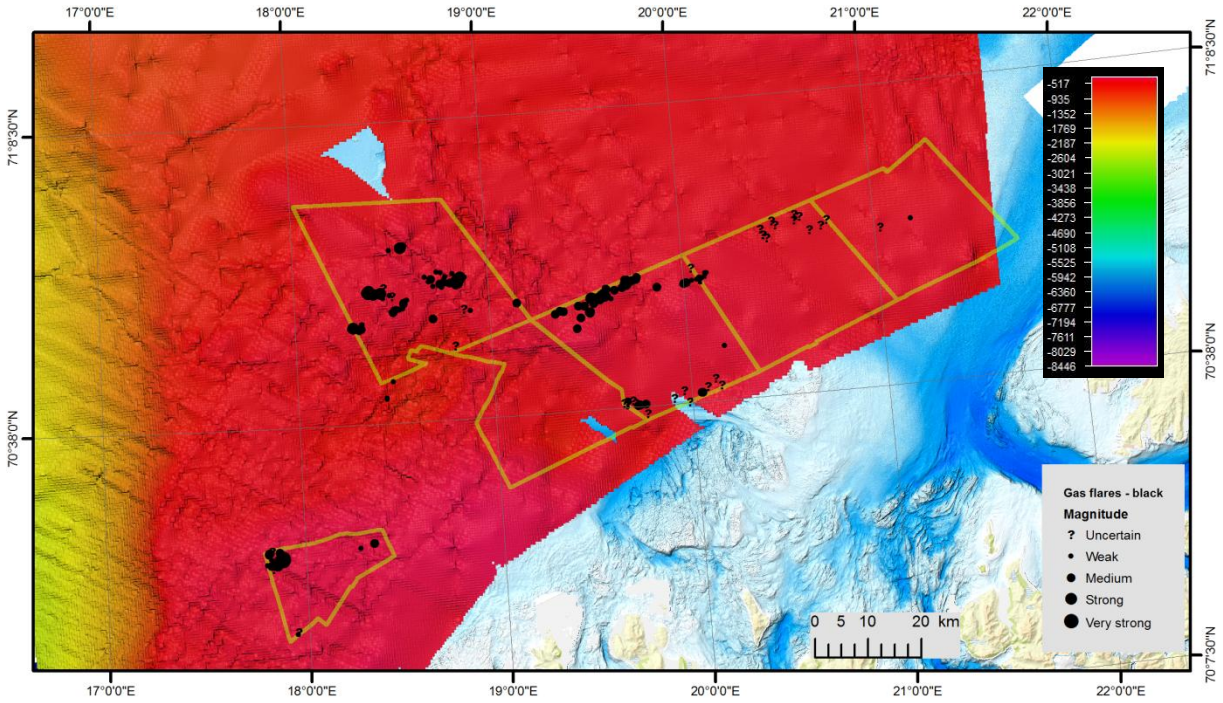

Figure 60. Two way travel time map of the URU showing gas flares (black dots). MAREANO bathymetry with water colum data (yellow polygons) overlaid on shaded relief bathymetry (background).

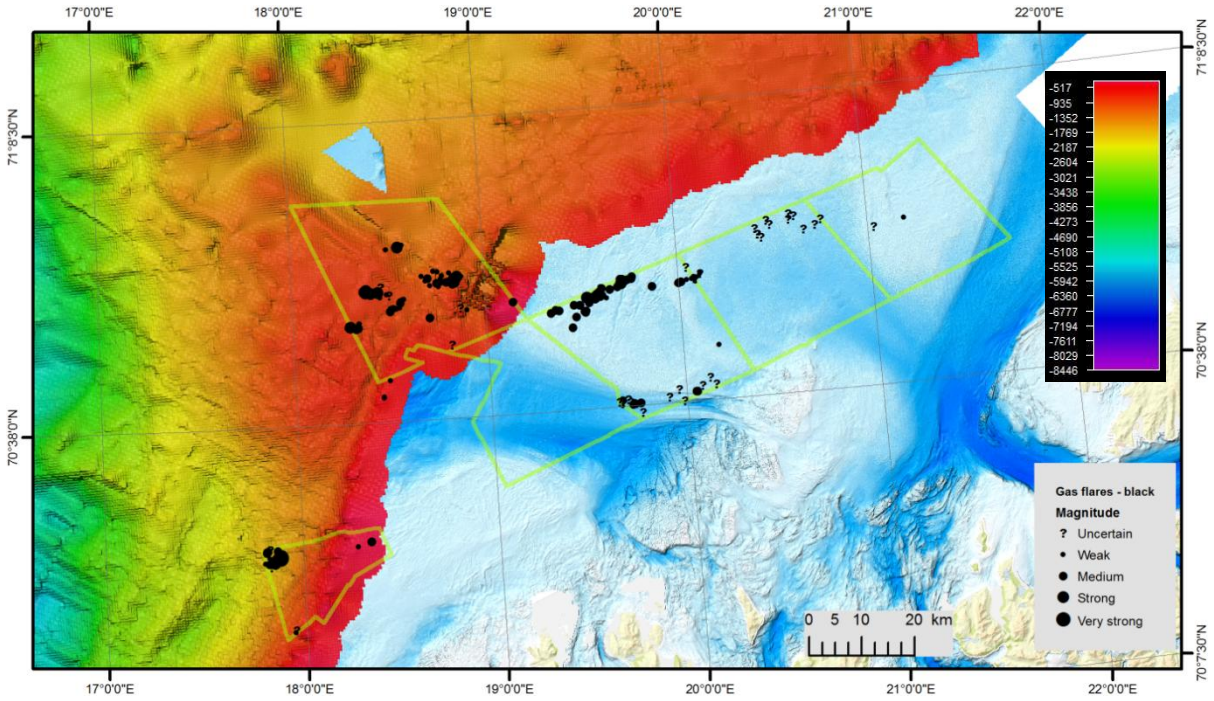

Figure 61. Two way travel time map of base Tertiary showing gas flares (black dots). MAREANO bathymetry with water colum data (yellow polygons) overlaid on shaded relief bathymetry (background).

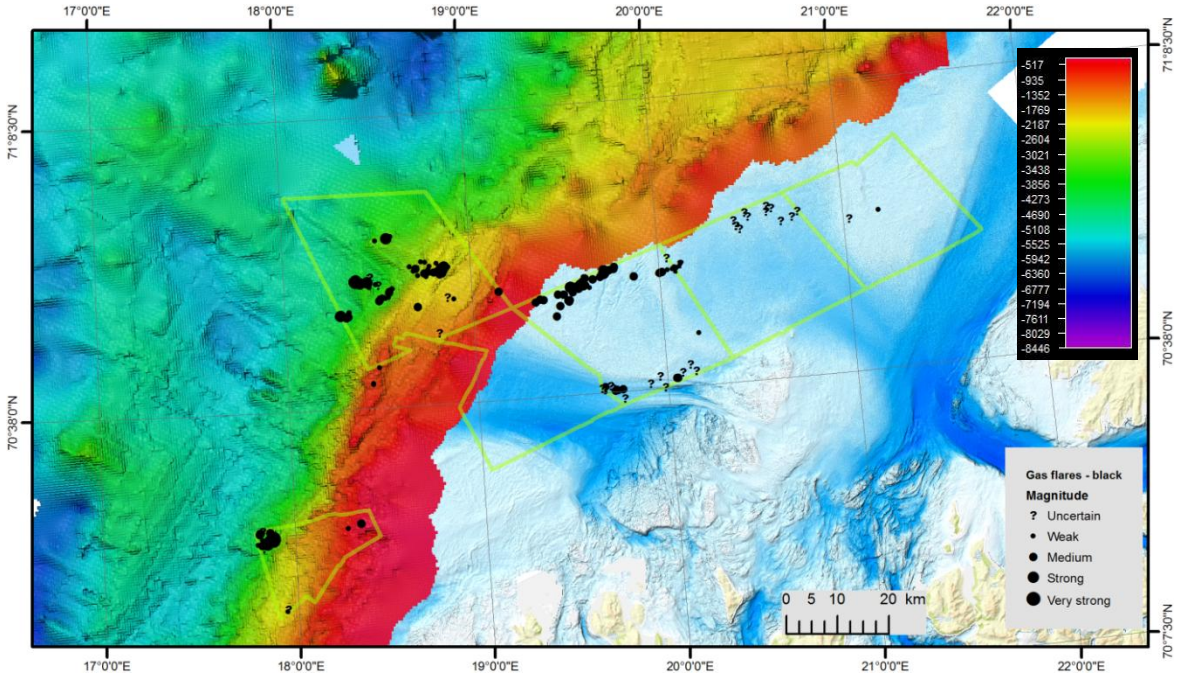

Figure 62. Two way travel time map of base Cretaceous showing gas flares (black dots). MAREANO bathymetry with water colum data (yellow polygons) overlaid on shaded relief bathymetry (background).

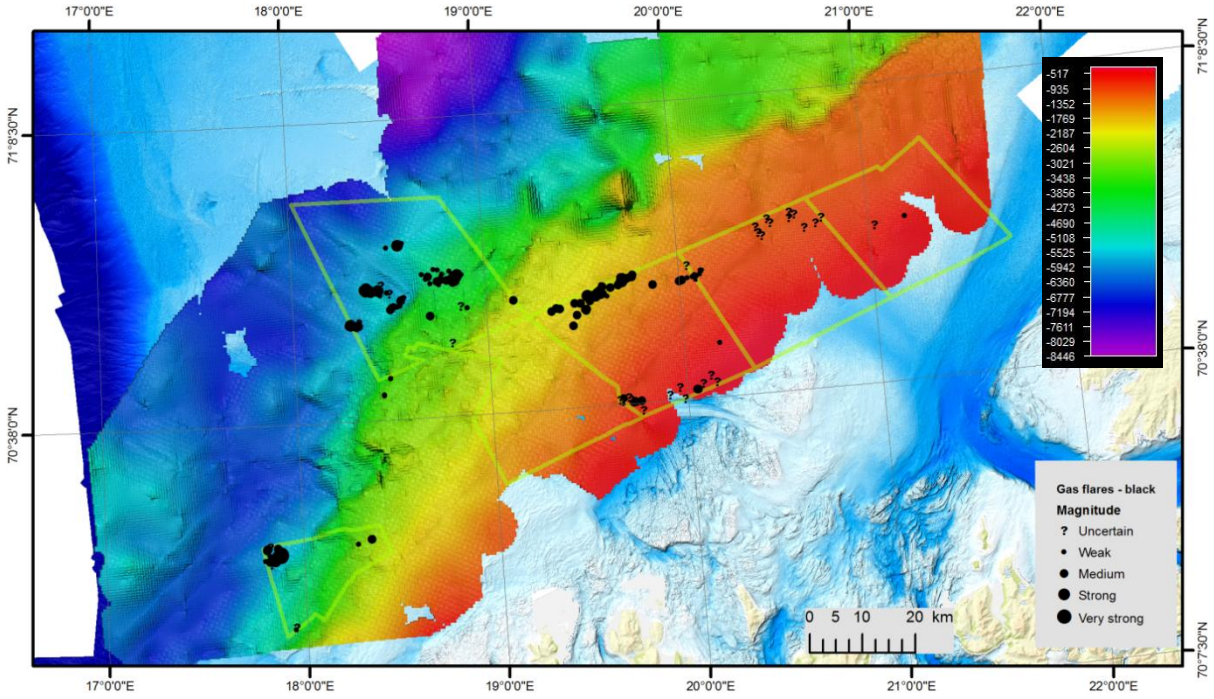

Figure 63. Two way travel time map of top Permian showing gas flares (black dots). MAREANO bathymetry with water colum data (yellow polygons) overlaid on shaded relief bathymetry (background).

The high resolution fluid flow study of the Harstad Basin was carried out using a 3D seismic cube. The 3D cube does not cover the entire study area but the data is useful for identifying the major factors affecting the fluid flow at three of the four carbonate crust areas (Fig. 44a). Three major horizons were interpreted along with the seafloor; the upper regional unconformity (URU) (Fig. 64a & b), the base Tertiary (Fig. 65a & b) and the base Cretaceous (Figs. 66a & b). The URU shows a depression shallowing in all directions within the southern part of the 3D cube area (Figs. 64a & b). The URU also shallows from the north towards the centre of the 3D cube, and the shallowest part of the URU coincides with the locations of flares and carbonate crust localities (Figs. 64a & b). The structure map of the URU indicates that the fluid flow probably was channelized towards the shallow part of the URU, where leakage occurred. Even though the depression of the URU coincides with the depression on the seafloor, the fluid flow is not directly linked to the smaller thickness of glacial sediments (Fig. 67) but rather dependent on the stratigraphic boundary of the layers abutting the seafloor.

The 3D structural map of the base Tertiary (Figs. 65a & b) doesn't give link between the gas anomalies observed and the morphology at this level. Two of the carbonate crust locations and some flare locations coincide where the base Tertiary abuts the URU (Figs. 65a & b). The morphology of the base Cretaceous (Figs. 66a & b) gives a totally different picture. The base Cretaceous shallows from the west and north towards the study area probably focusing the fluids (Figs. 66a & b). The major fluid focusing probably happens along this surface or stratigraphic layers parallel to this surface as shown by the regional stratigraphic boundaries (Figs. 60, 61, 62 & 63). One of the carbonate crust areas (C1) is located directly above a fault (Fig. 66a). The carbonate crust location (C1) above the fault probably gives a different geochemical signature than other sites since the fluids are directly linked to the deep subsurface instead of taking the longer route through stratigraphic units and boundaries.

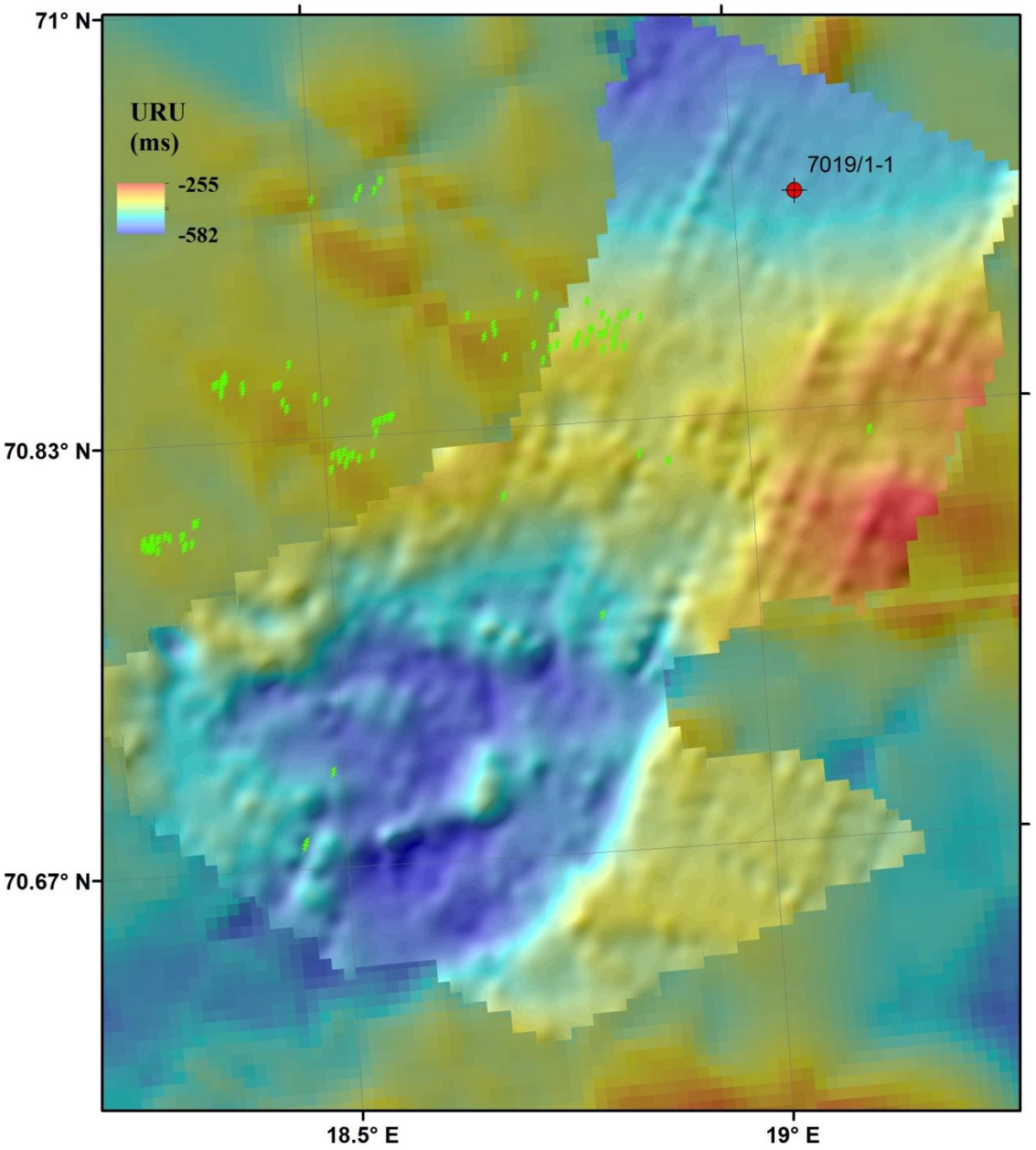

Figure 64a. Shaded relief topography of the URU. The green symbols indicate locations of gas flares. The low resolution background image of the URU is based on 2D seismic data (Fig. 60).

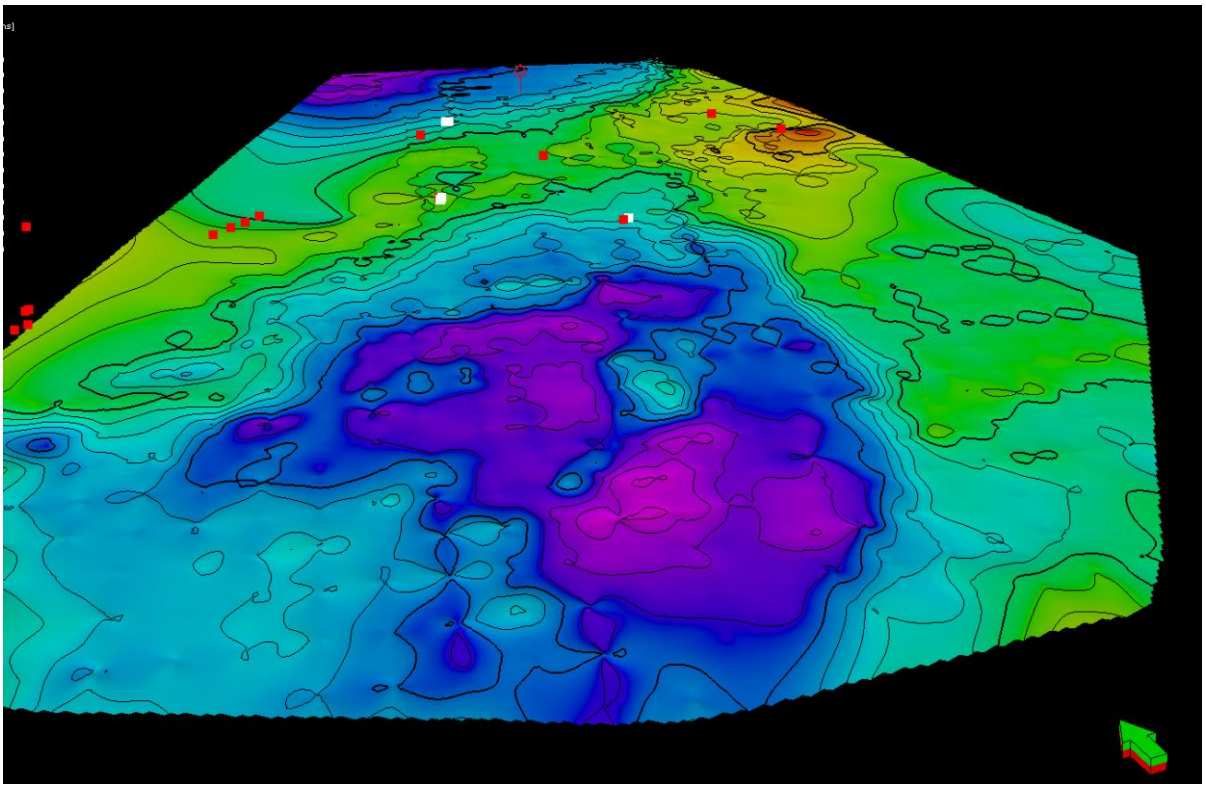

Figure 64b. 3D shaded relief map of the URU interpreted using 3D seismic data. The white and red squares indicate the locations of carbonate crusts and flares, respectively.

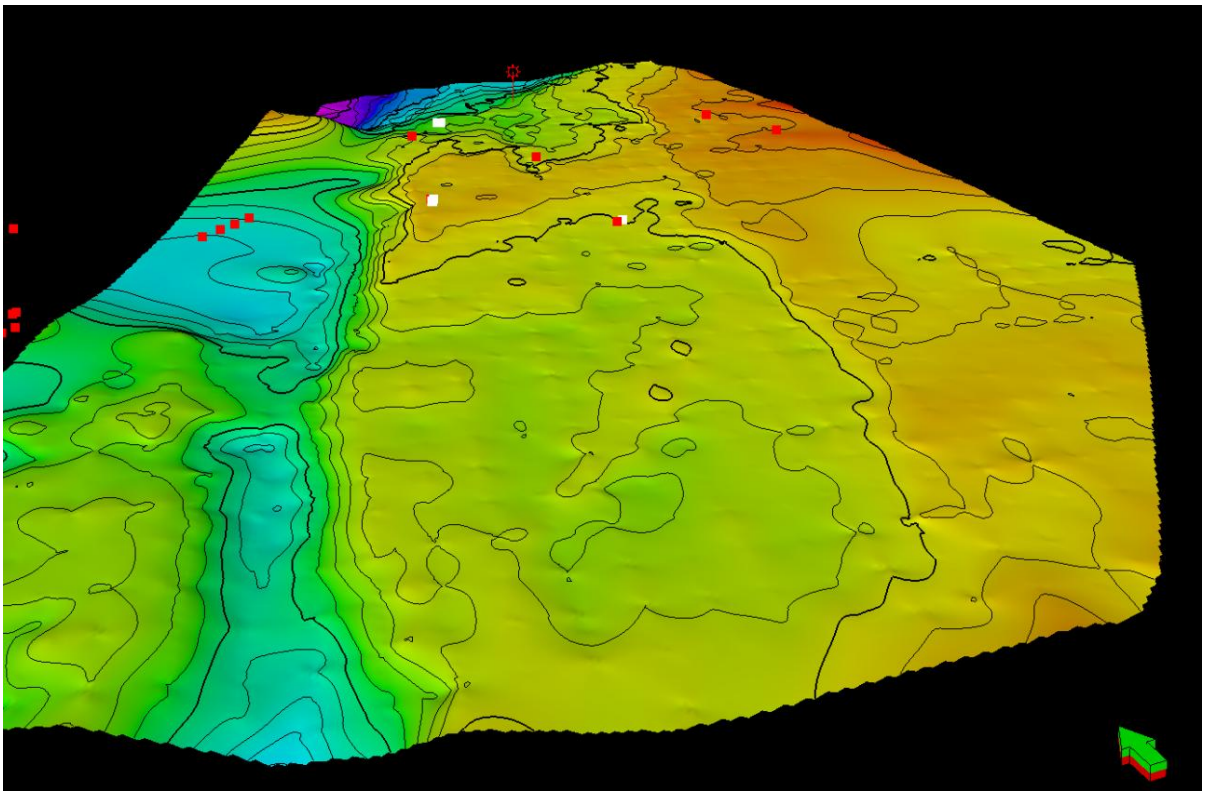

Figure 65a. 3D shaded relief map of the base Tertiary interpreted using 3D seismic data. The white and red squares indicate the locations of carbonate crusts and flares, respectively.

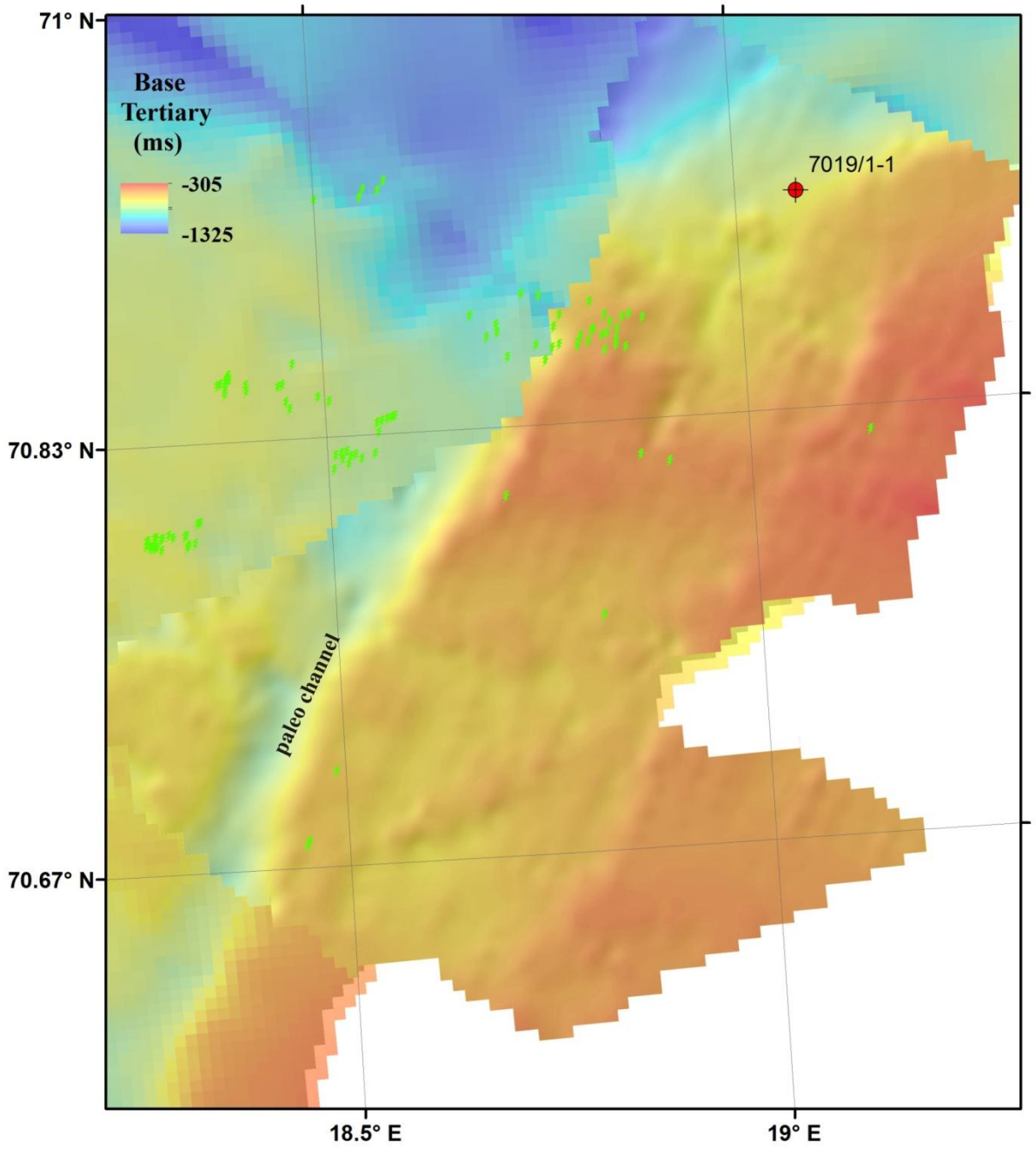

Figure 65b. Shaded relief topography of the base Tertiary. Notice the paleo-channel west of the Håkjerringdjupet. The green symbols indicate the locations of flares. The low resolution background image of the base Tertiary is based on 2D seismic data (Fig. 61).

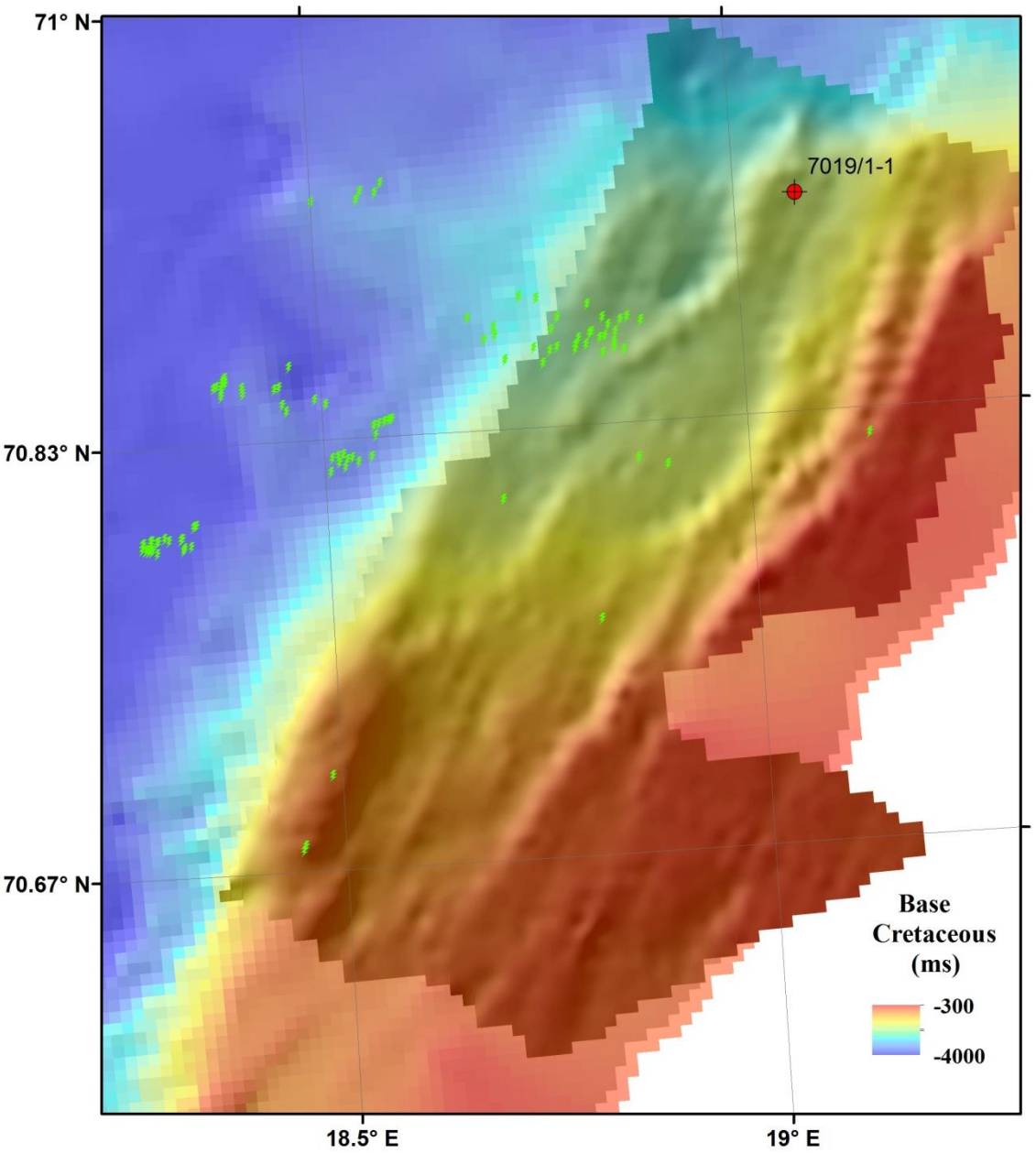

Figure 66a. Shaded relief topography of the base Cretaceous surface. The green symbols indicate the locations of flares. The low resolution background image of base Cretaceous is based on 2D seismic data (Fig. 62).

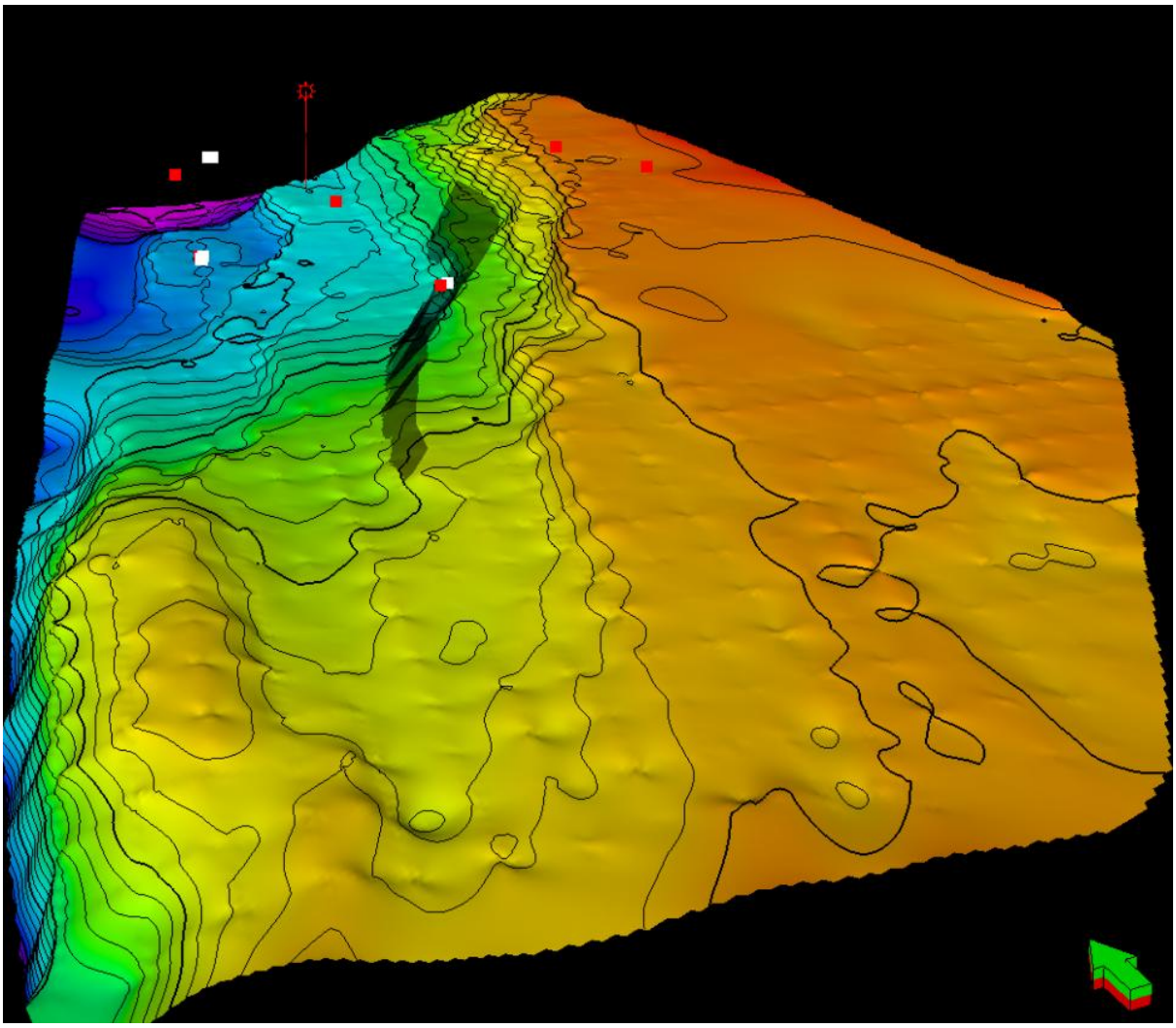

Figure 66b. 3D shaded relief map of the Base Cretaceous interpreted using 3D seismic data. The white and red squares indicate the locations of carbonate crusts and flares, respectively.

The focusing of fluid flow along stratigraphic boundaries is evident in seismic sections also (Figs. 69, 70, 71, 72, 73, 74, 75 & 76). The E-W seismic section across carbonate crust locality C1 indicates fluid leakage along the fault (Figs. 69, 70 & 75). The fault could be acting as a bypass conduit for fluids flowing along pre Tertiary formations dipping from the Tromsø basin as well (Fig. 70). The carbonate crust location in Area C is clearly linked to the pinching out of Tertiary formations at the base Tertiary boundary below the pre glacial deposits (URU) (Figs. 71, 72 & 76).

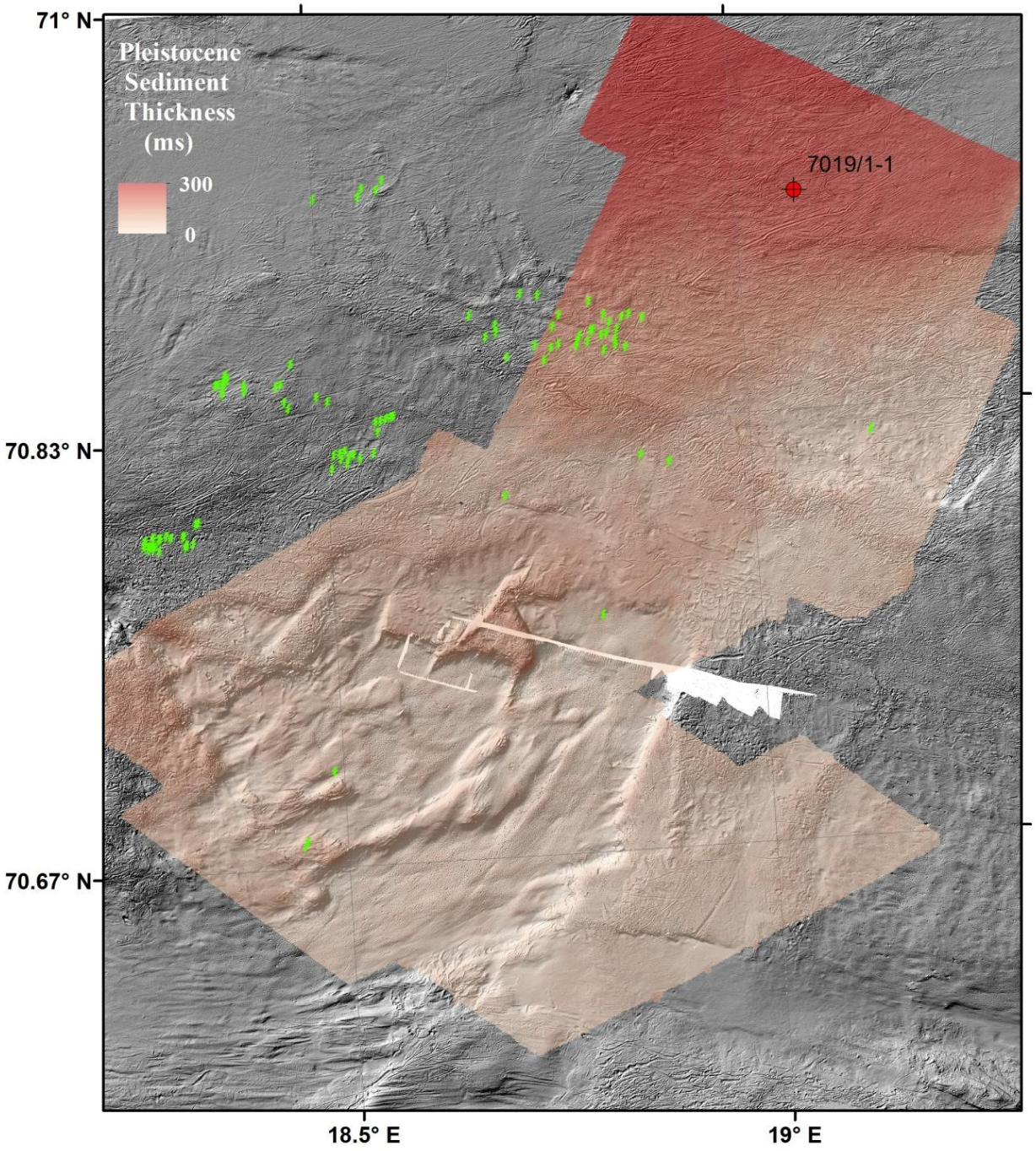

Figure 67. Thickness of Plio-Pleistocene deposits (ms TWT) on shaded relief bathymetry. The green symbols indicate the locations of flares. The location of well 7019/1-1 is also shown.

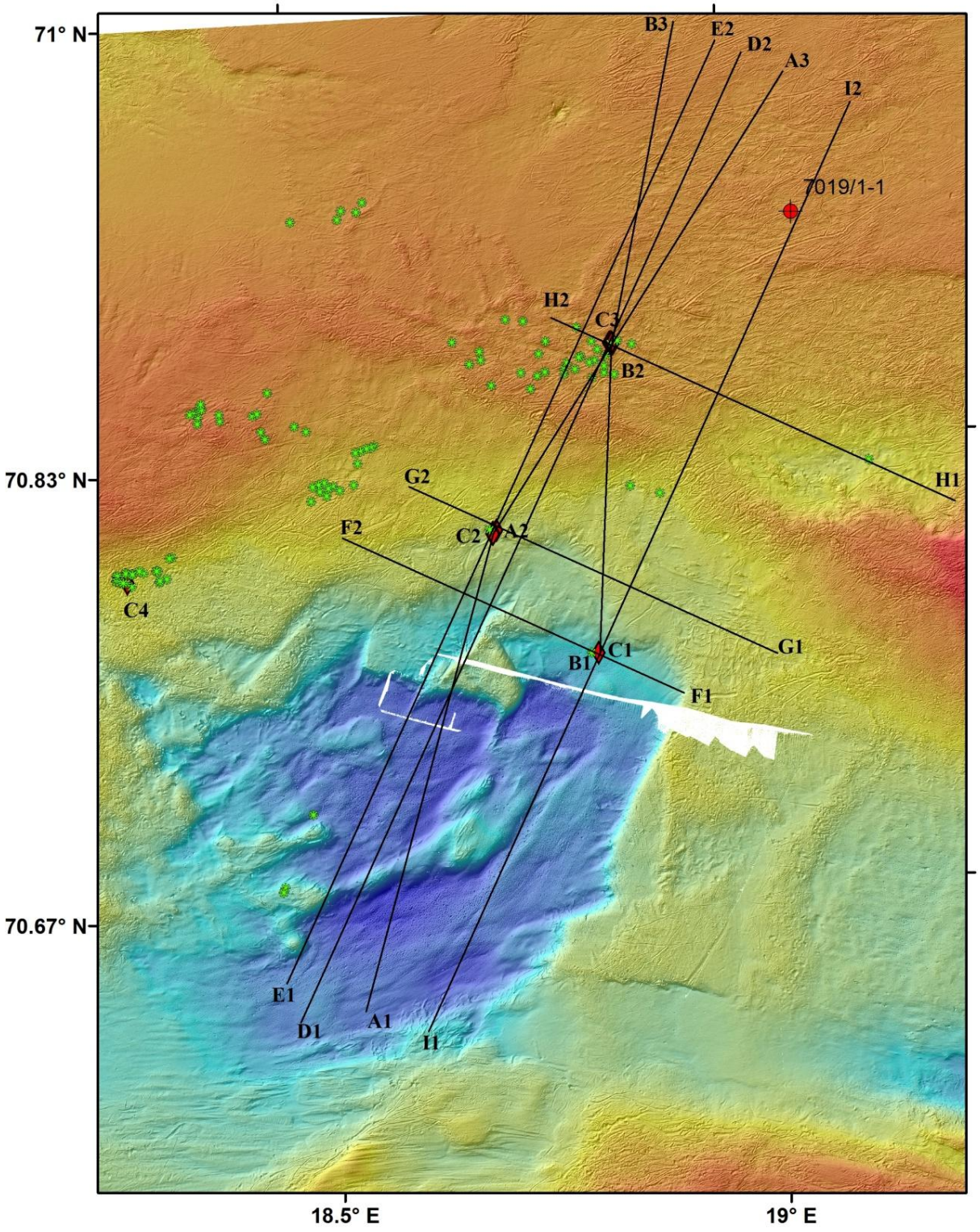

Figure 68. Shaded relief bathymetry (MAREANO) of the study area showing the locations of flares (green flowers) and carbonate crusts (red rhombohedra). Also shown are the locations of seismic sections given in Figures 69, 70, 71, 72, 73, 74, 75, 76 and well 7019/1-1. Crust samples are from these areas: C1 - Area C; C2 - Area B; C3 - Area A; C4- Area M.

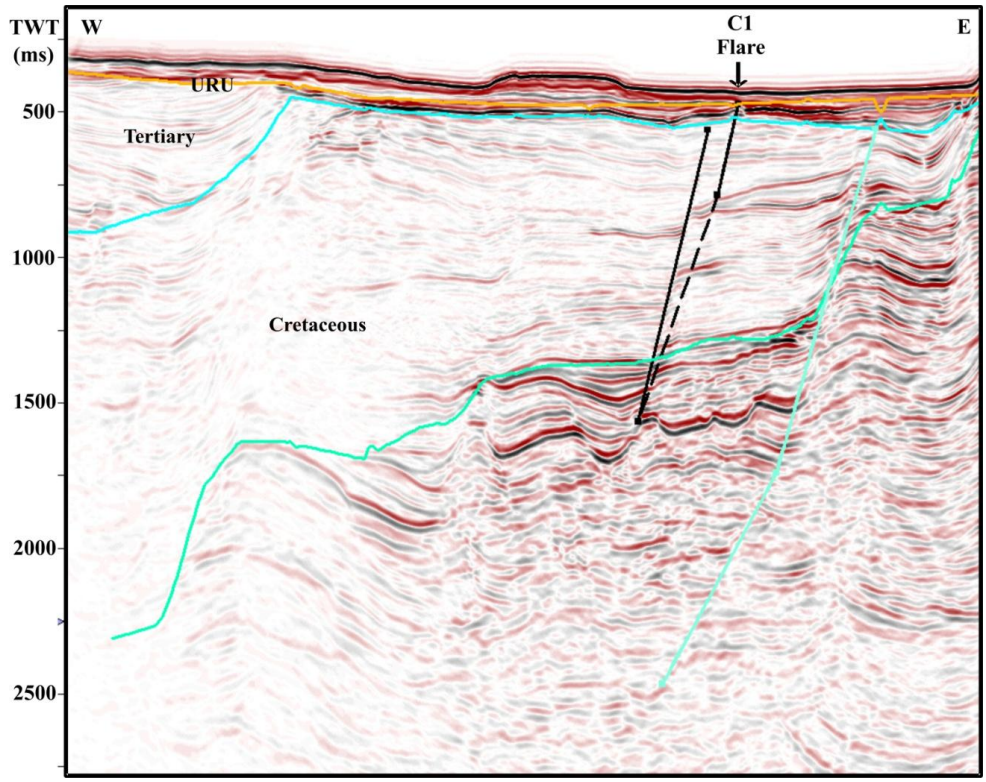

Figure 69. E-W seismic section (F1-F2; Fig. 68) across the carbonate crust location C1 in Area C showing the link between gas leakage at the seafloor and a subsurface fault (Fig. 66b).

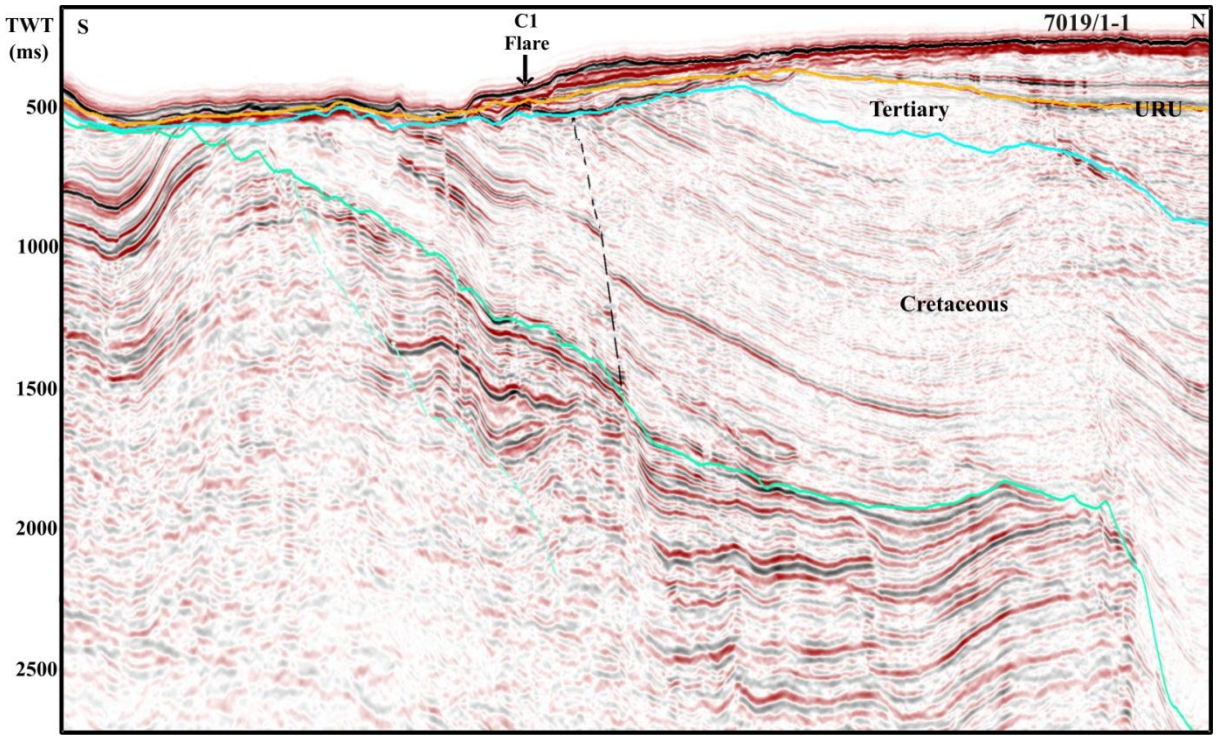

Figure 70. N-S seismic section (I1-I2; Fig. 68) across the carbonate crust location C1 in Area C showing the possible link between carbonate crust at the seabed and a subsurface fault (Fig. 66b).

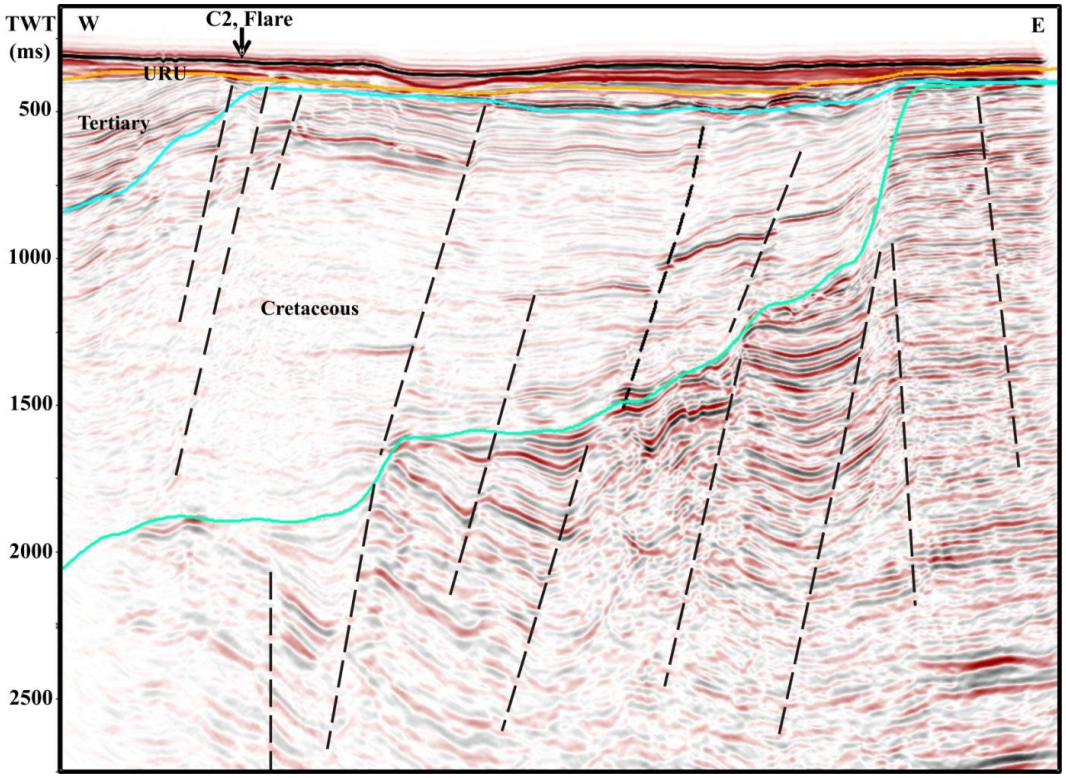

Figure 71. W-E seismic section (G1-G2; Fig. 68) across the carbonate crust location area C2 in Area B showing that the fluid flow could be focusing from the west along stratigraphic layers.

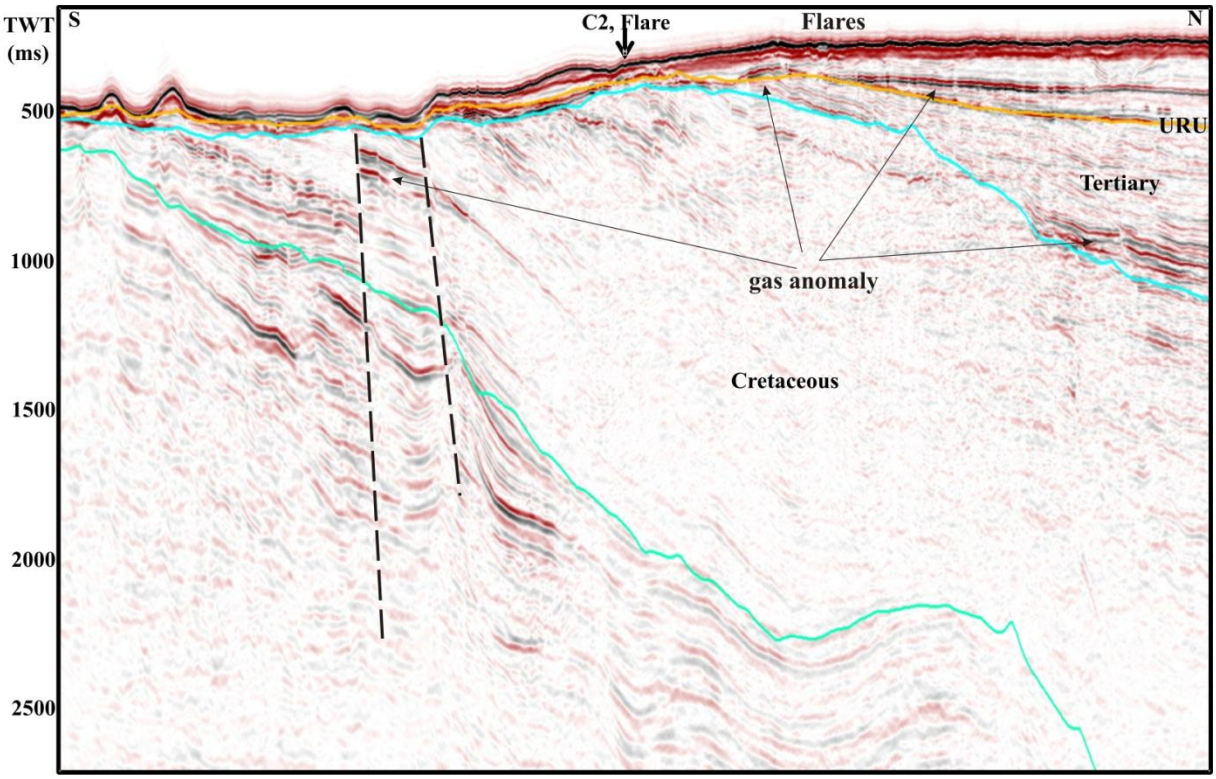

Figure 72. N-S seismic section (E1-E2, Fig. 68) across carbonate crust location C2 in Area B showing that the fluids could be focusing from the Tromsø Basin in the north along stratigraphic layers.

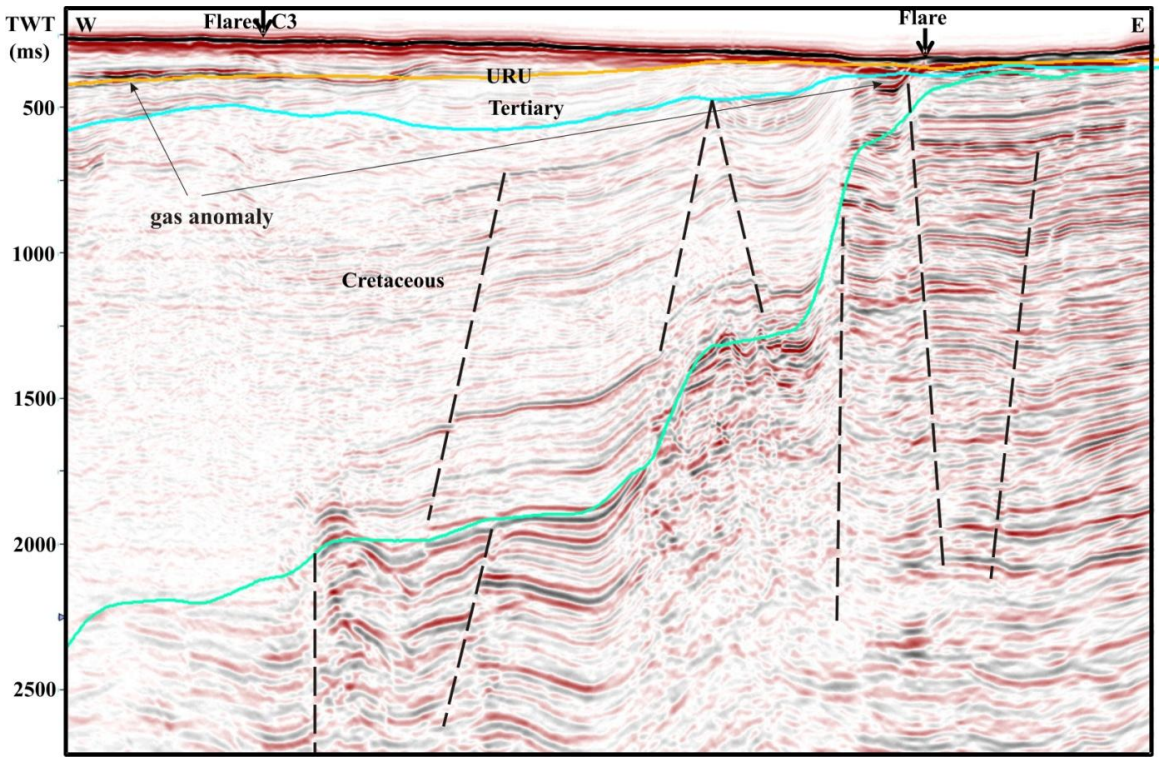

Figure 73. E-W seismic section (H1-H2; Fig. 68) across carbonate crust location C3 in Area A showing that the fluids could be focusing from the Tromsø Basin in the north along stratigraphic layers.

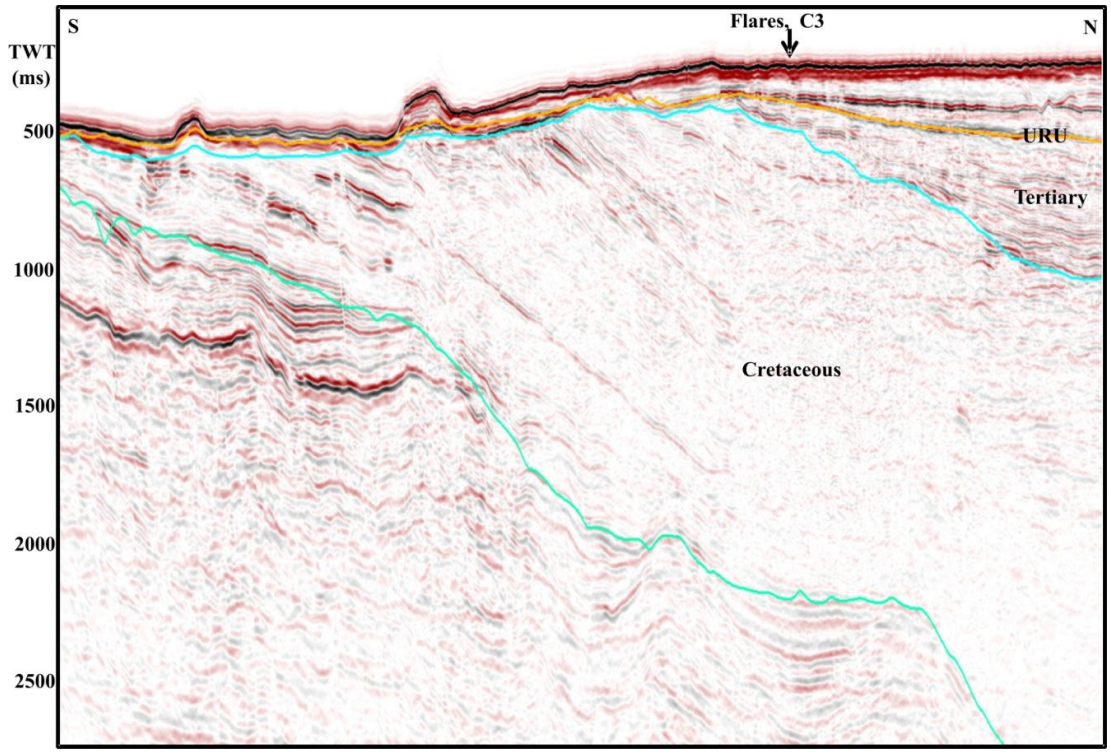

Figure 74. N-S seismic section (D1-D2; Fig. 68) across carbonate crust location C3 in Area A showing that the fluids could be focusing from the Tromsø Basin in the north along stratigraphic layers.

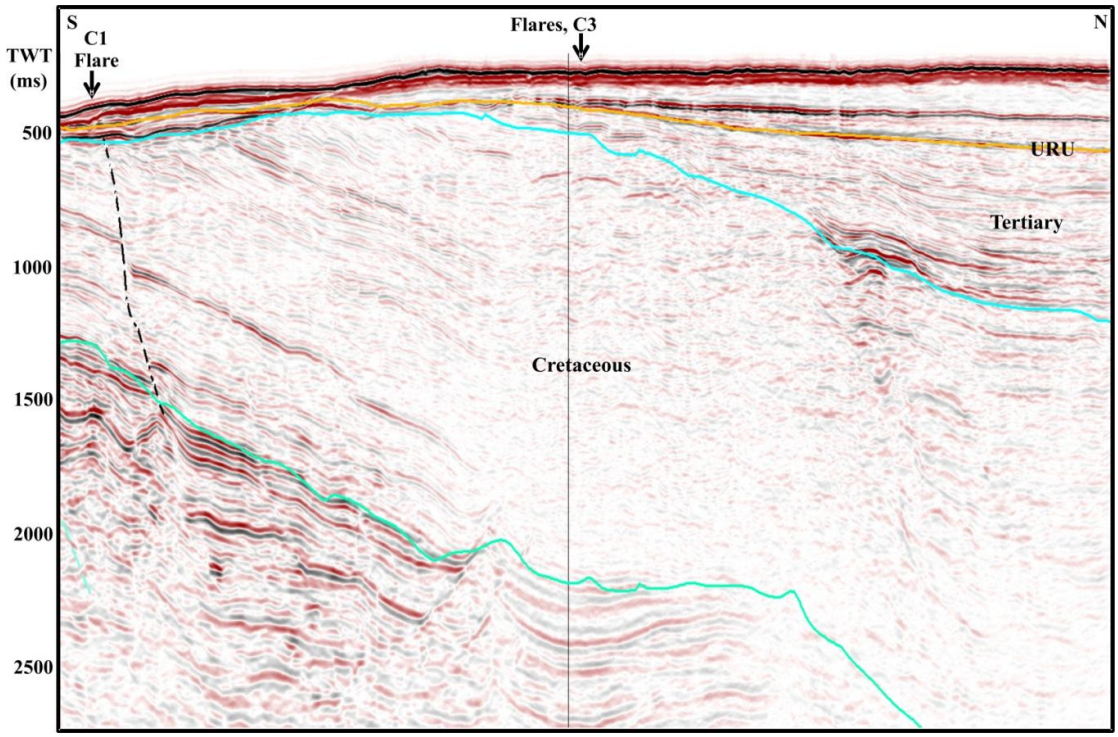

Figure 75. N-S seismic section (B1-B2-B3; Fig. 68) across carbonate crust location C1in Area C and crust location C3 in Area A showing that the fluids could be focusing from the Tromsø Basin in the north along stratigraphic layers for C3/Area A while the fluids at C1/Area C come directly from deep below through the fault.

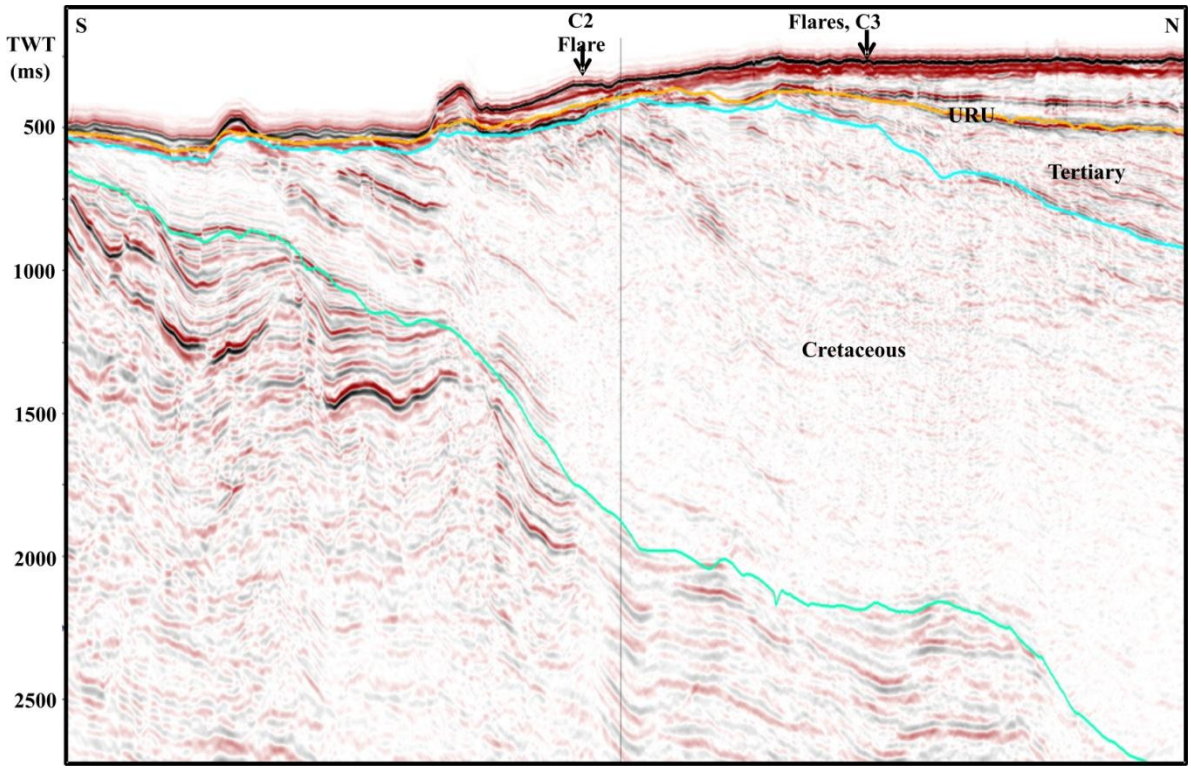

Figure 76. N-S seismic section (A1-A2-A3; Fig. 68) across carbonate crust location C2 in Area B and crust location C3 in Area A showing that the fluids could be focusing from the Tromsø Basin in the north along stratigraphic layers.

4.4 Glacio/Neotectonic structures

4.4.1 Alvheim

The new MBB data from the Alvheim study area do not show neotectonic structures. Two highs (Fig. 77) appear to be glacial dumping sites but they could be mud diapirs as well. They are also indicated by high backscatter.

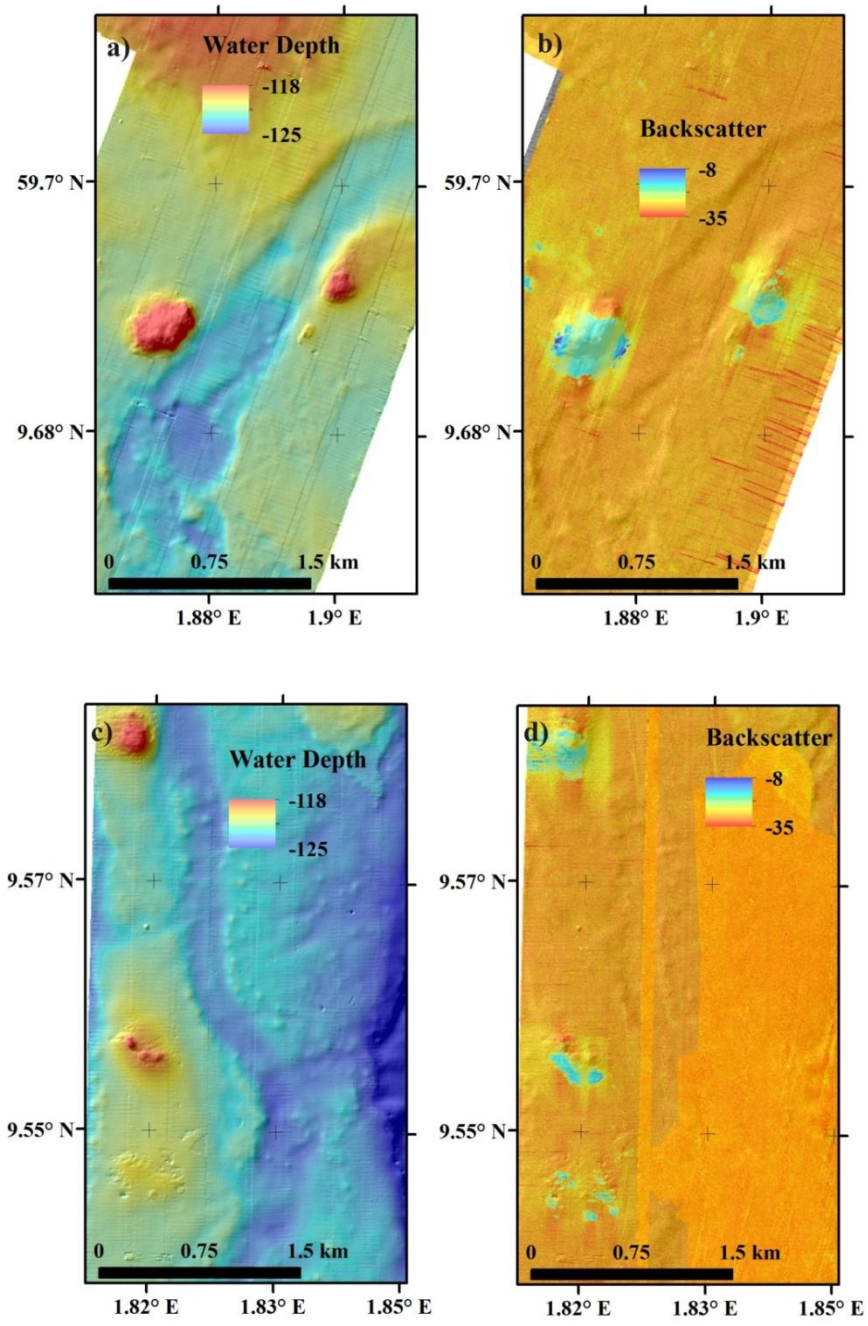

Figure 77. Topographic highs in the Alvheim study area. The highs, which may represent mud diapirs, have high backscatter values.

4.4.2 Utsira High

No neo tectonic features were observed in the Utsira High study area.

4.4.3 Harstad Basin

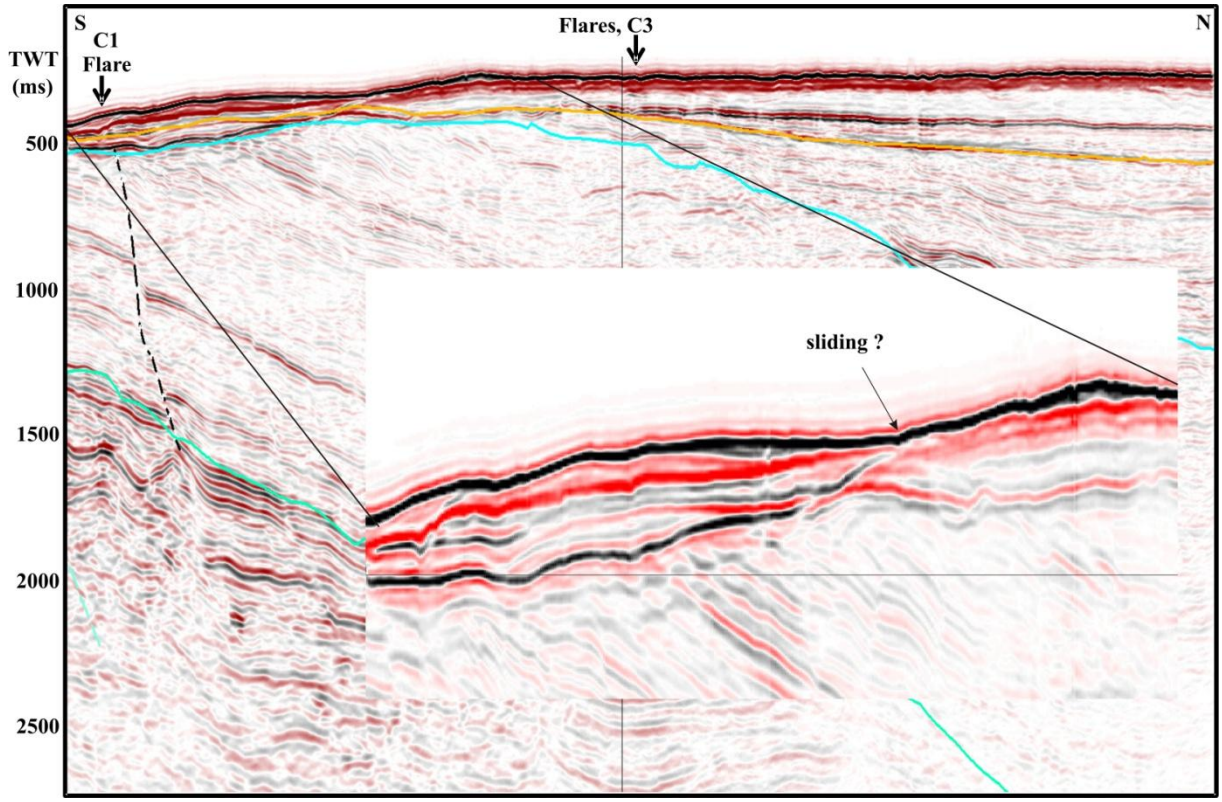

Figure 78. Seismic line (B1-B2-B3) showing possible glaciotectonic or neotectonic feature on the northern slope of Håkjerringdjupet (location given in Fig. 68)

A possible glacio or neotectonic feature has been identified in the Harstad Basin. This can be associated with glacial loading/sliding. The lobe of sediments towards the Håkjerringdjupet appears to be rotated or to have slid down towards the depression (Fig. 70, 72, 75, 76 & 78). The carbonate crust location C2 and one flare is associated with this feature in the north south direction (Fig. 76).

4.5 Gas hydrates and fluid flow

Gas hydrates in offshore areas are often associated with a bottom simulating reflector (BSR). A BSR is a seismic reflector which sub-parallels the seafloor reflection and is opposite in polarity (Shipley et al., 1979). The BSR indicates an acoustic impedance change across a high velocity layer of gas hydrate containing sediments overlying a gas filled layer (Stoll and Bryan, 1979). The BSR is paralleling the seafloor since the thickness of the gas hydrate

stability zone (GHSZ) is primarily decided by the hydrostatic pressure induced by the water column thickness (Sloan, 1990).

The nature and properties of BSRs and their occurrence vary depending on the sedimentary environment and fluid flow (Chand and Minshull, 2003). It is observed in many parts of the world that the BSR depths are determined by the presence of one or more of the gas hydrate inhibitors (NaCl, N_2, warm fluids, isostatic uplift, sliding, deglaciation) or facilitators (CO_2, H_2S, higher order hydrocarbon gases, increase in sea level, subsidence, glacial loading). Hydrates formed from pure methane assume molecular structure I while in the presence of higher order hydrocarbon gases it takes structure II. Structure I and II gas hydrates have different stability conditions and physical properties. Hence, it is complicated to interpret the presence of gas hydrates in areas with mixed gas/thermogenic gas causing disturbed BSRs, or in regions outside the methane hydrate stability field where all the gas hydrate is formed as structure II. The BSR or gas hydrate stability zone is shifted due to changes in sea level, variations in ice thickness or due to influx of warm or salty fluids from below, altering gas hydrate stability conditions.

Gas hydrate modelling was not carried out for the North Sea study areas since the bathymetry is too shallow for any gas hydrate to be stable. This was also suggested by previous studies where the methane hydrate stability ends north of the North Sea Fan (Vogt et al., 1999). The methane hydrates can be stable in some parts of the Norwegian Channel especially in the Skagerrak region where water depths exceed 400 m. With the presence of higher order hydrocarbon gases the hydrate stability zone can be even thicker. Previous studies from the North Sea indicated a stable gas hydrate scenario during the LGM. Gas hydrate modelling study by Fichler et al. (2005) estimated a methane hydrate stability zone of at least 400 m and as much as 1600 m if the glacial model thickness predicted for this region is correct.

The present regional gas hydrate stability estimated for structure II hydrates containing higher order hydrocarbon gases for the Barents Sea indicates a ~25 m deep base of the GHSZ covering the study area using a gas composition consisting of 96% methane, 3% ethane and 1% propane whereas for structure I MHSZ the thickness is zero (Chand et al., 2008). The estimated thickness of the GHSZ in two way travel time (TWT) in milliseconds (ms) is around 22-27 ms assuming 1990 m/s velocity for the sediments (observed at well 7220/2-1). High amounts of CO_2 (up to 6%) and H_2S (3 ppm) is reported from many wells in the Snøhvit area, indicating that CO_2 and H_2S may be of importance for modelling the gas hydrate stability in this region (NPD, 2005; e.g., NPD well report 7021/4-1).

During the LGM, about 20 000 ^{14}C years ago, a more than 1200 m thick ice cap covered the SW Barents Sea (Siegert et al., 2001). This made the whole SW Barents Sea stable for methane hydrate with MHSZ depths up to 600 m below the present seafloor (Chand et al., 2012b). The difference between the present MHSZ and that during LGM indicates a change of thickness by up to 600 m. The MHSZ within the Bear Island Trough (BIT) thinned to less than 250 m while most other parts of the southwestern Barents Sea including our study area

lie outside the MHSZ. The major change occurred outside the BIT, which made this region prone to release of methane accumulated during the last glaciation as methane hydrates.

4.5.1 Alvheim

Gas hydrates are not stable in this region.

4.5.2 Utsira High

Gas hydrates are not stable at Utsira High.

4.5.3 Harstad Basin

The study area in the Harstad Basin falls within the shallow water depths of Tromsøflaket and the area is modelled to be presently unstable for methane hydrate (Fig. 79a). In presence of higher order hydrocarbon gases, the region comes under gas hydrate stable conditions, especially the Håkjerringdjupet depression. Different theories could be suggested for the formation of this depression. One possible model is that the depression was an area of active leakage which resulted in the formation of gas hydrates and "freezing in" of the ground which was transported away by glaciers in the flow direction. Another possibility is that faults created weak lithologies which were eroded by glaciers and melt water flow and that were transported away by the ice streams (Ottesen et al., 2008). The second model is favoured since Håkjerringdjupet is located above easily eroded Cretaceous rocks and the Troms Finnmark Fault Complex (Figs 4a & b). Fluid flow appears to be controlled by dipping strata and open faults, isostatic uplift and glacial erosion. The fluid flow model for the study area is complex due to the two stage process which governed the accumulation and release of fluids and gases.

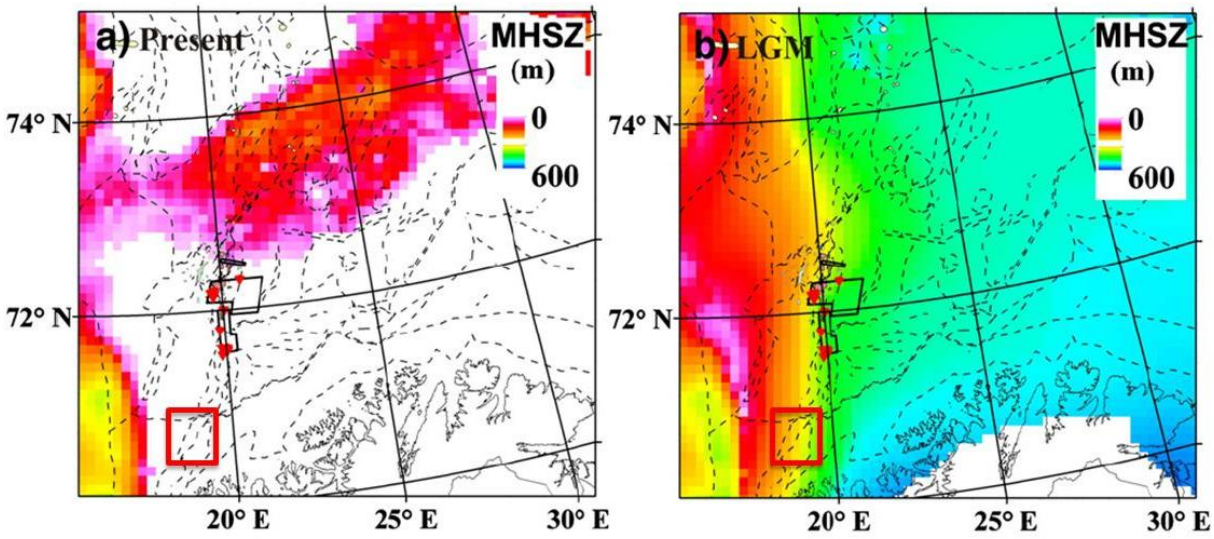

Figure 79. Methane hydrate stability zone map of the SW Barents Sea a) present and b) during LGM (Chand et al ., 2012b). The study area in the Harstad Basin is indicated with red square.

Fluids and methane accumulated as methane hydrates under glaciers during LGM (Fig. 79 b) and were later released during the deglaciation which created the pockmarks. Our study areas experienced a change in MHSZ thickness from 500 m to zero m during deglaciation. This can be confirmed in Håkjerringdjupet, where pockmarks were formed after the deposition of the glaciomarine and the lower part of the postglacial marine succession. The stratigraphic layers in the marine/glaciomarine units are cut by the pockmarks (Fig. 28b), indicating that the sediments were removed once the gas hydrates started melting after the glaciers retreated from this region. The process has a time delay and probably stopped after some time indicated by marine sediments a few centimetres thick of in pockmarks, similar to the observation in Loppa high. Thus the formation of pockmarks can be related to the deglaciation after the LGM.

5. SUMMARY AND CONCLUSIONS

- Studies in the North Sea indicate fluid flow along faults towards the seafloor dammed below postglacial deposits.
- A meltwater channel in the Alvheim area is a deep incision in the seafloor into the Quaternary succession, further facilitating fluid flow towards the seafloor.
- Gas flares were detected at 25 locations in the Alvheim area and at 21 locations in the Utsira high study areas.
- Carbonate crusts were located within pockmarks and along the side wall of the channel in the Alvheim study area whereas no carbonate crust locations were found in the Utsira high study area.

- Analysis of 12 gas samples collected from the Alvheim study area indicates microbial origin of the gas leaking through the seafloor.
- Several shallow gas seismic anomaly pockets were identified in the shallow subsurface in both the Alvheim and Utsira study areas.
- The Harstad Basin study area shows a two style fluid flow similar to that observed at the Loppa High where the fluids are either channelled along stratigraphic boundaries and/or facilitated by shallow and deep faults.
- Gas flares have been detected at 190 locations above the Harstad Basin. Some of these locations have multiple flares.
- Carbonate crusts are found in approximately 90% of the flare locations.
- Carbonate crusts were not found with confidence in Area N and area O above the Harstad Basin. These sites are located in the Håkjerringdjupet glacial trough, where the sediments have a higher content of mud compared to the flank areas north and south of the trough.
- In Area B, only one gas flare was recorded, but 116 occurences of carbonate crusts occur within a 1900 m long and 250 m wide belt trending WSW-ENE. This indicates that the majority of these crust fields are associated with extinct gas releases.
- Many of the carbonate crust fields have an abundance of sea trees, sponges and other hard bottom organisms, and locally high numbers of rock fish (Sebastes) and/or ling cod.
- Several occurrences of carbonate crusts show a close spatial relationship with coral mounds with abundant stony corals (*Lophelia pertusa)*, but so far it has not been observed that stony corals grow directly on the crusts. However, there are several sites in Area N where TFish imagery indicates this, but it needs to be confirmed by ROV observations and sampling.
- Extensive trawling has been documented by the SAS imagery. In some cases, this also affects coral mounds.
- Shallow and deep gas accumulations as well as pathways through faults and formation boundaries were identified in the Harstad Basin.
- Pure methane hydrates are not stable in the study area but similar to other parts of the Barents Sea, gas hydrates formed from methane and other hydrocarbon gases are stable.
- The thickness of the methane hydrate stability zone has changed from about 300 m to zero since the LGM in Harstad Basin area.

6. REFERENCES

Andresen, K.J., Huuse, M. & Clausen, O.R., 2008. Morphology and distribution of Oligocene and Miocene pockmarks in the Danish North Sea – implications for bottom current activity and fluid migration, Basin Research, 20, 445-466.

Brekke, T., Lønne, Ø., Ohm, S.E., 1997. Light hydrocarbon gases in shallow sediments in the northern North Sea, Marine Geology, 137, 81-108.

Cameron, T.D.J., Stoker, M.S., Long, D., 1987. The history of Quaternary sedimentation in the UK sector of the North Sea Basin, Jour. Geol. Soc., 144, 43-58.

Chand, S. & Minshull, T. A. 2003: Seismic constraints on the effects of gas hydrate on sediment physical properties and fluid flow: A review. Geofluids 3, 275-289.

Chand, S., Mienert, J., Andreassen, K., Knies, J., Plassen, L., Fotland, B., 2008: Gas hydrate stability zone modelling in areas of salt tectonics and pockmarks of the Barents Sea suggests an active hydrocarbon venting system. Marine and Petroleum Geology 25, 625-636.

Chand, S., Thorsnes, T., Rise, L. & Bøe, R. 2012a: Pockmarks, gas flares, tectonic features and processes leading to their formation, south western Barents Sea. NGU Report 2012.017.

Chand, S., Thorsnes, T., Brunstad, H., Stoddert, D., Bøe, R., Lågstad, P. & Svolsbru, T. 2012b: Huge gas flares, pockmarks and gas accumulation along the Loppa High, SW Barents Sea indicate multiple episodes of formation and fault controlled focused fluid flow. Earth and Planetary Science Letters 331-332, 305-314.

Chappell, J., Shackleton, N.J., 1986. Oxygen isotopes and sea level, Nature, 324, 137-140.

Clausen O.R, Nielsen O.B, Huuse M, Michelsen O., 2000. Geological indications for Palaeogene uplift in the eastern North Sea Basin, Global and Planetary Change, 24, 175-187.

Clayton, C.J., Hay, S.J., Baylis, S.A. & Dipper, B. 1997. Alteration of natural gas during leakage from a North Sea salt diapir field, Marine Geology, 137, 69-80.

Cremiere, A., Lepland, A., Sahy, D., Noble, S.R., Condon, D.J., Chand, S., Stoddart, D., Pedersen, J.H., Sauer, S., Brunstad, H., Pedersen, R.B., Thorsnes, T., 2014. Methane-derived carbonates as archives of past seepage activity along the Norwegian margin, EGU Conference, Vienna.

Eldholm, O., Sundover, E., Myhre, A.M. & Faleide, J.I. 1984: Cenozoic evolution of the continental margin off Norway and western Svalbard. In: AM Spencer (ed) Petroleum geology of the North European Margin, Graham and Trotman, London, 3-18.

Eidvin, T. & Riis, F. 1989: Nye dateringer av de tre vestligste borehullene I Barentshavet. Resultater og konsekvenser for den tertiære hevingen. NPD Contribution 27, 44 pp.

Eidvin, T., Brekke, H., Riis, F. & Rensaw, D.K. 1998: Cenozoic stratigraphy of the Norwegian Sea continental shelf 64^{o}N – 68^{o}N. Norsk Geologisk Tidskrift 78, 125-151.

Eidvin, T., Jansen, E. & Riis, F. 1993: Chronology of Tertiary fan deposits off the western Barents Sea: implications for the uplift and erosion history of the Barents Shelf. Marine Geology 112, 109-131.

Faleide, J.I., Solheim, A., Fiedler, A., Hjelstuen, B.O., Andersen, E.S., Vanneste, K. 1996: Late Cenozoic evolution of the western Barents Sea – Svalbard continental margin. Global and Planetary change 12, 53-74.

Fichler C, Henriksen S, Rueslåtten H, Hovland M., 2005. North Sea Quaternary morphology from seismic and magnetic data: indications for gas hydrates during glaciations? Petroleum Geoscience 11, 331-337.

Forsberg, C.F., Planke, S., Tjelta, T.I., Svanø, G., Strout, J.M., Svensen, H., 2007. Formation of pockmarks in the Norwegian Channel, Proceedings of the 6th International Offshore Site Investigation and Geotechnics conference, Confronting New Challenges and Sharing Knowledge, London, UK.

Grollimund, B., Zoback, M.D., 2000. Post glacial lithospheric flexure and induced stresses and pore pressure changes in the northern North Sea, Tectonophysics, 327, 61-81.

Haavik K.E, Landrø M., 2014. Iceberg ploughmarks illuminated by shallow gas in the central North Sea, Quaternary Science Reviews, 103, 34-50.

Haflidason H, King E.L, Sejrup H.P., 1998. Late Weichselian and Holocene sediment fluxes of the northern North Sea margin, Marine Geology, 152, 189-215.

Hald, M., Sættem, J. & Nesse, E. 1990: Middle and Late Weichselian stratigraphy in shallow drillings from the southwestern Barents Sea: foraminiferal, amino acid and radiocarbon evidence. Norsk Geologisk Tidskrift 70, 241-257.

Hovland, M. 1982a. Pockmarks and the recent geology of the central section of the Norwegian Trench, Marine Geology, 47, 283-301.

Hovland, M., 1982b. A coast parallel depression, possibly caused by gas migration, off western Norway, Marine Geology, 50, 11-20.

Hovland, M., 1991. Large pockmarks, gas charged sediments and possible clay diapirs in the Skagerrak, Marine and Petroleum Geology, 8, 311-316.

Hovland M., 2007. Discovery of profile natural methane seeps at Gullfaks, northern North Sea. Geo Marine Letters, 27, 197-201.

Hovland M, Sommerville J.H., 1985. Characteristics of two natural gas seepages in the North Sea, Marine and Petroleum Geology, 2, 319-326.

Hovland, M., Talbot, M.R., Qvale, H., Olaussen, S., Aasberg, L., 1987. Methane related carbonate cements in pockmarks of the North Sea, Journal of Sedimentary Petrology, 57, 881-892.

Hubscher, C. & Borowski, C., 2006. Seismic evidence for fluid esacpe from Mesozoic cuesta type topography in the Skagerrak, Marine and Petroleum Geology, 23, 17-28.

Huuse, M., Lykke-Andersen, H. and Piotrowski, J. A., 2003. Geophysical Investigations of Buried Quaternary Valleys in the Formerly Glaciated NW European Lowland: Significance for Groundwater Exploration, Journal of Applied Geophysics, 53, 153-300.

Huuse, M. & Lykke-Andersen, H. 2000. Overdeepend Quaternary valleys in the eastern Danish North Sea: morphology and origin, Quaternary Science Review, 19, 1233-1253.

Isaksen, D., Tonstad, K., 1989. A revised Cretaceous and Tertiary lithostratigraphic nomenclature for the Norwegian North Sea, Norwegian Petroleum Directorate Bull. 5, pp39.

Karstens, J. & Berndt, C., 2015. Seismic chimneys in the southern Viking Graben – Implications for palaeo fluid migration and overpressure evolution, Earth and Planetary Sceince Letters, 412, 88-100.

Knies, J., Matthiessen, J., Vogt, C., Laberg, J.S., Hjelstuen, B.O., Smelror, M., Larsen, E., Andreassen, K., Eidvin, T. & Vorren, T.O. 2009: The Plio-Pleistocene glaciation of the Barents Sea-Svalbard region: a new model based on revised chronostratigraphy. Quaternary Science Reviews 28, 812-829.

Laberg, J. S., Andreassen, K., Knies, J., Vorren, T.O. & Winsborrow, M. 2011: Late Pliocene-Pleistocene development of the Barents Sea Ice Sheet, Geology, 38, 107-110.

Landrø M, Strønen L.K, 2003. 4D study of fluid effects on seismic data in the Gullfaks Field, North Sea, Geofluids, 3, 233-244.

Lastochkin, A.N. 1977: Submarine valleys on the northern continental shelf of Europe, Izv. Vsesoy. Geogr. Obsh. 5, 412-417.

Lonergan L, Maidment S.C.R, Collier J.S., 2006. Pleistocene subglacial tunnel valleys in the central North Sea basin: 3-D morphology and evolution, Journal of Quaternary Science, 21, 891-903.

Løseth, H., Lippard, S.J., Sættem, J., Fanavoll, S., Fjerdingstad, V., Leith, L.T., Ritter, U., Smelror, M. & Sylta, O. 1992: Cenozoic uplift and erosion of the Barents Sea – evidence from the Svalis Dome area. In: TO Vorren et al (eds) Arctic Geology and Petroleum Potential (Norw. Pet. Soc. Spec Pub. 2, Elsevier Amsterdam, 639-661.

Mazzini, A., Duranti, D., Jonk, R., Parnell, J., Cronin, B.T., Hurst, A. & Quine, M., 2003. Palaeo-carbonate seep structures above an oil reservoir Gryphon Field, Tertiary, North Sea, Geo Marine Letters, 23, 323-339.

Mørk, M.B. & Duncan, R.A. 1993: Late Pliocene basaltic volcanism on the western Barents shelf margin: implications from petrology and ^{40}Ar -^{39}Ar dating of volcani-clastic debris from a shallow drill core. Norsk geologisk Tidskrift 73, 209-225.

Nansen, F. 1904: The bathymetrical features of the North Polar seas with a discussion of the continental shelves and previous oscillations of the shoreline. Norwegian Polar Expeditions 1893-1896, Scientific results, vol. IV, 231pp.

Norwegian Petroleum Directorate, 2005: NPD well report 7021/4-1, http://factpages.npd.no/ReportServer?/FactPages/PageView/wellbore_exploration&rs:Comma

nd=Render&rc:Toolbar=false&rc:Parameters=f&NpdId=135&IpAddress=193.156.2.1&CultureCode=nb-no

Nygård A, Sejrup H.P, Haflidason H, Bryn P., 2005. The glacial North Sea Fan, southern Norwegian margin: architecture and evolution from the upper continental slope to the deep sea basin, Marine and Petroleum Geology, 22, 71-84.

Nyland, B., Jensen, L.N., Skagen, J., Skarpnes, O. & Vorren, T. O. 1992: Tertiary uplift and erosion in the Barents Sea: Magnitude, timing and consequences. In: RM Larsen and H Brekke, TB Larsen and E Talleraas (eds), Structural and tectonic modeling and its application to petroleum geology, Norw. Pet. Soc. Spec. Publ. 1, Elsevier, Amsterdam, 153-162.

Nøttvedt, A., Berglund, T., Rasmussen, E. & Steel, R. 1988: Some aspects of Tertiary tectonics and sediments along the western Barents shelf. In: Morton AC, and Parson LM, (eds): Early Tertiary volcanism and the opening of the NE Atlantic. Geological Society of London, special publication 39, 421-425.

Ottesen D, Dowdeswell J, Bugge J., 2014. Morphology, sedimentary infill and depositional environments of the early Quaternary North Sea basin (56^{o} to 62^{o} N), Marine and Petroleum Geology, doi: 10.1016/j.marpetgeo.2014.04.007.

Ottesen, D., Stokes, C.R., Rise, L., Olsen, L., 2008. Ice-sheet dynamics and ice streaming along the coastal parts of northern Norway. Quaternary Science Reviews, 27, 922-940.

Pau, M., Hammer, Ø., Chand, S., 2014. Constraints on the dynamics of pockmarks in the SW Barents Sea: Evidence from gravity coring and high resolution, shallow seismic profiles, Marine Geology, 355, 330-345.

Rawson, P. F., Riley, L. A. 1982: La test Jurassic-Early Cretaceous events and the "Late Cimmerian unconformity" in North Sea area. AAPG Bull. 66, 2628-2648.

Riis, F. & Fjeldskaar, W. 1992: On the magnitude of the late Tertiary and Quaternary erosion and its significance for the uplift of Scandinavia and the Barents Sea. In: RM Larsen, H Brekke, BT Larsen, and E Talleraas (eds): Structural and tectonic modeling and its application to the Petroleum Geology NPF Special Publication 1, 163-185, Elsevier, Amsterdam.

Rise, L., Sættem, J., Fanavoll, S., Thorsnes, T., Ottesen, D., Bøe, R., 1999. Sea-bed pockmarks related to fluid migration from Mesozoic bedrock strata in the Skagerrak offshore Norway, Marine and Petroleum Geology, 16, 619-631.

Schroot B.M, Klaver G.T., Schuttenhelm R.T.E., 2005. Surface and subsurface expressions of gas seepage to the seabed – examples from the southern North Sea, Marine and Petroleum Geology, 22, 499-515.

Sheriff, R. 1980: Nomogram for Fresnel zone calculation. Geophysics 45, 968-972.

Shipley, T.H., Houston, M., Buffler, R.T., Shaub, F.J., McMillan, K.J., Ladd, J.W. & Worzel, J.L. 1979: Seismic reflection evidence for the wide spread occurrence of possible gas hydrate horizons on continental slopes and rises. American Association of Petroleum Geologists 63, 2204-2213.

Siegert, M.J., Dowdeswell, J.A., Hald, M., Svendsen, J.I. 2001: Modelling the Eurasian Ice Sheet through a full (Weichselian) glacial cycle. Global and Planetary Change 31, 367-385.

Sigmond, E.M.O. 1992: Bedrock map of Norway and adjacent ocean areas, NGU.

Sloan, E. D. 1990: Clathrate Hydrates of Natural Gases, Marcel Dekker, NewYork.

Solheim, A. & Kristoffersen, Y. 1984: Sediments above the upper regional unconformity: thickness, seismic stratigraphy and outline of the glacial history, Norsk Polarinstitutt Skrifter 179B, 26pp.

Spencer, A.M., Home, P.C. & Berglund, L.T. 1984: Tertiary structural development of western Barents shelf: Troms to Svalbard. In: AM Spencer (ed) Petroleum geology of the North European Margin, Graham and Trotman, London, 199-210.

Stoker, M. S., Long, D., Fyre, J. A. 1985. The Quaternary succession in the central North Sea, Newsletter on Stratigraphy, 14, 119-128.

Stoll, R.D. & Bryan, G.M. 1979: Physical properties of sediments containing gas hydrates. Journal of Geophysical Research 84, 645-648.

Sættem, J., Rise, L. & Westgard, D.A. 1992: Composition and properties of Glacigenic sediments in the southwestern Barents Sea. Marine Geotechnology 10, 229-255.

Vogt, P.R., Gardner, J., Crane, K., 1999. The Norwegian-Barents-Svalbard (NBS) continental margin: Introducing a natural laboratory of mass wasting, hydrates, and ascent of sediment, pore water, and methane. Geo Marine Letters, 19, 2-21.

Von Deimling J.S., Rehder G, Greinert J, McGinnis D.F., Boetius A, Linke P., 2011. Quantification of seep related methane gas emissions at Tommeliten, North Sea, Continental Shelf Research, 31, 867-878.

Vorren, T.O., Hald, M. & Lebesbye, E. 1988: Late Cenozoic environments in the Barents Sea. Paleocenography 3, 601-612.

Vorren, T.O., Kristoffersen, Y. & Andreassen, K. 1986: Geology of the inner shelf west of North Cape. Norsk Geologisk Tidskrift 66, 99-105.

Vorren, T.O., Lebesbye, E., Andreassen, K. & Larsen, B. 1989: Glacigenic sediments on a passive continental margin as exemplified by the Barents Sea. Marine Geology 85, 251-272.

Vorren, T.O., Lebesbye, E. & Larsen, K,B. 1990: Geometry and genesis of the glacigenic sediments in the southern Barents Sea, In: Dowdeswell JA and Scourse JD, (eds) Glacimarine environments, processes and sediments, Geol Soc London, Sp Publ. 53, 309-328.

Vorren, T.O., Richardsen, G., Knutsen, S.M. & Henriksen, E. 1991: Cenozoic erosion and sedimentation in the western Barents Sea. Marine and Petroleum Geology 8, 317-340.

Wingfield, R. 1989. Glacial incisions indicating Middle and Upper Pleistocene Ice limits off Britain, Terra Nova, 1, 538-548.

GEOLOGICAL
SURVEY OF
NORWAY

· NGU ·

Geological Survey of Norway
PO Box 6315, Sluppen
N-7491 Trondheim, Norway

Visitor address
Leiv Eirikssons vei 39
7040 Trondheim

Tel (+ 47) 73 90 40 00
E-mail ngu@ngu.no
Web www.ngu.no/en-gb/